Production rates of ^{36}Cl in basalts from the calibration site of Fuerteventura, Canary Islands

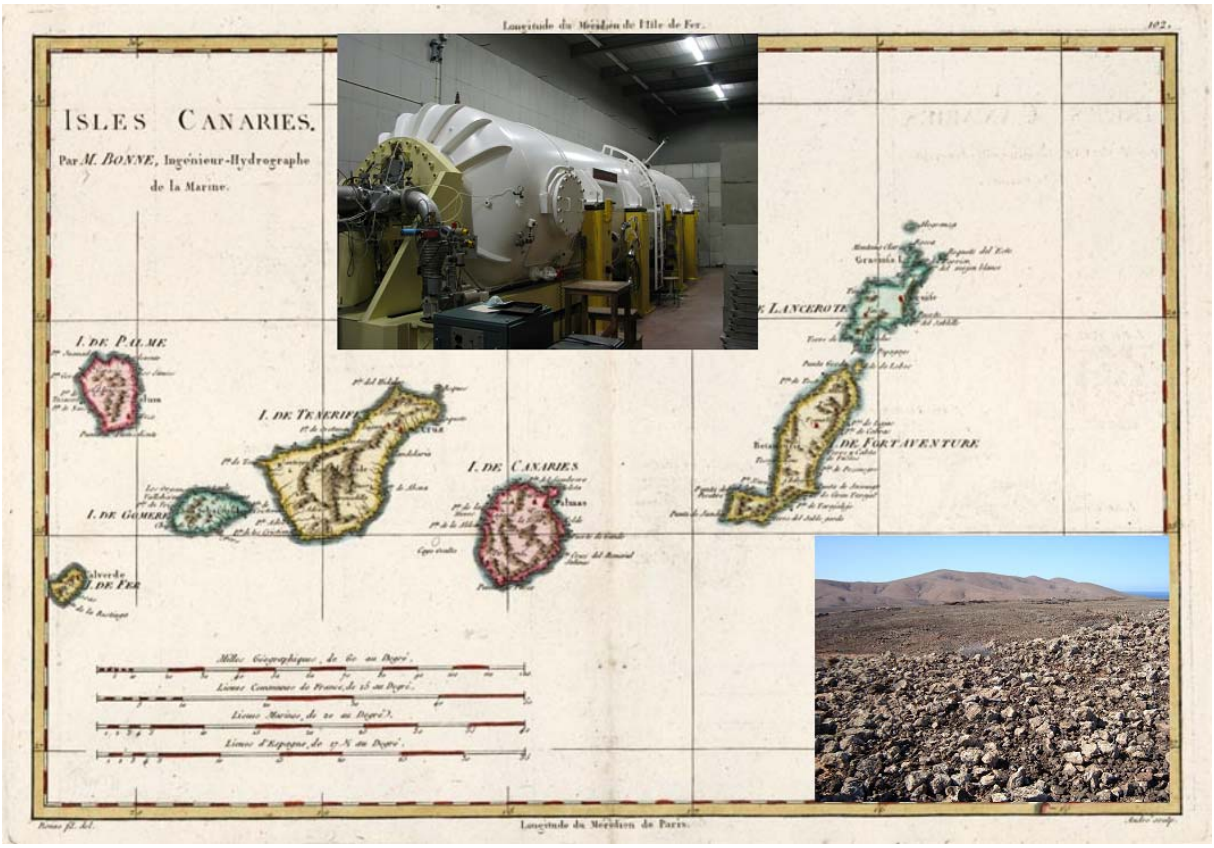

Katrin Mai

Production rates of ^{36}Cl in basalts from the calibration site of Fuerteventura, Canary Islands

Cover: Map of the Canary Islands, Isles Canaries, R. Bonne, 1787, Paris, hand colored.

ISBN: 978-90-393-5108-6

Print: This thesis was printed by CPI Wöhrmann Print Service

Production rates of ^{36}Cl in basalts from the calibration site of Fuerteventura, Canary Islands

Productiesnelheden van ^{36}Cl in basalten van de calibratielocatie Fuerteventura, Canarische Eilanden

(met een samenvatting in het Nederlands)

Proefschrift

ter verkrijging van de graad van doctor aan de Universiteit Utrecht
op gezag van de rector magnificus, prof. dr. J.C. Stoof,
ingevolge het besluit van het college voor promoties
in het openbaar te verdedigen
op woensdag 2 september 2009 des middags te 12.45 uur

door

Katrin Mai

geboren op 10 augustus 1975 te Berlijn, Duitsland

Promotor: Prof. dr. R. Kamermans

Co-promotor: Dr. K. van der Borg

Dit onderzoek werd mogelijk gemaakt met financiële steun van de Marie-Curie Fellowship als deel van het Europese Unie programma “Improving the human research potential and socio-economic knowledge base”

To my parents

Content

1. Introduction and overview

1.1 Introduction

The history of landforms is an important field of research in geosciences because their development affects the welfare and even the existence of human civilization. Dramatic changes of the landscape because of landslides, floods, volcanic eruptions or (de-)glaciations have had and still have strong influence on people throughout human history. To understand the progression, the time frame and probable periodicity of these processes it is necessary to investigate the development of the land surfaces over geological as well as historical time. This includes determining the ages of land surfaces, and rates of geological and geomorphic processes such as erosion rates and rates of motion of crustal segments along faults (fault slip rates).

The landscape is continuously exposed to cosmic rays. These cosmic rays, which are high-energetic particles from the outer space, produce special isotopes in nuclear reactions with target elements in surface rocks. These isotopes can be discriminated from the elements present in the earth's matter. Some of them are stable nuclides, such as ^{3}He and ^{21}Ne, while others like ^{10}Be, ^{26}Al, and ^{36}Cl are radionuclides. These isotopes formed by interaction of cosmic rays with terrestrial matter are called cosmogenic nuclides. The concentrations of the formed stable nuclides are proportional to the exposure time, while for the radionuclides an equilibrium between production and decay is reached, dependent on its half-life. The intensity of the cosmic rays at the earth surface is low and therefore only a few atoms per gram rock per year are produced. Measurements of these isotopes require a sensitive method to determine their concentration in comparison with their natural background, which has to be extremely low, and discriminate them against an overwhelming number of common isotopes. In the case of the isotopes ^{3}He or ^{21}Ne the measurements are performed with noble gas spectrometers (for details see e.g. Niedermann et al., 1993; Niedermann, 2002). The radio-nuclides ^{10}Be, ^{26}Al, ^{36}Cl are determined with the ultra-sensitive method of Accelerator Mass Spectrometry (AMS) (Litherland, 1984). During the last thirty years the sensitivity of AMS measurements has been increased to isotope ratios of $1{:}10^{15}$ and a precision of 0.3 to 2 % for isotope analyses of ^{10}Be, ^{14}C, ^{26}Al, and ^{36}Cl (see Table 1.1) (Freeman et al., 2007). It has now become a method with a wide spectrum of applications such as volcanology, tectonics, geomorphology, and hydrology, but also in pre-historic archaeology and medicine. The methods of determination of surface ages based on cosmogenic nuclides cover a relatively wide range of geologically younger ages, which may lead to important progress especially for

studies of Quaternary geology. Because a fairly large number of different cosmogenic nuclides are formed in a great variety of matter there are many possibilities in terms of employed cosmogenic nuclide and analysed material.

Isotope	Half-life $T_{1/2}$	Detection limit in AMS measurements	Precision in AMS measurements
^{10}Be	1.34 ± 0.07 Ma	$3*10^{-15}$	3 %
^{14}C	5730 ± 40 years	10^{-15}	1-3 ‰
^{26}Al	0.705 ± 0.024 Ma	$1*10^{-15}$	3 %
^{36}Cl	0.301 ± 0.005 Ma	$3*10^{-15}$	5 %

Table 1.1. Half-lives, sensitivity and precision of cosmogenic isotopes typically measured with AMS (Freeman et al., 2007).

The concentration of the isotopes formed by exposure to cosmic rays depends on the time of exposure and on the intensity of the irradiation but also on the cross sections of nuclear reactions and the chemical composition of the rock. The production rate describes the production of a cosmogenic nuclide from target material, which here is rock at the earth surface. It is defined as the production of the number of atoms of an isotope per gram target material in a year. Since rocks show a wide variety of chemical composition, the production rates given in atoms per gram rock per year are difficult to inter-compare. Therefore, the production rate is preferably related to the individual target elements, and given in atoms per gram target element in a year This provides a parameter that is independent of chemical variation in composition of the target material. There is, however, still a considerable uncertainty about the absolute production rates of the cosmogenic nuclides from the individual target elements. Furthermore there is a variety of factors that influence the production rates at any place on earth such as the earth's magnetic field depending on the geomagnetic latitude, the elevation, shielding by surroundings, or temporary coverage with snow or ash. To take these influences into account, scaling factors have been developed which are also still debated.

To reduce these uncertainties and to establish cosmogenic nuclide dating securely as a method for age determination the CRONUS-EU programme (Cosmic Ray prOduced NUclide Systematics on Earth; http://www.cronus-eu.net/) was initiated. One of the tasks of CRONUS-EU was to determine in situ production rates of a number of cosmogenic nuclides such as ^{3}He, ^{10}Be, ^{26}Al, and ^{36}Cl on natural and artificial samples at a number of calibration

sites such as Cape Verdes, Canary Islands, Etna or Mt. Kilimanjaro. Further, numerical models of the production of cosmogenic nuclides and of the terrestrial influences such as the earth magnetic field or the shielding effect of the atmosphere were developed.

For the study presented in this thesis, which was part of the CRONUS-EU programme, samples were collected on the island of Fuerteventura, Canary Islands, to contribute calibration data for the production of ^{36}Cl from the target elements common in basalts (mainly calcium, potassium, and chlorine) from a mid-latitude, low-altitude calibration site. The reason why in the CRONUS-EU programme a strong focus was placed on basalt as a natural target material is its exceptionally wide distribution as preserved lava flows over latitude and elevation. No other type of rock surface, such as moraines or glacial polish, provides such a wide range of sampling sites for calibration. Furthermore, basaltic lavas do not contain any cosmogenic nuclides from a prior exposure due to their origin from sources deep below the earth's surface. In addition, they do not have a long formation process but rather form instantaneously through eruption. Basaltic rocks are also fairly resistant against weathering and their surface structures make it possible to estimate their geomorphic stability and the amount of erosion (Zreda & Phillips, 2000). In addition, the largely similar composition of basalts facilitates the comparison of the total production rates of e.g. ^{36}Cl in the rocks from different sites on earth. All these particulars together made basalt the preferred rock for this project of calibrating the production rates, despite the chemical complexity of the rock. Due to the largely arid climate of Fuerteventura the surfaces of the lava flows are mostly well preserved and the overall condition of the rocks' surface structures indicated geomorphic stability and extremely low rates of chemical weathering. To ensure minimum erosion and weathering, relatively young lava samples with ages ranging from about 50 ka to 400 ka were collected.

1.2 Outline of the thesis

The production rates of ^{36}Cl in the basalts were obtained by measuring the amount of ^{36}Cl for several flows of different ages and by determining independently the ages of the samples with the ^{40}Ar/^{39}Ar-dating method (Schneider et al., submitted). This included the establishment of the preparation and measurement methods for ^{36}Cl determination at the accelerator laboratory at the Utrecht University. The results are values, which are integrated over time and consequently include all the variations of the cosmic radiation throughout the

exposure time of the samples. These variations depend on changes in earth's magnetic field, the climate and other factors. These data were then scaled with respect to sea level and high latitude (SLHL) to remove the site-specific features that influence the production rate and to provide data comparable to production rates from other sites. Basalts are chemically fairly complex i.e. they include target elements for several different possible production mechanisms whose contributions are superposed. In spite of the general compositional similarity of basalts even basalts from the same site show some chemical variation among the individual eruption periods throughout the time. This means that the concentrations of the different target elements change (for the samples from Fuerteventura the element concentrations varied within a range of approximately 10 %). Therefore the production rate values for the whole rock vary, which is a serious restriction to the viability of the inter-comparison of whole rock production rates because even for the material from the same place and generally the same magmatic system the variation of the total rock production rates can reach 40 %. To improve this situation it was tried to deduce the production rate of ^{36}Cl from calcium alone for each flow from the production rates of ^{36}Cl obtained for the whole rock. Calcium was chosen for its high and relatively stable abundance in the rocks and its expected high production rate for ^{36}Cl.

Chapter 2 contains details of exposure dating. The cosmic radiation is characterised and its behaviour which is influenced by the earth magnetic field, attenuation in the atmosphere and rock is illustrated. The production of cosmogenic nuclides by cosmic radiation in general and specifically for ^{36}Cl is discussed in detail. Furthermore, the scaling factors that are applied to correct for a variety of conditions influencing the production for example the geographic position of the site or the surrounding hillside, and the build-up of cosmogenic nuclides are explained. Examples are given to illustrate the effects uncertainties in the determination of the conditions (e.g. angular measurements for the topography) may have on the respective scaling factors and error estimates for the scaling factors obtained for the site of Fuerteventura are presented.

Chapter 3 gives an introduction to the origin, geological development and recent setting of the Canary Islands and Fuerteventura. The geological units relevant to this research are characterised and their historical relation is specified.

The experimental methods are described in chapter 4. The sampling strategy and the sample selection criteria are delineated. The sample processing and the preparation of the AMS samples are described in detail. Furthermore the measurement techniques, tests on some preparation issues and the data analysis including error analysis are discussed.

In chapter 5 the results of the measurements are presented and analysed. The production rates for the total rock and for the individual target elements based on these data are calculated and compared to published production rates.

The discussion and interpretation of the data are provided in chapter 6. The influences of different environmental conditions on cosmogenic nuclide production and nuclide storage are examined. Special attention is directed to what effects preparation and measurement have on the results, but geological, geochemical and geophysical aspects as well as influences of the (paleo-)climate are also discussed.

Chapter 7 provides the conclusions and suggestions for the work that needs to be done for further progress in the field of cosmogenic nuclide dating.

The appendices give detailed measurement results, the site specific data and the elemental compositions of the samples from XRF and ICP-MS measurements. The laboratory protocol which was followed during the sample preparation is also provided.

2 Theory of exposure dating

2.1 Cosmic radiation as a source of cosmogenic nuclide production

Cosmogenic nuclides are continuously produced by interaction of cosmic rays with target elements on terrestrial or extraterrestrial matter. On the earth the production occurs mainly from secondary particles resulting from interaction of primary cosmic rays with atoms in the uppermost layers of the atmosphere. These secondary particles are mainly neutrons and muons. The primary cosmic radiation can be separated into (high energy) galactic cosmic radiation (GCR, 0.1 - >10 GeV), which originates from within the Milky Way galaxy, outside the solar system, and the (lower energy) solar cosmic radiation from solar outbursts (SCR, typically 0.1 - 100 MeV; 1-10 GeV rarely can be reached during highly energetic flares), which usually gives only a small contribution to the total cosmic ray flux at the earth's surface even at high latitudes (e.g. Lingenfelter & Flamm, 1964; Reedy & Arnold, 1972; Reedy et al., 1983; Simpson, 1983; Cerling & Craig, 1994). The intensity of solar cosmic radiation increases by orders of magnitude during solar flares, which occur usually around sunspot maxima (Reedy & Arnold, 1972; Tuniz et al., 1998) and it may even exceed the galactic ray flux for short periods. In periods of high sun spot activity the GCR flux at the earth is reduced (especially the lower energy part of the spectrum) by up to 20-30 %, through the stronger solar magnetic field, which creates an additional magnetic field around the earth. At the times of a quiet sun with a weaker magnetic field the GCR flux is higher (Finkel & Suter, 1993; Ziegler, 1996). An additional but small component of the primary cosmic radiation is the anomalous cosmic radiation (ACR), which is thought to originate from the neutral interstellar gas that drifts into the heliosphere and becomes ionized near the sun.

The galactic cosmic rays (GCR) comprise protons (87-90 %), α-particles (9-12 %), electrons, neutrons, and heavy particles (together 1 %) (Simpson, 1983). The solar cosmic radiation (SCR) comprises protons (98 %) and α-particles (2 %). The component of interest in terms of the production of terrestrial cosmogenic nuclides is restricted to the high energy particles with an energy range of roughly 1 to 10^{10} GeV (Gosse & Phillips, 2001).

The cosmic ray flux on earth has changed substantially with time because of a variety of both extraterrestrial and terrestrial factors. Extraterrestrial factors like nearby supernovae, variations in solar activity or the movement of the solar system through the galaxy or relative

to the galactic plane are expected to affect the production rate uniformly everywhere on earth. On the other hand, terrestrial factors like variations of the earth magnetic field or the climate cause local and regional variations in the effective production rate (Reedy et al., 1983; Klein & Gosse, 1996). These different parameters have specific effects on the time-integrated cosmic ray flux. Long-term variations in the primary galactic cosmic ray flux occur over times of million years, whereas variations induced by solar activity occur within 1 to 100 years. Both have only a small influence on the terrestrial cosmogenic nuclide production, which usually integrates over a time range of 10^3 to 10^5 years (Pigati & Lifton, 2004). In contrast, the variations of the geomagnetic field strength and the magnetic pole positions occurring over a time of 10^3 to 10^4 years have significant impact on the cosmogenic nuclide production on surfaces with such an exposure age (Table 2.1) (Pigati & Lifton, 2004).

Time Range (year)	**Impact Factor**
10^0-10^2	Solar outbursts Polar wander (orientation of the magnetic pole position)
10^3-10^4	Variation of the geomagnetic field strength Long-term solar cycles (2400 year period)
10^6	Variation of cosmic ray flux

Table 2.1 Periodicity of factors influencing the cosmic ray flux at the earth's surface (see text).

The magnetic field of the earth consists of a main component that follows to a good approximation the field of a somewhat eccentric dipole, which at present is inclined relative to the rotation axis of the earth by about 11.5˚. The field lines surround the earth from north to south. Besides the main field strong non-dipole components also occur, which can extend over regions being several thousand kilometres wide and may locally add up to 10 % of the dipole field strength (Pigati & Lifton, 2004). These non-dipole components originate mainly from the geodynamo in the earth core, which also produces the main component i.e., the dipole part of the geomagnetic field, and from the earth lithosphere (so-called crustal magnetic field) (Constable, 2007). The non-dipole components "deform" the pure dipole structure of the geomagnetic field (Fig. 2.1).

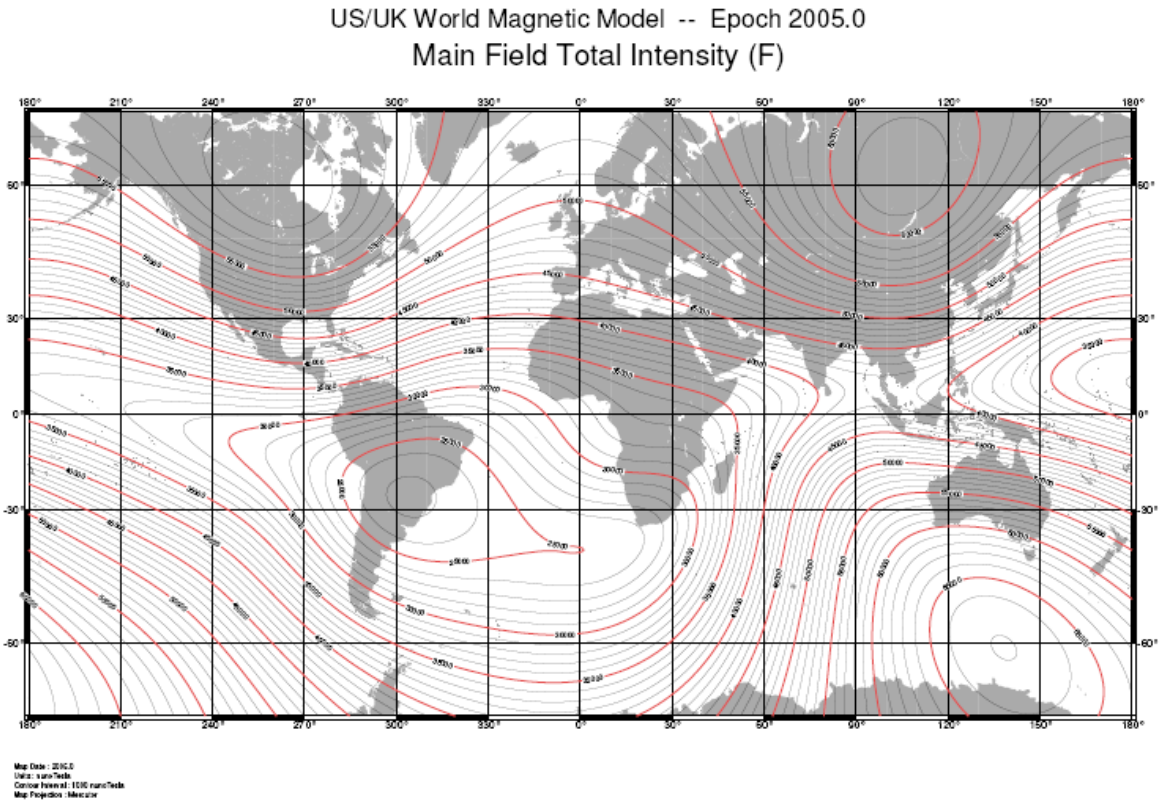

Fig. 2.1 Map of the geomagnetic main total field intensity (F), (from http://www.ngdc.noaa.gov/seg/WMM/data/wmm-F05.pdf, 2007). IGRF (International Geomagnetic Reference Field) epoch 2005.0. Clearly the magnetic field is not a perfect dipole field.

The geomagnetic field intensity and orientation have changed significantly throughout time (secular variations). The information about the time-dependent variation of the magnetic field has been obtained from countless historical, archeomagnetic and paleomagnetic investigations. For the purpose of comparison of data from all over the world the paleointensity data are commonly transformed into virtual axial dipole moments (VADM) or virtual dipole moments (VDM) that would generate the intensity and direction observed at the site[1] (Salis et al., 1989). Both VADM and VDM are proxies for the true dipole moment, but they also may include non-dipole contributions assigned to the dipole intensity, which can cause the VADM and VDM values to deviate from the true dipole moment, especially for averaging over short time scales (Usoskin et al., 2006). There are different time series of field intensity data, e.g. SINT800 (Guyodo & Valet, 1999), SINT2000 (Valet et al., 2005), or by Yang et al. (2000b), which cover time spans of up to 2000 kyr (note: kyr = 1000 years of

[1] The VADM assumes that the earth's magnetic dipole axis equals the earth's (geographic) axis of rotation while for the VDM the dipole axis is obtained from the magnetic inclination for the site of observation (Merrill et al., 1998).

duration, ka = 1000 years of age; C. Langereis, UU 2009, pers. comm.). The investigations throughout this thesis refer to the data set of SINT800 (Guyodo & Valet, 1999; based on recommendation by N. Lifton and C. Constable, 2007, pers. comm.; SINT data kindly provided by J.-P. Valet, 2007, written comm.).

The trajectories of the charged particles are bent by the earth's magnetic field depending on the strength of the field, the direction of incidence of the particles, and the momentum and the charge of the particles, which define their rigidity. The magnetic rigidity R (momentum over charge) of a particle determines its ability to penetrate the magnetosphere:

$$R = \frac{pc}{q} \quad \text{(in GV)}, \tag{2.1}$$

where p is the particle's momentum (kg.m.s^{-1}), q its charge (C), and c is the speed of light (m.s^{-1}). The higher the energy of the particle the deeper the particle invades the magnetosphere, i.e. the more magnetic field lines it crosses. The threshold value of the cut-off rigidity, R_c, describes the minimum kinetic energy per charge a particle needs to penetrate the magnetosphere at the point of incidence and to arrive at the upper atmosphere. Primary particles with a rigidity lower than R_c are deflected back into space or move toward higher latitudes along the field lines (e.g. Störmer, 1935; Quenby & Wenk, 1962).

The cut-off rigidity[2] R_c for protons is given by (Dunai, 2001)

$$R_c = \frac{Mc\mu_0}{16\pi r^2}\cos^4 \Lambda \quad \text{(in GV)}, \tag{2.2}$$

where M is the earth's dipole momentum (in A.m^2), μ_0 the permeability of the free space (4π*10^{-7} N.A^{-2}), r the earth radius (m), Λ the geomagnetic latitude (in degree). The geomagnetic rigidity is based theoretically on the geomagnetic coordinates. However, since the magnetic field is very variable, and only little information about the ancient pole positions is available, the time-averaged geomagnetic pole positions over periods of a few (>10) kyr are in most cases assumed to be to a first order approximation identical with the geographic poles (see chapter 2.3 for scaling issues).

The shielding effect of the magnetic field varies with the latitude and shows the strongest variation ("knee") around 40-45° (Millikan & Neher, 1935)[3]. Despite the fact that the

[2] The theoretical basis for the cut-off rigidity was developed by Störmer (1935) using a pure and undisturbed dipole approximation for the earth's magnetic field. However, during periods of high magnetic activity the cut-off rigidity is significantly lower than under "normal" conditions (Boberg et al., 1995).

[3] Millikan & Neher (1935) found that the cosmic ray intensity varies not only with the latitude but also with the longitude, which proved that the earth magnetic field is not a simple dipole but has a more complex structure.

intensity of the magnetic field is two times lower at the equator than at the poles, the magnetic shielding indicated by the cut-off rigidity is significantly stronger at the equator due to the orientation of the field lines (Table 2.2). At the magnetic equator the magnetic field lines are oriented parallel to the earth's surface and thus perpendicular to the incoming radiation. Hence, the repulsion effect caused there by the horizontal component of the geomagnetic field is strongest. Towards the poles the field lines turn more and more into vertical orientation with respect to the earth's surface and the cosmic rays reach the earth quasi parallel to the field lines, so that the repulsion effect decreases (e.g. Lal & Peters, 1967; Raisbeck & Yiou, 1989). This means that close to the poles a particle has to possess less energy in order to penetrate the magnetic field, i.e. more primary particles can reach the top of the atmosphere. At latitudes higher than 55°, R_c reaches a minimum and basically all primary particles reach the atmosphere. Therefore, the intensity of the cosmic radiation and its variation (e.g. due to solar cycles) is highest at high geomagnetic latitudes (>55°) together with the production rate of cosmogenic nuclides (e.g. Millikan & Neher, 1935; Cerling & Craig, 1994; Zreda & Phillips, 1994).

Place	Geographic Latitude (degree)	Geographic Longitude (degree)	Geomagnetic Latitude (degree)	Cut-off rigidity (GV)
Reykjavik (Iceland)	64.2	-21.9	66.0	0.41
Prague (Czech Rep.)	50.1	14.5	48.7	2.84
New York (U.S.A.)	40.7	-74.0	46.0	3.47
Puerto del Rosario (Fuerteventura, Spain)	28.5	-13.9	29.9	8.42
Hanoi (Vietnam)	21.0	105.8	15.7	12.82
Caracas (Venezuela)	10.5	-66.9	15.6	12.83
Quito (Ecuador)	-0.2	-78.5	5.2	14.67
Lima (Peru)	-12.1	-77.0	-6.7	14.51
Windhoek (Namibia)	-22.6	17.1	-23.9	10.42
Perth (Australia)	-31.9	115.8	-36.9	6.10
Wellington (New Zealand)	-41.3	174.8	-41.8	4.61

*Table 2.2 Cut-off rigidities for several cities of the world. The geographic coordinates are given in numbers positive to the north and the east. The transformation into geomagnetic coordinates is based on the position of the geomagnetic N-pole in 1950: 84.52˚N, -87.63˚E., based on data from CAS7K.2 (Korte & Constable, 2005; Korte et al., 2005) (pole position data kindly provided by M. Korte (GeoForschungsZentrum Potsdam (GFZ), 2007, pers. comm.)). The rigidity was calculated based on a VADM of 8.072*10²² Am² for 1950.*

A muonic and an electromagnetic cascade that emerge together with the hadronic cascade contain mainly weakly interacting particles such as muons and photons (Masarik & Reedy, 1995). The trajectories of the charged secondary particles are also bent by the magnetic field lines so that the number of particles that reach the earth surface is further reduced.

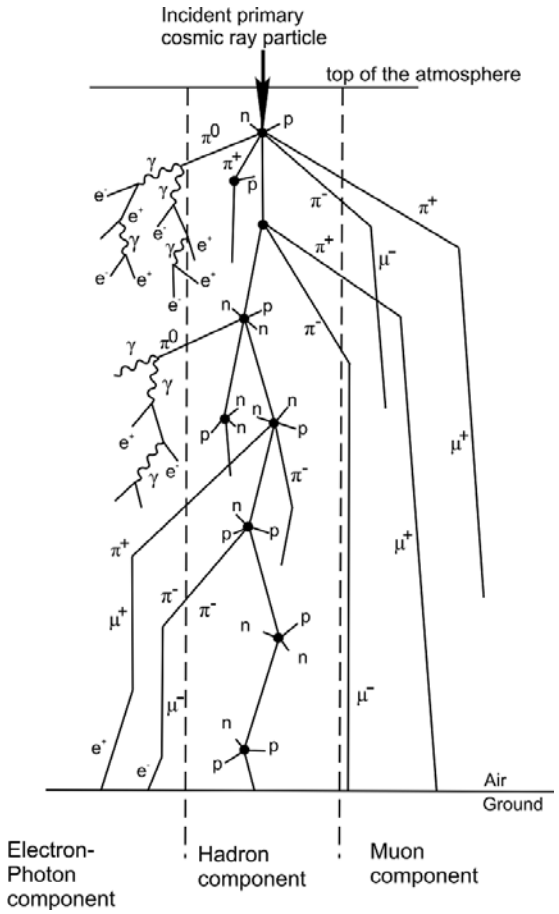

Fig. 2.2 Cascades of secondary cosmic rays produced in the atmosphere. Filled dots represent nuclear disintegrations, π pions, μ muons, γ gamma radiation, n neutrons, p protons, e^- electrons and e^+ positrons. (After Allkofer & Grieder, 1984; Simpson, 2000).

The atmosphere strongly attenuates the particle flux and shifts the spectrum of the flux to lower energies. This is described by the attenuation length or absorption length for a particle, which is usually given in $g.cm^{-2}$ and calculated by multiplying the penetration depth in cm with the density of the permeated material in $g.cm^{-3}$. This makes the value of the invasion depth independent of the material density and thus comparable for all materials. The attenuation length is the distance the particle has moved into a material before the probability that the particle has not been absorbed has dropped to 1/e. In air it is about 130 to 140 g/cm^{-2} (e.g. Dunai, 2000, 2001). The secondary flux decreases approximately exponentially with increasing atmospheric depth due to energy loss through successive collisions. Its

composition also changes because the neutrons increasingly dominate over the protons (Zreda et al., 1991; Desilets & Zreda, 2003; Pigati & Lifton, 2004). The intensity of the cosmic radiation (and thus the production rate) increases with the altitude of the site because of the decreasing thickness of the overlying atmospheric layer. The intensity of the interaction of cosmic ray particles with the atmospheric particles depends not only on the energy but also on the mass and the charge of the cosmic particles. Light charged particles (electrons) experience the strongest attenuation, whereas non-charged heavier particles (neutrons) are significantly less attenuated. A large portion of the neutrons produced in the atmosphere are captured by nuclear reactions with nitrogen and oxygen or leak out of the atmosphere into the free space. Muons and neutrons are the main components of the particle spectrum at the earth's surface that occur at an energy and quantity adequate to produce measurable amounts of cosmogenic nuclides. Protons, electrons and pions do not play a significant role in cosmogenic nuclide production at the earth's surface and therefore will not be considered here in detail.

At sea level, nucleonic attenuation lengths in rock and soil have been observed ranging between 150 $g.cm^{-2}$ at high latitude to 170 $g.cm^{-2}$ at low latitude (e.g. Cerling & Craig, 1994). The attenuation length is greater at low latitudes because the incident cosmic ray spectrum is harder (its intensity is decreased in the low energy part) due to the higher cut-off rigidity at low latitudes (Lingenfelter, 1963). This means that the primary particles with a higher energy produce cascades of secondary particles with higher mean energies that have slightly lower interaction cross sections with the particles of the atmosphere (Ziegler, 1996). Particles showing little interaction with atmospheric and terrestrial material (e.g. muons and neutrons) have a longer attenuation length, i.e. they are less strongly attenuated and their flux differs less when different elevations are compared (Ziegler, 1996). These are the particles that finally produce cosmogenic isotopes in rock surfaces by spallation reactions, muon-induced reactions and neutron-capture reactions (Ivy-Ochs, 1996).

2.2 Chlorine-36

There are several important cosmogenic nuclides such as ^{10}Be, ^{14}C, ^{26}Al, ^{36}Cl that are employed for the determination of exposure ages, erosion rates, burial periods and other geological and geomorphic aspects. The focus of this thesis is lain on ^{36}Cl. Chlorine occurs in nature in two stable isotopes: ^{35}Cl (75.76 %) and ^{37}Cl (24.24 %), and the radioactive ^{36}Cl (half-life 301 ka). ^{36}Cl can be formed at the earth's surface in several different nuclear

reaction mechanisms caused by diverse components of the secondary cosmic radiation (Fig. 2.3). The relevant components are essentially fast and slow muons, and highly energetic (≥10 MeV), epithermal (0.5 eV-0.1 MeV) and thermal neutrons (<0.5 eV). The highly energetic collision of fast neutrons with a target nucleus can cause a spallation reaction. In this process the neutron hits the target nucleus and severely shatters it, but it may even leave the nucleus with reduced momentum. Subsequently the target nucleus disintegrates releasing a number of nucleons until the excitation energy of the nucleus has fallen below the binding energy of the individual nucleons. As a result a new nucleus with a somewhat smaller mass is left behind (Templeton, 1953). Nuclei that are commonly involved in ^{36}Cl production by spallation are ^{39}K and ^{40}Ca:

$^{39}K(n,2n2p)^{36}Cl$

$^{40}Ca(n,2n3p)^{36}Cl$.

These reactions account for between 16 and 80 % of the total ^{36}Cl production close to the earth surface depending on the rock composition (Zreda et al., 1991).

Epithermal and thermal (low-energy) neutrons form when for example high energy neutrons slow down through elastic collisions with other particles (Lal, 1987). Epithermal neutrons behave similarly to the thermal neutrons and often end up as thermal neutrons by energy loss (Gosse & Phillips, 2001). The capture of thermal neutrons by ^{35}Cl is another major source of ^{36}Cl production in rocks with a significant amount of chlorine (the numbers in brackets give an estimate of the contribution of the mechanisms to this total ^{36}Cl production) (Zreda et al., 1991):

$^{35}Cl(n_{th},\gamma)^{36}Cl$ (11-80 %)

$^{39}K(n_{th},\alpha)^{36}Cl$ (0-2 %)

$^{36}Ar(n_{th},p)^{36}Cl$ (does not play a role in rocks but rather in the atmosphere for the production of meteoric ^{36}Cl)

Near the earth's surface muogenic production plays a minor role, but at depths larger than 1-2 m (250-500 g.cm^{-2}), the cosmogenic nuclide production by slow negative muons, which are captured by (charged) nuclei, becomes significant (Fabryka-Martin, 1988; Zreda et al., 1991):

$^{39}K(\mu^-,p2n)^{36}Cl$

$^{40}Ca(\mu^-,\alpha)^{36}Cl$

$^{40}K(\mu^-,p3n)^{36}Cl$.

The process of muon reactions is very complex and still not fully understood. A slow negative muon that is caught by the Coulomb field of a nucleus reaches the muonic 1s level.

There it either decays or it is finally captured by the nucleus forming a muonic atom, which then releases a neutron (for details see Charalambus, 1971). These muon-generated neutrons may be involved in neutron absorption reactions generating cosmogenic nuclide (Gosse & Phillips, 2001). High energy muons can also cause spallation.

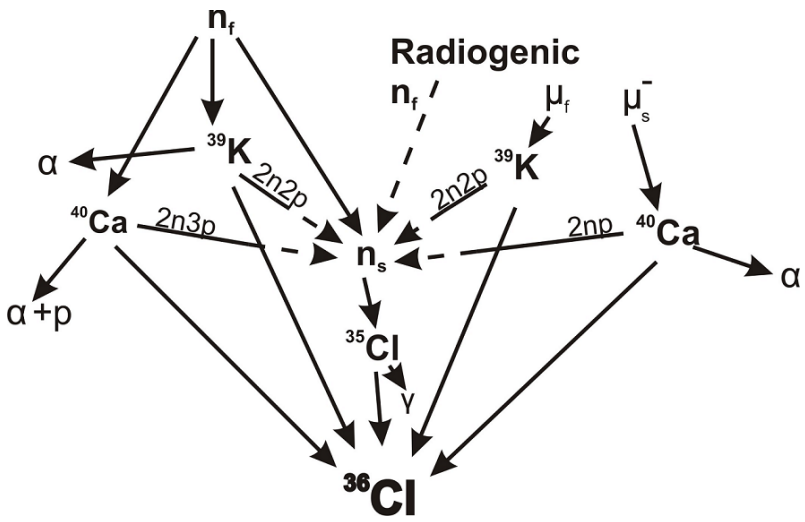

Fig. 2.3 The main production mechanisms of cosmogenic ^{36}Cl in basalt. (After Zreda & Phillips, 2000). Here, f denotes fast, high energy; s symbolizes slow, low energy.

Production of ^{36}Cl from heavier atoms such as iron or titanium occurs as well but at a lower production rate than the production from calcium and potassium.

All these mechanisms contribute to a different extent to the total production of ^{36}Cl depending on their individual production rates and the concentration of the target elements:

$$P = \left(P_{Ca,sp}[Ca] + P_{K,sp}[K] + P_{Cl,n}[Cl] + P_{K,n}[K] + P_{K,\mu}[K] + P_{Ca,\mu}[Ca] + P_{Ti,sp}[Ti] + P_{Fe,sp}[Fe] \right), \tag{2.3}$$

where $P_{Ca,sp}$, $P_{K,sp}$ $P_{Ti,sp}$ $P_{Fe,sp}$ are the production rates based on spallation of calcium, potassium, titanium, and iron, repectively, $P_{Cl,n,}$ $P_{K,n}$ are the production rates due to thermal neutron capture by chlorine and potassium, and $P_{K,\mu}$ $P_{Ca,\mu}$ are the production rates based on interaction with muons. [Ca], [K], [Cl], [Ti], and [Fe] are the concentrations of the target elements in the rock.

Table 2.3 gives some examples from the literature of production rates for the individual production mechanisms. The values naturally differ significantly from mechanism to mechanism, but even for one single production path there are severe variations. There are numerous possible reasons for this, for example the fact that different methods are employed to subdivide the total ^{36}Cl production into the individual mechanisms: Some calibration

Production Mechanism	Production Rate	Reference
Spallation of ^{39}K	106 ± 8 at.(g(K).yr)$^{-1}$	Zreda et al., 1991
$^{39}K(n, \alpha)^{36}Cl$	154 ± 10 at.(g(K).yr)$^{-1}$	Phillips et al., 1996
	161 ± 9 at.(g(K).yr)$^{-1}$	Fifield et al., 2002
	170 ± 25 at.(g(K).yr)$^{-1}$	Evans et al., 1997
	192 ± 17 at.(g(K).yr)$^{-1}$	Zreda & Phillips, 1994
Spallation of ^{40}Ca	48.8 ± 3.4 at.(g(Ca).yr)$^{-1}$	Stone et al., 1996b
$^{40}Ca(n, 2n3p)^{36}Cl$	57.3 ± 5.2 at.(g(Ca).yr)$^{-1}$	Licciardi et al., 2008
	72 ± 6 at at.(g(Ca).yr)$^{-1}$	Zreda & Phillips, 1994
	73 ± 5 at.(g(Ca).yr)$^{-1}$	Phillips et al., 1996
	76 ± 3 at.(g(Ca).yr)$^{-1}$	Zreda et al., 1991
	91 ± 5 at.(g(Ca).yr)$^{-1}$	Swanson & Caffee, 2001
Neutron Capture by ^{35}Cl	(3.07 ± 0.24)*10^5 n.(kg(rock).yr)$^{-1}$	Zreda et al., 1991
$^{35}Cl(n,\gamma)^{36}Cl$	(3.14 ± 0.28)*10^5 n.(kg(rock).yr)$^{-1}$	Zreda & Phillips, 1994
	(3.53± 0.07)*10^5 n.(kg(rock).yr)$^{-1}$	Swanson, 1996
Muon Capture by ^{39}K	6.9 ± 1.3 at.(g(K).yr)$^{-1}$ (μ_f)	Heisinger et al., 2002a
$^{39}K(\mu^-, p2n)^{36}Cl$	**9.5 ± 1.3 at.(g(K).yr)$^{-1}$ (μ^-)**	Heisinger et al., 2002b
	10.2 ± 1.3 at.(g(K).yr)$^{-1}$	Evans, 2002
Muon Capture by ^{40}Ca	0.74 ± 0.2 at.(g(Ca).yr)$^{-1}$ (μ_f)	Heisinger et al., 2002a
$^{40}Ca(\mu^-, \alpha)^{36}Cl$	**4.8 ± 1.2 at.(g(Ca).yr)$^{-1}$**	Stone et al., 1996b
	5.2 ± 1.0 at.(g(Ca).yr)$^{-1}$	Stone et al., 1998
	6.5 ± 0.7 at.(g(Ca).yr)$^{-1}$ (μ^-)	Heisinger et al., 2002b
Spallation of Fe	**1.9 ± 0.2 at.(g(Fe).yr)$^{-1}$**	Stone, 2005
Spallation of Ti	**13 ± 3 at.(g(Ti).yr)$^{-1}$**	Fink et al, 2000

Table 2.3: Overview of the different production mechanisms of ^{36}Cl and the corresponding production rates from the literature (yr = year). The production rates show quite some variation. The bold values were used for calculations in the present study. The values given for the neutron capture are neutron absorption rates (see eqn. 2.4) rather than production rates but included in this table for completeness.

studies are based on mineral separates, others on whole rock; some treat Ti- and Fe-spallation and muogenic production as individual mechanisms, others disregard Ti- and Fe-spallation or combine them with spallogenic and muogenic production from another element (e.g. Ca-

spallation), which overestimates the production from this element, when the contribution of titanium and iron is more than 2 or 3 %, and so forth (e.g. Stone et al., 1996a,b, 1998; Evans et al., 1997; Phillips et al., 2001; Swanson & Caffee, 2001). Other reasons for these discrepancies between the production rates could be differences in the chemical treatment of the samples for chlorine extraction, unidentified periods of prior exposure, inaccurate age determination, unknown degree of erosion, geomagnetic, solar or climate modulation, scaling uncertainties and others (e.g. Easterbrook, 2003; Lifton, et al., 2005; Licciardi et al., 2008). The boldly printed production rate values in Table 2.3 were used for the calculations in this study because they represent approximately the mean values avoiding the extremely high or low values. Generally higher values were supported by the measurements and test calculations performed for the research presented here (e.g. for thermal neutron based production from ^{35}Cl).

Since elements like lithium, boron and gadolinium have very large thermal neutron absorption cross-sections, they may distort the amount of thermal neutron really available for the ^{35}Cl atoms. Thus, the calculation of the production rate of ^{36}Cl due to neutron capture has to include the fact that only a certain proportion of all neutrons present really goes into ^{36}Cl production. The production rate of ^{36}Cl due to neutron capture in a rock is calculated depending on the rock's composition (Phillips et al., 1986; Dep, 1995):

$$P_{Cl,n} = \Phi_n \frac{N_{35}\sigma_{35}}{\sum_{n=i} N_i \sigma_i} \quad \text{atoms } (^{36}\text{Cl}).\text{g(rock)}^{-1}.\text{yr}^{-1} \tag{2.4}$$

where Φ_n is the thermal neutron absorption rate (e.g. $(3.07 \pm 0.24)*10^5$ n. kg(rock)$^{-1}$.yr^{-1}, Zreda et al., 1991, see Table 2.3), σ_{35} and σ_i are the elemental thermal neutron cross sections of ^{35}Cl and of the i-th element (in barns, here per atom), respectively, and N_{35} and N_i are the concentrations of ^{35}Cl and of element i (atoms.g^{-1} or moles.g^{-1}), respectively.

The different ^{36}Cl production processes have the maxima of their production rates at different depth levels (Fig. 2.4). Spallation and neutron capture are prominent in the ^{36}Cl production within the uppermost 500 to 600 g.cm^{-2}. Spallation caused by fast neutrons that move on essentially straight paths has its maximum at the surface and decreases with increasing depth approximately exponentially (according to *exp(-depth/Λ)*, Zreda et al., 1991). Thermal neutrons that are produced in the uppermost few centimetres of the rock tend to leak out of the rock into the overlying air because of their diffuse motion and the neutrons' long free attenuation length **(**Zreda & Phillips, 2000). There they are absorbed by atoms of atmospheric gases such as nitrogen, since the macroscopic thermal neutron absorption cross

section of the atmospheric gases is significantly higher than that of common rock material (Yamashita et al., 1966). Therefore thermal neutrons are somewhat reduced in the top layer of the rock and the maximum of ^{36}Cl production due to thermal neutron capture lies at a depth of roughly 50 g.cm^{-2} (for basalt at about 15-20 cm). Below that level the thermal neutron flux decreases approximately exponentially with increasing depth, at a rate comparable to the attenuation of the fast component (Zreda & Phillips, 1994).

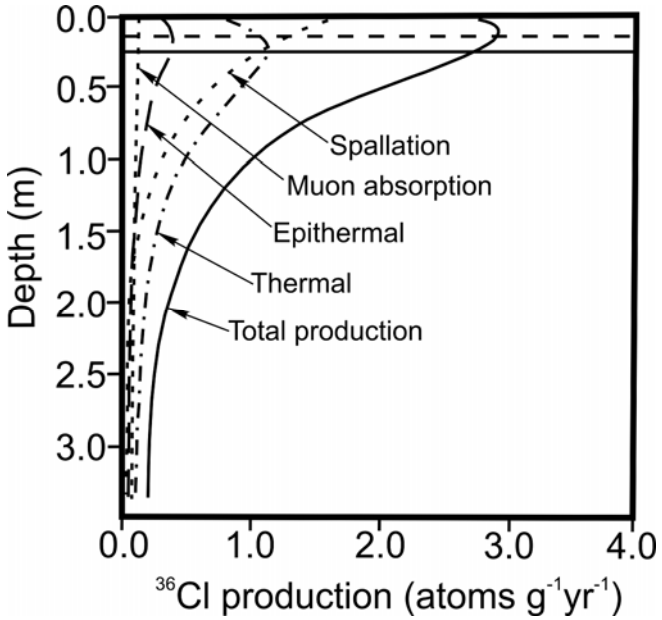

Fig. 2.4 Depth dependence of ^{36}Cl production in the earth surface (after Fabryka-Martin, 1988; Gosse & Phillips, 2001). The dashed horizontal line indicates the average thickness of the samples collected in Fuerteventura and the solid line the maximum sample thickness.

The exact position and magnitude of the maximum are functions of the chemical composition of the rock and the possible coverage (Zreda & Phillips, 2000). Attenuation of the cosmic radiation by a thin coverage (snow, soil, water in vesicles close to the rock surface) shifts the maximum of thermal-neutron induced ^{36}Cl production closer to the rock surface and tightens it, and so increases the apparent production rate because it result in an increased ^{36}Cl concentration in the top layer. Also small amounts of erosion can shift the maximum of ^{36}Cl production by thermal neutron capture towards the surface and thus increase the ^{36}Cl concentration there (Licciardi et al., 2008). At a depth greater than about 1000 g.cm^{-2} the influence of neutrons is insignificant and muon-induced nuclide production becomes dominant. The negative-muon-induced production of cosmogenic nuclides decreases exponentially with depth like the neutron-induced spallogenic production, but considerably more slowly than the latter (Lal, 1988; Gillespie & Bierman, 1995). Due to their weak

interaction with matter, muons penetrate the rock far more deeply than other particles. The attenuation length for muons is about 1500 g.cm^{-2} (Brown et al., 1995). Below 6000 g.cm^{-2} the capture of neutrons produced by fast muons becomes important. At very large depths the cosmogenic ^{36}Cl production ceases and background radiogenic production dominates (Stone et al., 1996a,b and 1998). This non-cosmogenic ^{36}Cl production results from capturing neutrons originating from the spontaneous fission of ^{238}U, and from secondary (α,n) reactions induced by decay chains of thorium or uranium (Ivy-Ochs, 1996). The resulting ^{36}Cl/Cl ratios are usually of the order of 10^{-15} (Fabryka-Martin, 1988), but they can also reach significantly higher values depending on the concentrations of uranium and thorium. The non-cosmogenic contribution is calculated from the concentrations of uranium and thorium, the concentration of target nuclides of (α,n) reactions and the chlorine concentration. This contribution is finally subtracted from the measured ^{36}Cl/Cl ratio of the rock.

The production rate determines how many atoms of ^{36}Cl can be formed in a certain time interval. However, in natural systems ^{36}Cl is not only accumulated but also lost by different processes. First of all, ^{36}Cl is radioactive and decays with a half life of 0.301±0.002 Ma through β^--decay (98 %) into ^{36}Ar and by electron capture (2 %) into ^{36}S (e.g. Zreda et al., 1993). For rocks and surfaces older than approximately 20 % of the half-life of a radionuclide, which is about 60 ka for ^{36}Cl, the radioactive decay becomes important for the determination of the age.

Furthermore, rocks exposed at the earth's surface are subject to erosion. Samples with a minimum loss of mass by erosion are ideal (Zreda & Phillips, 1994). As a first guess in the field the loss by erosion is usually estimated from the condition of the rock surface. For example if very fine structures of about 1-2 mm are preserved on the surface of volcanic rock samples, the loss by erosion can only be at most of few mm. When several cm of rock have been lost from a surface due to erosion, the surface structures do not exhibit fine structures of mm size anymore but only coarser ones of cm size. The intensity of the erosion depends on the climatic conditions, the relief at the sample site and on the resistance to weathering of the rocks themselves. Erosion can affect the surface either by removing material directly from it (rock erosion) or by gradually exposing surfaces (e.g. of boulders) by erosion of the overlying material. In either case the ages determined are lower than the true ones (Zreda & Phillips, 2000). If little erosion has occurred it is presumed that it did so at a constantly low rate, which for many cases is a reasonable assumption that can be included in the calculation of the age or the production rate by introducing an appropriate factor. However, this does not apply when the erosion rate changes, for example due to climatic variation, or for a sudden increase in the

loss of material such as by exfoliation of thick slabs, spalling or frost riving, or sudden removal of large blocks (e.g. in floods or landslides) (Gillespie & Bierman, 1995). Chemical weathering may also affect the dating results by changing the bulk composition by loss (other than that due to decay) or the gain of atoms of interest and by the formation of secondary minerals. Non-cosmogenic or ^{36}Cl not formed in-situ (e.g. meteoric) could be included in the newly created minerals (Zreda & Phillips, 1994). The error in the exposure age resulting from the error in the estimated erosion rate included in the formulas for the age determination is usually not very large (of the order of 1 %), but it can be significant (easily 10 % and more) if the erosion rate was severely under- or overestimated. The longer the half-life of the radionuclide the less the erosion rate is overestimated (Lal, 1991).

In most applications of exposure dating it is assumed that the samples have not been exposed to cosmic radiation before their current exposure and thus do not contain any cosmogenic nuclides at the beginning of their exposure. That is commonly true for volcanic rock samples coming from a clearly defined eruption or for surfaces that were newly exposed after deep rooted landslides. Samples that have been exposed to cosmic radiation before the exposure period of interest may contain a certain amount of cosmogenic nuclides stemming from these earlier periods. This is typically the case for material that has been transported by glaciers or where an originally free surface has been covered and later uncovered again. Generally, these pre-exposure contributions lead to higher exposure ages and thus have to be taken into account. Finally a few factors have to be considered that influence the radiation within the sample. These are the sample thickness, the shielding due to the surrounding topography and the geographic position of the sampling site in terms of latitude and elevation. These scaling factors ($SF_{Thickness}$, $SF_{Topo,}$ $SF_{El,Lat}$) are discussed in more detail in chapter 2.3. Taking all these considerations together, the concentration of ^{36}Cl (in atoms.g^{-1}) is calculated as follows (Ivy-Ochs, 1996):

$$[^{36}Cl] = \left(\frac{P}{\lambda + \rho\varepsilon/\Lambda} \left(1 - \exp\left(-\left(\lambda + \rho\varepsilon/\Lambda \right) t \right) \right) + [^{36}Cl]_0 \exp(-\lambda t) \right) \cdot SF_{Thickness} SF_{Topo} SF_{El,Lat} \quad (2.5)$$

where [^{36}Cl] is the concentration of ^{36}Cl atoms, [^{36}Cl]$_0$ is the concentration of ^{36}Cl atoms already present at the beginning of the exposure, ρ the rock density (g.cm^{-3}), ε the erosion rate (cm.yr^{-1}), P is the production rate (atoms.g(rock or target element)$^{-1}$.yr^{-1}), λ the decay constant of ^{36}Cl (2.302*10^{-6} yr^{-1}), Λ the cosmic ray attenuation length (NOT the latitude as in eqn. 2.2) in the rock surface (160 ± 10 g.cm^{-2}, Granger & Smith, 2000), and t the exposure age (years).

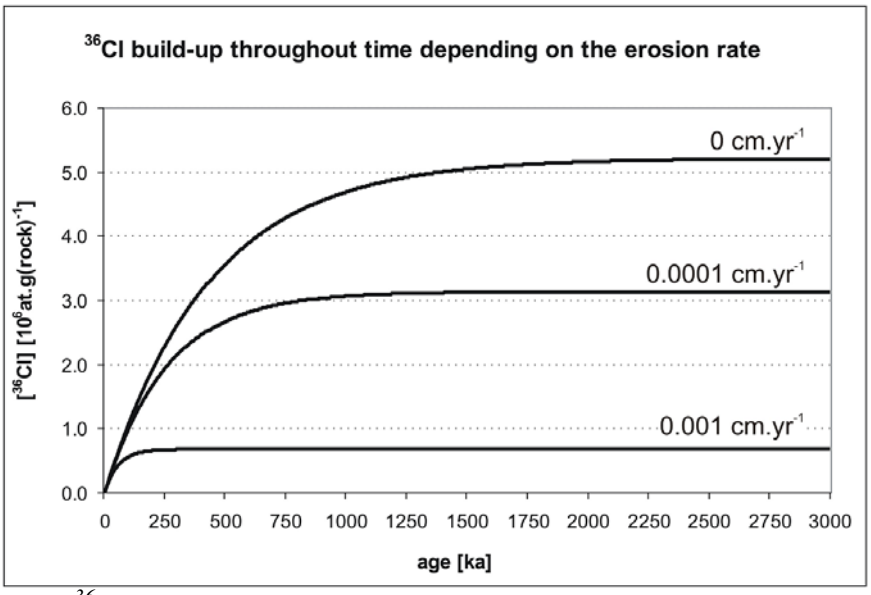

Fig. 2.5 ^{36}Cl build-up throughout the time for different erosion rates. The higher the erosion rate is the earlier the equilibrium is reached and the lower the amount of ^{36}Cl is in the equilibrium (calculated for a production rate of 12 atoms.g(rock)$^{-1}$.yr^{-1}).

The build-up of cosmogenic radionuclides in an exposed rock surface occurs in a three phase process (Lal, 1991; Gillespie & Bierman, 1995). Fig. 2.5 shows that the first phase is essentially a linear increase of the number of atoms with the time. After roughly one half-life for surfaces without erosion the build-up becomes increasingly slow, and after about six half-lives it approaches a secular (saturation) equilibrium between the production of the radionuclide and its decay. So the change in concentration over the time becomes very small. This determines an estimated limit of two to three half-lives of the nuclide (presuming no erosion) for the application of cosmogenic build-up methods based on radioactive nuclides (Zreda & Phillips, 2000). The equilibrium is reached faster as the half-life of the isotope shorter is. Erosion usually affects the accumulation of cosmogenic nuclides within time spans shorter than the theoretical limit (Zreda & Phillips, 2000). The higher the erosion, the faster the build-up reaches the saturation equilibrium and the lower is the ^{36}Cl concentration of that equilibrium. This shortens significantly the theoretical limit of applicability for exposure dating. Therefore information about erosion has to be gathered independently to extend the range of times that can be dated. Zreda & Phillips (2000) give 200 to 500 ka as a realistic upper limit for exposure dating with ^{36}Cl. Two different isotope systems have to be used on the same sample when both the erosion rate and the exposure age have to be determined. Occasionally ^{36}Cl is used to determine the amount of erosion and the erosion rate by measuring a ^{36}Cl depth profile (e.g. Dep et al. 1994a,b; Ivy-Ochs, 1996).

The lower limit for a determination of the exposure age depends on the production rate, the analysing technique, the inherited nuclide concentration due to prior exposure to cosmic radiation and the radiogenic isotope production. Surface exposure ages should generally be taken to represent minimum ages. In the case of some variance of cosmogenic ages for multiple samples from a single surface the opinions about how to interpret the ages obtained differ considerably. For example Zreda & Phillips (1995, 2000) argue that the oldest age is closest to the true age of the surface. Benson et al. (2005) in contrast consider the youngest apparent ages to be the best estimate for a landform's age. Ivy-Ochs et al. (1999) take the arithmetic average and the standard deviation to be the best age estimate.

2.3 Scaling factors

A number of factors, which systematically influence the production of cosmogenic nuclides, are included as scaling factors in the calculations. These scaling factors are based on models that describe the modification of the incoming cosmic radiation by effects such as the attenuation by passing through material or by shielding depending on the position of the site within the geomagnetic field.

Scaling for Topographic shielding

The surrounding relief and the dip angle of a sample not being horizontal can cause topographic shielding. Stone (2000) provided a formula to determine the angular dependence of the cosmic ray flux relative to the vertical flux:

$$I(\alpha) = I_v \sin^{3.3} \alpha \tag{2.6}$$

where I(α) is the angular intensity distribution of the incoming cosmic radiation, α the inclination angle to the horizontal, and I_v is the intensity at α = 90°. For a sector of width β (horizontal angle) and the inclination angle α within which the incoming radiation is blocked by topography (Fig. 2.6), the attenuation is calculated as (Stone, 2000):

$$f_{blocked} = \frac{\beta}{2\pi} \sin^{3.3} \alpha \tag{2.7}$$

In practice the topographic shielding is determined by approximating the horizon in the field as a series of straight line segments. The average horizontal angle is obtained with a series of small sectors (5°, if the relief of the horizon varies strongly, otherwise in larger steps

of 15˚). For all of these sectors separate values for $f_{blocked}$ are calculated and finally summed for the whole circle (Stone, 2000):

$$SF_{Topo} = 1 - \sum_i f_{blocked,i} \tag{2.8}$$

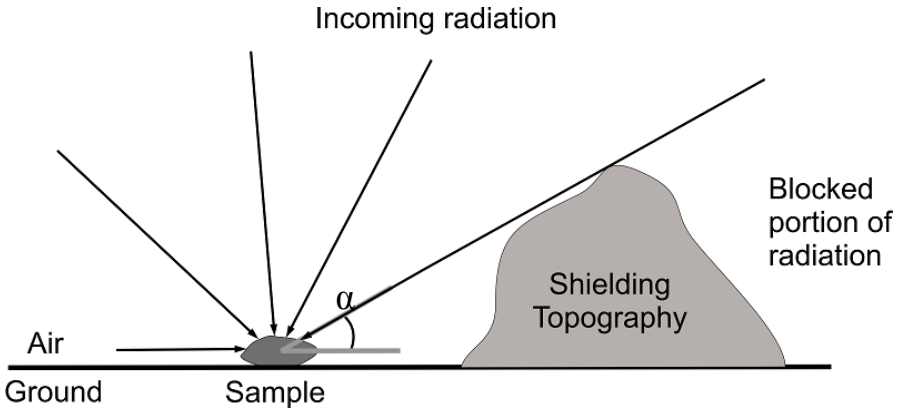

Fig. 2.6 Shielding effect of surrounding topography. The inclination angle of the horizon determines the portion of the radiation that does not reach the sample.

The scaling factor is close to unity for inclination angles between 0 and 5° and decreases the faster the stronger the inclination angles increase. This rather simple method works well for low inclination angles and introduces only little uncertainty to the shielding correction. The errors are calculated for all (e.g. 5°-) sectors of the 360° of the whole horizon that are employed for the topographic scaling:

$$\Delta f_{blocked} = \sqrt{\left(\frac{\partial f}{\partial \alpha}\Delta\alpha\right)^2 + \left(\frac{\partial f}{\partial \beta}\Delta\beta\right)^2} \quad , \tag{2.9}$$

which is then included into the total error:

$$\Delta SF_{topo} = \sqrt{\sum_i \Delta f^2_{blocked,i}} \tag{2.10}$$

For inclination angles of up to 6° measurement errors of about 1° cause only a deviation of the scaling factor of up to 1 %. Larger inclination angles are more sensitive to a given measurement error, and thus the deviation of the calculated scaling factors from the true value increases with increasing inclination. For inclinations of 10° a measurement error of 1° causes already a deviation of 7 % (Fig. 2.7). For larger inclination angles as would be obtained for sampling sites in gulches, a more accurate method of integration might be desirable.

The sampling sites in Fuerteventura all have a very simple topography. No steep hills or strongly varying relief surrounded the lava flows sampled. The inclination angles obtained were mostly between 0° and 4°. The inclination angle only exceptionally exceeded 6° for a range of horizontal angles of 15° to 45°. Thus, assuming a measurement error of 0.5° for both the horizontal and the inclination angles, the deviation of the scaling factor in most cases results in a total error of 1-3 %. For sites with higher surrounding hillside causing lager inclination angles the errors are somewhat higher and can reach more than 5 %.

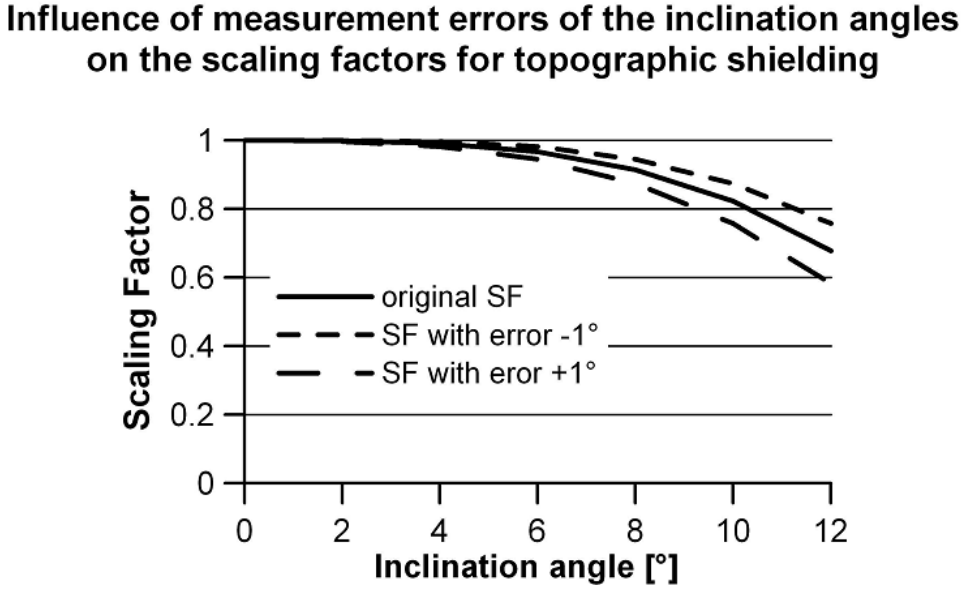

Fig. 2.7 Scaling factors of topographic shielding as a function of the inclination angle. Low inclination angles cause only minute shielding and are little sensitive to errors in the determination of the angle, whereas larger inclination angles cause increasingly severe shielding and are more sensitive to errors (dashed lines).

Scaling for sample thickness

Since secondary particles are attenuated on their way through the material, the production rate of the cosmogenic nuclides decreases with increasing depth of penetration. This is described by the equation (Stone, 2000):

$$P_z = P_0 \cdot \exp\left(-\rho z / \Lambda\right) \tag{2.11}$$

where P_z is the production rate at depth z (atoms.g^{-1}.yr^{-1}), P_0 the production rate at the surface (atoms.g^{-1}.yr^{-1}), ρ the rock density (g.cm^{-3}), z the depth (cm), Λ the cosmic ray attenuation length (g.cm^{-2}). Integration of this equation leads to the integrated production rate from spallation over a given depth interval:

$$P = P_0 \frac{\Lambda}{\rho z}\left(1 - \exp\left(-\rho z / \Lambda\right)\right) \tag{2.12}$$

Thus, the scaling factor for a given depth range, i.e. also for the thickness of the sample piece, is

$$SF_{thickness} = \frac{\Lambda}{\rho z}\left(1 - \exp\left(-\frac{\rho z}{\Lambda}\right)\right) = \frac{\Lambda}{\frac{m}{V} z}\left(1 - \exp\left(-\frac{\frac{m}{V} z}{\Lambda}\right)\right) \tag{2.13}$$

The scaling factor decreases with increasing sample thickness, increasing sample density and decreasing mean free path. The rate of decrease of the scaling factor with increasing sample thickness becomes less as the density of the sample is lower (Fig. 2.8). The uncertainties introduced into this parameter originate mainly from the determination of the sample thickness, and from the mass and the volume measured to determine of the density.

$$\Delta SF_{thickness} = \sqrt{\left(\frac{\partial SF}{\partial z}\Delta z\right)^2 + \left(\frac{\partial SF}{\partial m}\Delta m\right)^2 + \left(\frac{\partial SF}{\partial V}\Delta V\right)^2} \tag{2.14}$$

Rock samples collected from a lava flow do not usually have a perfectly regular shape. This means especially that when the sample shows some keel or dent the extreme and the average thicknesses differ by a few centimetres. The deviation of the scaling factor based on measurement errors of the thickness increases with increasing rock density. The contribution to the error of the scaling factor is about 1-2 % when the uncertainty in the thickness is 2 cm for rock densities between 2.5 and 3.3 g.cm^{-3}. The error introduced by the determination of the density of the rock in a hand specimen is based on measurements of volume and of mass. The volume measurement is performed as simple volume displacement in a water-filled measurement cylinder of one litre of total volume. Considering a 10 ml scaling, a maximum reading error of 5 ml is assumed to be possible, which introduces an error of about 1 % in the scaling factor. The balance on which the specimens' mass is determined has an uncertainty of 2 g, which introduces errors of about 0.1 % in the scaling factor. The total error of the scaling factor for the thickness of the samples from Fuerteventura are fairly low (2-3 %, except for the samples of the flow MQ, which is 8 % due to a higher thickness uncertainty).

Additional shielding may be caused by covering by snow, volcanic ash, soil, dust and sand after exposure. The intensity of the cosmic radiation approaching the surface is reduced by this additional layer and the apparent age may therefore deviate from the true surface age giving younger values (Zreda & Phillips, 2000). Shielding can also be caused by vegetation.

Cerling & Craig (1994) found a reduction of cosmogenic isotope production by roughly 40 % for samples taken in a forest due to trees and leaves. It is hardly ever possible to estimate shielding by ancient vegetation. Usually, recent vegetation differs strongly from that in the past, and often only a little information about the earlier conditions is preserved.

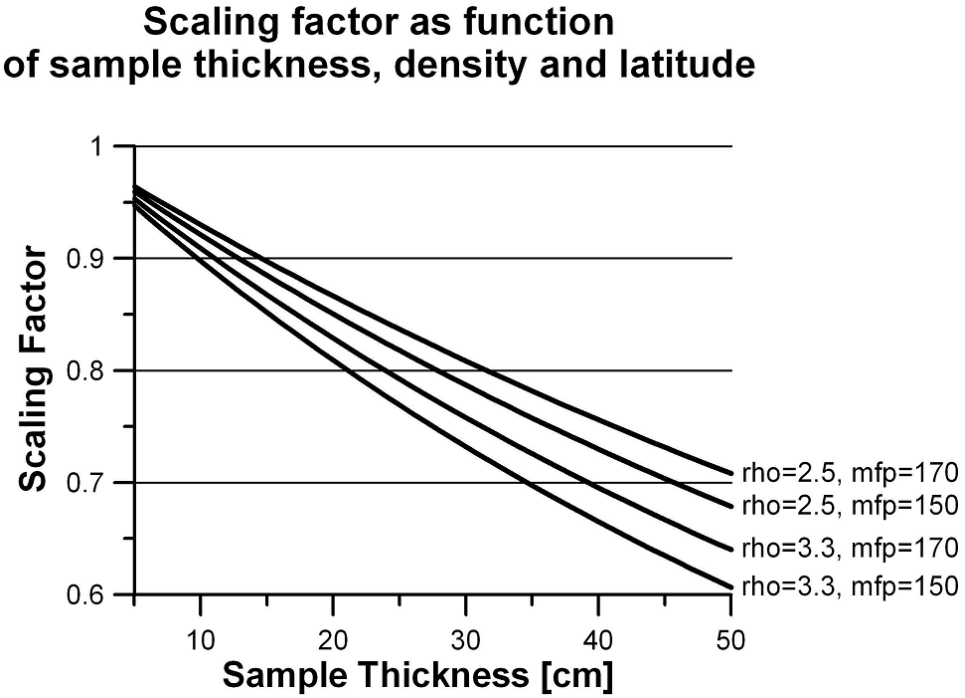

Fig 2.8 Scaling factor for sample thickness depending on rock density (rho in g.cm^{-3}) and mean free path (mfp in g.cm^{-2}). The mean free path depends on the site latitude. The scaling factors are the larger the higher the mfp, the lower the density and the thinner the sample.

Scaling for latitude and elevation

The production of cosmogenic nuclides is also a function of the position of the site within the earth's magnetic field, of the intensity of the magnetic field, and of height of the site. Therefore the geographic position of the site, the position of the magnetic poles and mean annual air pressure and temperature at the site are needed to interpret the amount of the isotope of interest in the material in terms of cosmogenic nuclide production and age. There are a number of models for in-situ production of cosmogenic nuclides that take the magnetic field and the geographical information of the site into account and allow for the scaling of the production rate with respect to the conditions of the site, e.g. Lal (1991), Dunai (2000, 2001), Desilets & Zreda (2003), Pigati & Lifton (2004), and Desilets et al. (2006). These scaling

models all relate the production at a given site on earth to a standard site at sea level and high latitude.

Lal (1991) based the parameterization of his model on a purely dipole shaped earth's magnetic field and included information on the altitude of the sites by extrapolations of values of the absorption cross sections obtained at high altitudes down to the sea level. This model cannot include temporal changes of the earth magnetic field and spatial variations of the atmospheric pressure systems. Nishiizumi et al. (1989) integrated the effect of the variability of the magnetic field on the production rates for cosmogenic nuclides into the model.

Dunai (2000, 2001) developed a model similar to that by Lal (1991) but allowed for variations in the magnetic field intensity and in the atmosphere, i.e. for climatic variation and anomalous pressure systems. For samples for which the magnetic inclination at the site has been obtained the effects of non-dipole components of the magnetic field together with polar wander can be included in the calculation of the cut-off rigidity (Dunai, 2000). For samples with less abundant information the cut-off rigidity is calculated from their geographic latitude. This also applies to the samples of Fuerteventura but because of their rather large ages (50-400 ka), the effects of polar wander and the non-dipole components are assumed to average out.

Desilets & Zreda (2003) found during neutron monitoring that the attenuation lengths for high energy neutrons and slow neutrons are different and they produced separate scaling factors for the thermal and the high-energy, spallation-inducing components of the neutron flux. Their model is based on trajectory-traced cut-off rigidity values for the geocentric axial dipole field of changing field intensity. However, there is no thorough description of the energy dependence of nucleon attenuation lengths for any of these components. An extended version of the model was developed by Desilets et al. (2006).

Pigati & Lifton (2004) developed a model based on Desilets & Zreda (2003) to investigate the effect that the temporal variation of the geomagnetic field has on the production of cosmogenic nuclides integrated over time. Like Desilets & Zreda (2003) they apply separate scaling for fast and slow neutrons. Lifton et al. (2005) presented a model that additionally includes the influence of solar activity since different solar cycles affect the overall intensity and the energy spectrum of the galactic cosmic rays. Lifton et al. (2008) also included geomagnetic influences in their model suspecting that for certain periods (Holocene to Pleistocene) the earth's magnetic field may not have been approximately that of an axial dipole but rather might have averaged to that of an eccentric dipole and exhibited strong non-dipole components.

The examination of the scaling factors presented here and the following analysis of the data is based on Dunai (2001). The physical reasoning behind this model is considered to be the most consistent. Even though the energy spectrum of the cosmic radiation shifts to the lower end (Desilets & Zreda, 2003), the neutrons that reach the earth's surface must have been high energy neutrons for most of their way through the atmosphere because otherwise they en route would have been absorbed by atmospheric particles or decayed, and would never have reached the ground. Only for the last centimetres of their path can they have been slowed down to (epi)thermal energies and still cause neutron-capture reactions in the rock. Many of the thermal neutrons are only formed within the rock by successive collisions or are the result of collisions of secondary particles in the rock forming quasi ternary particles. Thus there is no reason to scale for anything else than a general neutron component. Since all scaling equations are based on a collection of fitting coefficients instead of a consistent physical concept that describes the processes and interactions, it is doubtful if the scaling separately for increasingly more components with increasingly more coefficients really provides any improvement. The basis of Dunai's model to assume a dipole field when the cut-off rigidity is applied for scaling turns out to be not too much of a restriction because of the lack of information on pole positions and the strength and global distribution of non-dipole components. For ancient periods we have to go back to the geocentric axial dipole (GAD) assumption anyway at the same time being aware of this inherent inaccuracy. However, the models by Pigati & Lifton (2004) and Desilets et al. (2006) are tested as well for comparison in this study. The scaling factors and thus the production rates for whole rock production and Ca-spallation derived for all sites on Fuerteventura differ by about 1 – 4 % for the different scaling models. This means that despite the different theoretical approaches the scaling factors are comparable within their own errors, which are also consistently 3 to 4 %.

Because of the fairly high ages of the samples from Fuerteventura and the position of the island at rather low latitude, the model of Lifton et al. (2005) was not investigated further. The relatively high cut-off rigidity at low and mid latitudes blocks the low energy portion of the incoming cosmic radiation. So the solar modulations of the galactic cosmic rays (GCR), which mainly affect the low energy part of the GCR spectrum, have little effect on the radiation at these latitudes. In addition, over the periods of time considered here the effects of the solar cycle are assumed to cancel out (Lifton et al., 2005). There is also too little data about the strength, duration and absolute time spans of especially the long-term ancient solar and cosmic ray variation available to develop a decent model from them in the present study.

The models of Stone (2000) and Zreda & Phillips (2000) are only tested for comparison but they are not included in any way in the data analyses because these models do not allow for temporal magnetic field variations. These models consistently produced scaling factors 15 to 20 % lower than those from the models by Dunai (2000, 2001), Pigati & Lifton (2004) and Desilets et al. (2006). The model by Lal (1991) has been disregarded completely because it does not include the coefficients specifically for ^{36}Cl.

The Latitude effect

For the following analyses the equations from Dunai (2000, 2001) were employed. For details of the model the reader is referred to these publications. Here only the equations and the abbreviations used are summarized for completeness and convenience.

Cut-off rigidity at the site: $$R = \frac{M \mu_0 c}{16 \pi r^2} \cos^4 \lambda \text{ (in GV)}$$

Average atmospheric pressure at the site: $$p = p_0 \left(1 - \frac{\beta_0 h}{T_0} \right)^{\frac{g_0}{R_d \beta_0}} \text{ (in mbar)}$$

Atmospheric depth at the site: $$d = 10 p / g_o \text{ (in g.cm}^{-2}\text{)}$$

Atmospheric depth at sea level: $$d_0 = 10 p_0 / g_0 \text{ (in g.cm}^{-2}\text{)}$$

Depth difference: $$z(h) = d_0 - d \text{ (in g.cm}^{-2}\text{)}$$

Neutron flux normalised to sea level: $$N_{1030}(R) = Y + \frac{A}{\left[1 + \exp\left(-\left(\frac{R - X}{B} \right) \right) \right]^C}$$

Attenuation length for neutrons: $$\Lambda(R) = y + \frac{a}{\left[1 + \exp\left(-\left(\frac{R - x}{b} \right) \right) \right]^c}$$

Scaling factor concerning the neutron flux at the site:

$$N(z,R) = N_{1030}(R) \cdot \exp(z(h)/\Lambda(R))$$

Scaling factor concerning the neutron and muon flux at the bsite:

$$N(z,R) = N_{1030}(R) \cdot \exp(z(h)/\Lambda(R)) \cdot (1-f) + N_{1030}(R) \cdot \exp(z(h)/\Lambda_{\mu}) \cdot f = SF_{El,Lat}$$

M	earth's dipole momentum (in $A.m^2$)
μ_0	permeability of the free space ($4\pi*10^{-7}$ $N.A^{-2}$)
r	earth radius (in m)
c	speed of light (in $m.s^{-1}$)
λ	geomagnetic latitude (in degree)
p	atmospheric pressure of the sampling site (in mbar)
p_0	mean annual sea level pressure at the sampling site (in mbar)
β_0	temperature lapse (in $K.m^{-1}$)
h	altitude of the site (in m)
T_0	mean annual sea level temperature at the sampling site (in K)
g_0	acceleration constant due to gravity (in $m.s^{-2}$)
R_d	gas constant
d	atmospheric depth of the site (in $g.cm^{-2}$)
d_0	atmospheric depth of sea level (in $g.cm^{-2}$)
f	muon-induced fraction of cosmogenic nuclide production
Λ_{μ}	attenuation length of muons in the atmosphere (in $g.cm^{-2}$)

Fitting coefficients (dimensionless):

A	0.5221	a	17.183
B	-1.7211	b	2.06
C	0.3345	c	5.9164
X	4.2822	x	2.2964
Y	0.4952	y	130.11

Influence of the field intensity

The intensity of the magnetic field controls directly the intensity of the primary cosmic radiation impinging on the earth's magnetic field. Fig. 2.9 shows the dependence of the scaling factors on the latitude from 0 to 60 degrees for magnetic field intensities of $2*10^{22}$, $6*10^{22}$, and $10*10^{22}$ Am². The lowest field intensities produce the highest scaling factors (i.e. the least modification to the values to be corrected such as production rates) and considering the range of variation throughout the latitudes it shows the lowest sensitivity to the latitude.

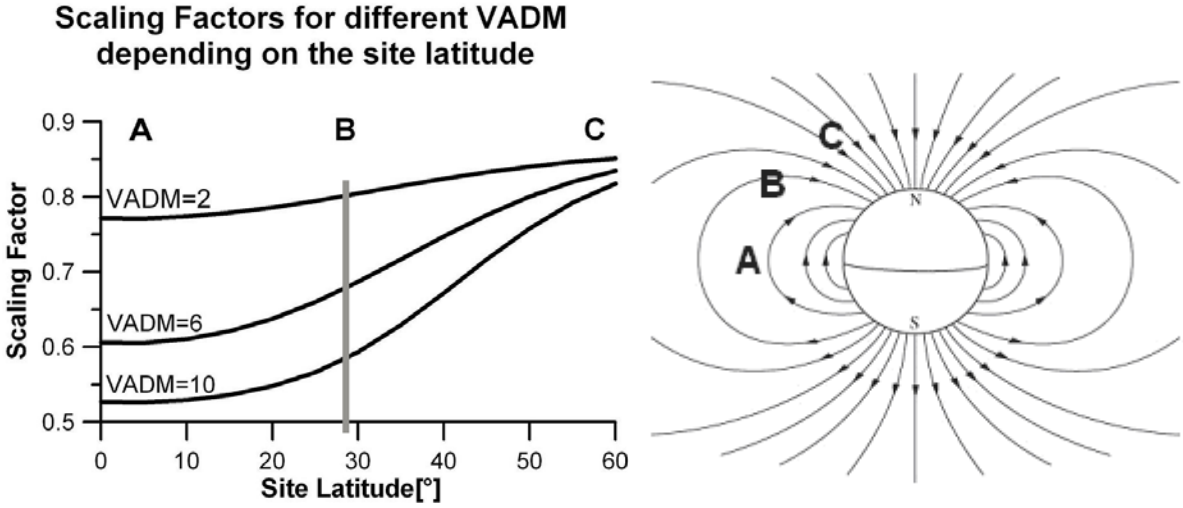

Fig. 2.9 Scaling factors as functions of latitude (A: low latitude, B: mid-latitude, C: high latitude) and field intensity represented by the values of VADM (left) and simplified image of the field lines of the earth magnetic dipole (right). The variation of the magnetic field intensity has most effect on the mid and low latitudes but affects the cosmic radiation at high latitudes only little. The grey line denotes the position of Fuerteventura.

With increasing field intensity the scaling factors decrease, especially at low latitudes, and the range of the values of the scaling factors throughout the latitudes increases, which indicates a higher sensitivity of the cosmic ray flux to latitudes. At high latitudes the scaling factors for all field intensities are high and very similar. Sites at high latitudes are not very sensitive to variations of the field intensity. The sensitivity to latitude is also reduced at high latitudes compared with mid-latitude sites because the orientation of the field lines with respect to the earth's surface, which directs the particles towards the earth surface, is not influenced by the field intensity. The stability of the radiation effects at high latitude is the reason why the scaling factors for the latitude effect are chosen to be normalized for high latitude. Towards low latitudes the sensitivity to the field intensity increases. Since the field lines above the magnetic equator are horizontal, which causes maximum shielding, the intensity of shielding (cut-off rigidity) mainly depends here on the field strength. The differences between scaling factors based on different field intensities are therefore maximum for the lowest latitudes.

Effects of the pole position

The position of the geomagnetic poles with respect to the geographic coordinate system determines the geomagnetic coordinates of the site and defines the orientation of the field lines at the site. The effect of changing the pole positions on the scaling factor at a given site is investigated briefly using a simple dipole field model for the earth's magnetic field. A set of sites at three different latitudes (0°, 30°, 60°) and the same longitudes is chosen and a set of pole positions at latitudes of 90° and 85°, for all longitudes. The geographic coordinates of the sites are transformed into geomagnetic coordinates (Yang et al., 2000a):

$$\sin\Lambda = \sin\lambda \sin\lambda_p + \cos\lambda \cos\lambda_p \cos(\varphi - \varphi_p) \qquad \text{for the magnetic latitude} \qquad (2.15)$$

$$\sin\Phi = \frac{\cos\lambda \sin(\varphi - \varphi_p)}{\cos\Lambda} \qquad \text{for the magnetic longitude} \qquad (2.16)$$

where Λ and Φ are the geomagnetic latitude and longitude of the sites, respectively, λ and φ are the sites' geographic latitude and longitude, respectively, and λ_p and φ_p the geographic latitude and longitude of the magnetic pole.

The scaling factors for each given site vary with the pole position (Fig. 2.10). The strongest impact is seen for the site at mid-latitude (30/0), whereas it is significantly less for the low (0/0) and the high (60/0) latitude sites. The more the magnetic pole latitude deviates from the geographic pole the stronger is the effect on the scaling factor. The larger the latitude shift of the pole becomes the more important is the longitude of the shift. The scaling factors increase when the pole moves along a longitude that is between 0° and 90° away from the longitude where the site is located (see also Pigati & Lifton, 2004). The maximum increase occurs when the pole shifts along the site's longitude, i.e. when the pole moves directly towards the site and thus the site moves to higher magnetic latitudes by the rotation of the magnetic coordinate system. The reverse effect, i.e. a decrease of the scaling factor for a site not located at the equator, is observed when the pole shifts along a longitude between 90° and 180° away from the site's longitude. The maximum decrease occurs when the pole moves along the longitude 180° away from the site's longitude. In this case the site effectively reaches a lower magnetic latitude because the pole moves away from it.

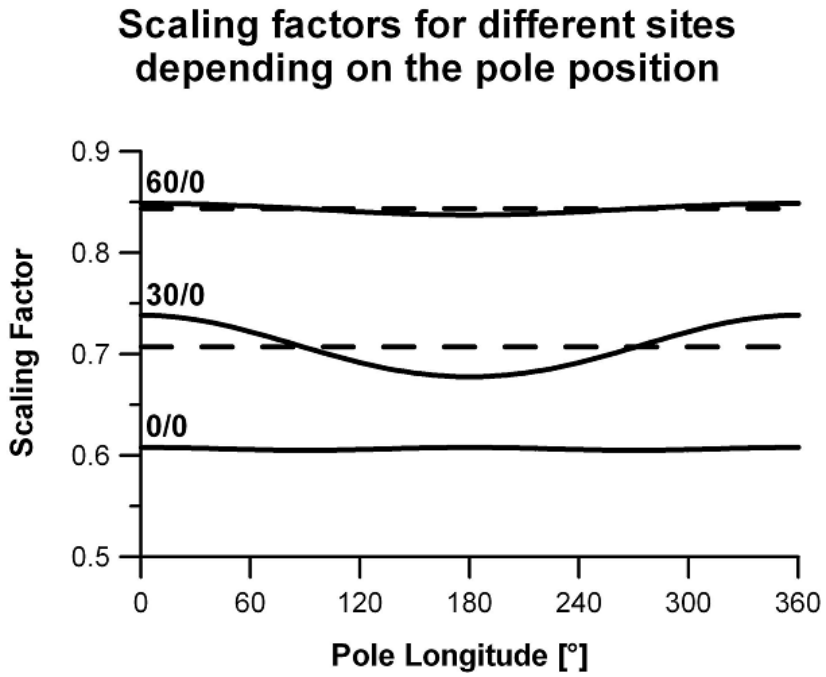

*Fig 2.10 Variation of scaling factors for certain fixed sites (see (latitude/longitude)-notations on the left of the graphs) caused by shifts in the pole latitude and summarized for all pole longitudes (VADM for all 6*10²² Am²). Variations in the pole position (polar wander) affect the production rates of cosmogenic nuclides at low and high latitudes considerably less than at mid-latitudes. The curves for pole position at latitude 90° are dashed lines, the curves for pole position at latitude 85° are solid lines.*

For a site at the equator the scaling factor is lowest for a magnetic pole position equal to the geographic pole. A shift of the magnetic pole along longitudes equal to and 180° away from the site longitude causes the same increase in the scaling factor because the site is equally far from both the north and the south poles. Thus, moving one pole along the longitude 180° away from the site drives the other one towards the site by the same amount. So shifts of the pole along the same longitude or 180° away produce the same geomagnetic situation for the site, just being either a few degrees north or south of the geomagnetic equator. A shift of the magnetic pole away from the geographic pole along longitudes at an angle of 90° to the site longitude does not cause any deviation of the scaling factor because the coordinate system rotates around a point right at the site. The scaling factor is not very sensitive to longitude uncertainties of the pole when the pole is around the longitude of the site or 180° away from it. Within a range of ±30° in the longitude around these positions, the scaling factor shows a deviation of less than 1 %. For pole positions 90° away from the site longitude, the scaling factor is significantly more sensitive to uncertainties of the pole longitude: within only 10° of deviation the scaling factor varies about 1 %.

Altitude effect

The effect of the altitude on the intensity of radiation is included together with the latitude in all models quoted here. The height of the site determines the thickness of the atmospheric layer above the site. The higher a site the thinner is the atmospheric layer. The site experiences less shielding and thus the intensity of the radiation is higher. The scaling is performed with respect to sea level with a standard pressure and temperature. The annual mean temperature of the site and either the standard atmospheric pressure or a regional mean

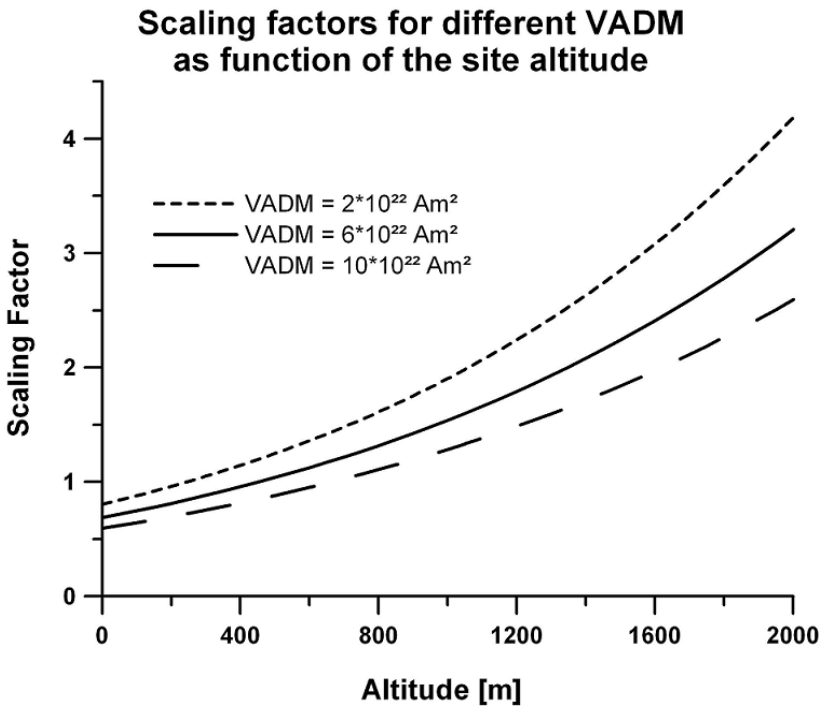

Fig.2.11 Scaling factors for different VADM as function of altitude for the site of Fuerteventura. The lower the VADM is the stronger is the effect of height.

pressure, where the standard pressure is not appropriate (e.g. Iceland), are taken as a reference. The equation for the standard atmosphere (ICAO) is usually applied to calculate the atmospheric pressure and the atmospheric depth at the site for the specific altitude (for details see Dunai, 2000). The scaling factors for each value of VADM increase with altitude because the attenuating effect of the atmosphere decreases with increasing height and thus the degree of shielding from radiation by the atmosphere decreases. The increase is stronger and the rate of increase grows faster for lower VADM values and for higher altitudes (Fig. 2.11). That also means that uncertainties in the determination of the height are less severe for large VADM.

Error analysis for the elevation/latitude scaling factor

A thorough error analysis based on classical error propagation methods is performed in this study for the models by Dunai (2000, 2001), Pigati & Lifton (2004), and Desilets et al. (2006) to calculate which parameters may be critical for the errors. The derivations are calculated using Mathematica 5.1 and 6 routines. Attention is directed at uncertainties of dipole moment, latitude, pressure, temperature, and the fraction of muons contributing to the production of cosmogenic nuclides. The earth's radius, temperature lapse rate, gas constant, and permeability of free space are taken as natural constants or as parameters with negligible uncertainty.

The scaling factors calculated for the different sampling sites on Fuerteventura lie between 0.8 and 1. The contribution to the scaling factor from the uncertainty of the latitude, λ, which is based on the uncertainty of positioning of the site by means of GPS (horizontal error about 10 m) and the coordinate transformation, is very small (of the order of magnitude of 10^{-4}) and it is neglected as source of error for the samples given. The influence of the muon fraction, f, on the error is also minute (10^{-4}) for the samples considered here, which are mainly (with the exception of two profiles) samples taken directly from the surface and are not more than 25 cm thick. For samples from a greater depth the influence of the uncertainty of the muon fraction may be higher due to the larger contribution of the muon-induced production of cosmogenic nuclides. The contributions of the uncertainties of standard pressure P_0 and mean annual temperature T_0 are of the same order of magnitude and relatively small (10^{-3}). Considering the age of the samples the approximation of the magnetic pole by the geographic pole is a reasonable one and at present the only feasible approach.

The main contribution (10^{-1} to 10^{-2}) comes from the uncertainty of the magnetic dipole moment, which is especially important with view on earth history, the uncertainty of the altitude measurement from the low quality of GPS-height determinations (vertical error about 20 m), and the uncertainty of the magnetic latitude from assigning the magnetic pole to the geographic pole. For very young samples the uncertainty of the magnetic latitude from polar wander is more critical than that of the VADM. According to Dunai (2000) the sea level neutron flux and the attenuation coefficient, which are determined through fitting coefficients, also have an uncertainty of 2 % and 3 %, respectively. So, the overall uncertainty in the scaling factor lies between 2 and 4 % for the site of Fuerteventura.

Pigati & Lifton (2004) determine the scaling factors for elevation and latitude by applying a series of fitting coefficients for each of the components of the radiation. For the high energy

neutron component that causes spallation reactions, the error contribution of the latitude in terms of GPS positioning is very small (10^{-5}) and is thus negligible. The contribution of the uncertainty of the geomagnetic latitude is of the order of 10^{-2}. Temperature uncertainties also do not contribute significantly (10^{-3}). However, the influence of pressure uncertainties is stronger in this model than in Dunai (2000, 2001). The uncertainties of the pressure, the dipole moment, and the height give errors of the order of 10^{-2}. The estimation of the uncertainty of the fitting coefficients is rather complicated, but they may contribute approximately 10^{-3}. (A simplified error calculation by Pigati and Lifton (2004) gives similar results.) For the fast and slow muon fractions of the scaling factors all the contributions to the total error are half an order to one order of magnitude smaller than for the part for spallation. Also here the dipole moment together with height, pressure and (for the slow muons) temperature are the main contributors. The total uncertainty of the scaling factors according to the error estimation is about 4 to 5 %.

The calculation of the scaling factors for the models by Desilets & Zreda (2003) and Desilets et al. (2006) is in principle similar to that for the model by Pigati & Lifton (2004) but includes an extra step for the calculation of the contribution of the production based on thermal neutrons. The contributions of the individual parameters to the error are very similar to the ones of the former model. The error contribution of the latitude in terms of GPS positioning is very small (10^{-5}) for the high energy neutron component that causes spallation reactions and is thus neglected. The contribution of the uncertainty of the geomagnetic latitude is of the order of 10^{-2}. Temperature uncertainties also do not contribute significantly (10^{-3} for the high energy component of the radiation and 10^{-4} to 10^{-7} for the muon and thermal neutron components, respectively). The uncertainties of the pressure, the dipole moment, and the height give errors of the order 10^{-2} to 10^{-3} for all components. The uncertainty of the fitting coefficients may contribute all together about 10^{-2}. Again the largest contribution to the total error in the scaling factor comes from the spallation part, whereas the error for the thermal neutron part is smallest. The uncertainty of the scaling factor is with about 5 % comparable to the one for the Pigati & Lifton (2004) model.

3 Geological development and recent setting of the Canary Islands and the island of Fuerteventura

The Canary Islands are located in an intraplate setting on the northwestern African shelf on a passive continental margin (Almendros et al., 2004). Fuerteventura is the easternmost island of the Canary Islands, approximately 100 km away from the west coast of Africa and extends roughly from 28.04˚N to 28.76˚N and from 13.82˚ W to 14.51˚W (Fig. 3.1).

The island of Fuerteventura consists of two main lithological units: the older Basal Complex and a younger, subaerial series of volcanic flows (e.g. Coello et al., 1992; Steiner et al., 1998). The Basal Complex is exposed in the western central part of Fuerteventura (mainly in the Betancuria Massif and small areas north and south of it) and represents the seamount (pre-shield) stage of the submarine and subaerial volcanism of the island. It includes (Jurassic to Oligocene) sedimentary successions and volcaniclastic sediments, and (Paleocene to Early Eocene) submarine volcanic rocks (see geological time scale in Appendix E) (e.g. Rothe, 1986; Le Bas et al., 1986; Ancochea et al., 1996). A series of alkaline ultramafic to intermediate plutons and a NNE-SSW trending dike complex intruded the succession in several episodes in the Late Oligocene to Early Miocene (e.g. Ahijado et al., 2001; Balogh et al., 1999). Due to Miocene tectonic uplift it now crops out above sea level (Coello et al., 1992).

The younger, less abundant basaltic activity of Fuerteventura is subdivided into four series (I to IV) representing successive eruptive cycles (Coello et al., 1992). The lavas of the Canary Islands, which comprise predominantly basalts (picrites, tholeiites, basanites) and associated differentiated rocks (phonolites, trachytes) (Carracedo et al., 1998; Stillman, 1999), are alkaline throughout all eruptive periods. The Miocene age series I is interpreted to be the shield-building stage of the island (Carracedo et al., 1998). The base of the series of all volcanic centres (edifices) is cut by numerous trachytic dikes and locally trachytic domes (e.g. Coello et al., 1992; Steiner et al., 1998). The morphology and the structure of the dike systems point to the existence of old large scale volcanic complexes with the centres being located offshore (southern volcanic centre) or onshore (central and northern volcanic centres) (Fig. 3.1) which have formed successively over a time span of approximately 10 Myr. The activity episodes were separated by temporal gaps, which provide evidence that independent magmatic cycles have occurred (for details see Ancochea et al., 1996).

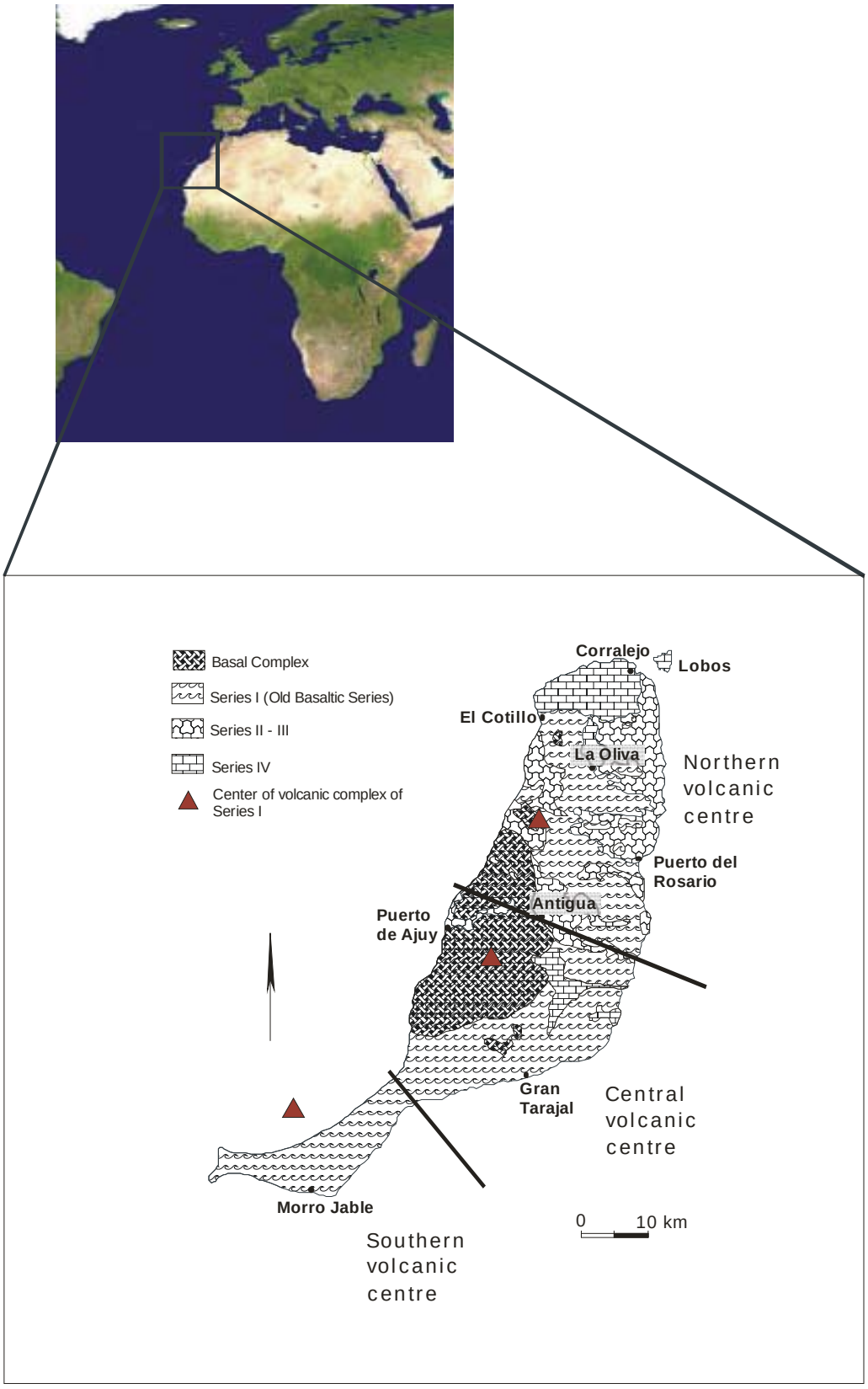

Fig. 3.1 Location of the island of Fuerteventura and geological map of Fuerteventura (after Ancochea et al., 1996; Coello et al., 1992); (http://plasma.nationalgeographic.com/ mapmachine/, http://www.sage.wisc.edu/riverdata/images/world_map_small.jpg; 2005).

A period of volcanic quiescence of about 7 Myr during which the three volcanic centres were denuded rapidly separated the Miocene series I from the Pliocene to recent post-erosional series II – IV that contained exclusively basaltic rocks (Coello et al., 1992). The older rocks of the post-erosional stage are basanites and alkali-basalts, whereas the younger ones also include transitional tholeiites, which is probably due to magma contamination by crustal material (Lundstrom et al., 2003). The new period of activity is characterized by numerous scattered small volcanoes and associated lava fields, which are concentrated in the central and northern part of Fuerteventura. The (K-Ar) age data however for these younger activity periods are in significant disagreement with new $^{40}Ar/^{39}Ar$-data (Schneider et al., submitted). This discrepancy is very likely because of limits in the detection devices for K-Ar measurements performed ten to twenty years ago, which restricted the resolution of the age determination for very young rocks. Therefore the new $^{40}Ar/^{39}Ar$-data are used in this research.

The origin of the archipelago has already been under debate for a long time. A slowly moving mantle plume of changing shape appears at present to be the best explanation of the features of the archipelago. This seems to be confirmed by results of finite-frequency tomography which provide an indication of a deep-rooted plume structure underneath the Canary Islands that may possibly be connected to the plumes of the Azores and the Cape Verdes (Montelli et al., 2004). The plume model is also supported by isotope evidence of the magmas (e.g. Hart et al., 1992; Faure, 2001; Gurenko et al., 2006). Based on the plume model, the development of the Canary Island archipelago might be sketched as follows. The lithosphere beneath the Canary Islands developed between 180 and 190 Myr (older, eastern islands) and 150 Myr (younger, western islands) ago during the opening of the central Atlantic Ocean (e.g. Hoernle, 1998; Schmincke et al., 1998). A 10 km thick sedimentary cover of the crust at the continent-ocean transition zone is assumed to have weakened the lithosphere and to have provided a location for the onset of Canarian volcanism parallel to the African coast. The initial stage of the volcanism could have spread out to the northeast and southwest along the weak transition zone between continental and oceanic crust producing the Fuerteventura-Lanzarote ridge (Carracedo et al., 1998). Subsequently, the slow easterly motion of the African tectonic plate relative to the hotspot, i.e. the plume, could have caused the general westward trend of the subaerial volcanic activity of the Canary archipelago so that the western islands started to develop significantly later (about 1-4 Myr ago) than the central islands (12-15 Myr ago) and the eastern ones (about 20 Myr ago) (Abratis et al., 2002; Gurenko et al., 2006). According to e.g. Muñoz et al. (2005) the older subaerial volcanic

activity on Fuerteventura started even 25 Myr ago. The extremely slow motion of the African plate in relation to the hotspot reference frame (20 mm/yr during the last 19 to 30 Myr, according to O'Connor et al. (1999)) was also the reason for the Canaries' exceptionally long volcanic activity. Including the stages of early submarine volcanism the activity of Fuerteventura has started 35 Myr, probably even more than 50 Myr ago (Coello et al., 1992). Volcanological, structural and geomorphological features such as triple armed active rifts and giant landslides that are assumed to be typical for the shield-building phase of hotspot-related islands have been found on the younger islands (Tenerife, La Palma, El Hierro). On the older islands these characteristics cannot easily be determined because of the age and geological stage of the islands which are in long-lasting activity gaps with intense erosion. This wide range of island development is a clear sign for long-lasting volcanic activity throughout the archipelago.

The slow motion of the African plate probably together with slight wiggling of the plume itself there is apparently not a straight linear and simple age-distance correlation as found in Hawaii. Some authors see a slight step backward to the east in the overall western movement of the activity reporting ages for Tenerife being younger than for La Gomera (e.g. Carracedo et al., 1998). However this has been questioned recently (e.g. Guillou et al., 2004) suggesting that the west-directed motion of the activity in the archipelago might not have been interrupted. However, during the last 5000 years almost all of the major islands (even the older Canary Islands like Lanzarote) were volcanically active (only exception La Gomera) (e.g. Schmincke, 1982; Gee et al., 2001; Guillou et al., 2004), and islands being 500 km apart showed volcanic activity in very short time spans (La Palma between 1585 and 1971, Lanzarote 1730 till 1824) (Anguita & Hernán, 2000). This also provides strong indication that the volcanic activity of the Canary Islands is initiated by a plume that may wiggle or initiate volcanism by forming sub-plumes originating from the main-plume within the crust.

4 Experimental methods

4.1 Sampling strategy

Nine flows of young basaltic lava have been sampled on the island of Fuerteventura with 7 or 8 samples each (see Figs. 4.1 and 4.2, and Appendix A1 for location, for detailed sample description see Appendix A2). The lava was broken into countless separate pieces of rock distributed on the ground but did not form a compact cover of lava on the earth surface. The samples were collected from places with minimum shielding, i.e. from hill tops or from flow tops distant to surrounding hills, ridges, volcanic cones, and vegetation.

Fig. 4.1 Location of the sampling sites (http://plasma.nationalgeographic.com/mapmachine/, http://www.sage.wisc.edu/riverdata/images/world_map_small.jpg; 2005;)

Attention was directed to samples that did not show any indication of having been formerly covered by volcanic ash and lava layers, which was inferred from the cleanliness of the rock surfaces. Pieces with sediment or (in dents sometimes slightly compacted) ash deposits on top were rejected. Sites with no or little development of desert pavement, caliche, soil formation, or debris deposition in close-by surface depressions were preferred because this was considered to provide evidence for only minimum erosion (Cerling & Craig, 1994).

For older flows this only could be attained with certain restrictions. Further, samples were rejected, which were suspected of probably having originated from lower levels within the flow because they were less vesicular than their surroundings (lava flows are usually more vesicular at the top and become denser with depth (Cerling & Craig, 1994)) or when lava layers of apparently similar age on top of each other were found nearby. The samples collected were large and flat in shape and generally in a stable position to make sure that they had not turned or rolled downhill. To ensure this, only samples were collected that showed the typical flow top structures. When a sample had moved after its deposition, e.g. by rolling downhill, it would expose a new surface to the radiation so that the apparent age would be lower than the true age of the surface (Zreda & Phillips, 2000). Volcanic bombs and other loose deposits as well as the cinder cones were not considered for sampling because of the uncertainties regarding geomorphic instabilities and erosion of loose and soft material. Samples with excessively large sharp edges of flow top structures were rejected to exclude leak-out of thermal neutrons from the sides, which would be difficult to quantify.

Samples of each flow were taken close to each other to make sure that they had identical exposure histories. This provided an additional possibility of controlling the internal consistency (Tuniz et al., 1998). In places where younger and older flows formed interlayered unclear boundaries samples were only taken from unique spots in the flow top centres. Furthermore, only samples away from anthropogenic features such as little walls running across the field were taken. The mass of the samples ranged between 4 and 20 kg, with a thickness between 10 and 25 cm. This made it possible to concentrate on the neutron-based production because muon-based production provides only a minor contribution at this depth. Two samples were taken at the MA-flow to obtain chlorine depth profiles. No samples for chlorine depth profiles could be taken at any other flow, since the depth range of the lava pieces was not sufficient. The positions of the sampling sites were determined with a handheld GPS (Gekko). The relief of the surrounding topography was recorded using a clinometer.

The samples collected showed well preserved ropy or cauliflower surface structures indicating an erosion as little as 1-2 mm for the younger and 10 mm (in one case (flow VF) up to maximum 15 mm) for the apparently older samples. To avoid errors coming from chemical weathering (loss or gain of ions) only rock with a thin weathering crust, along the outer surface, fracture surfaces and on pore walls (not more than 2-3 mm of crust with altered colour and no textural alteration along the surface) was collected. In some cases the weathering rind extended to more than 5 mm with decreasing intensity of alteration. In a

number of the samples, sediment had entered the pore space and fractures and secondary carbonate had formed there. The porosity of the samples varied considerably from flow to flow, but also between the samples within a flow. It was estimated to be between almost none to 25 %, in extreme cases even up to 40 %, with pore sizes varying between less than 1 and 30 mm. Samples with a rather high amount of sediment and/or with extremely high porosity were rejected from further preparation.

(a)

(b)

(c)

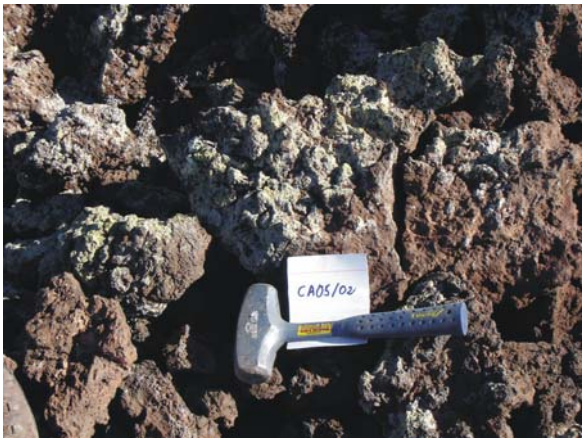

(d)

Fig. 4.2 Examples of sampling sites on Fuerteventura: (a) site MQ, (b) site MR. The positions of the blue bags are approximately the positions of the samples taken. (c) and (d) show examples of the samples collected.

4.2 Sample processing

The sample surfaces, fracture planes and pores were brushed with a wire brush to remove lichen and other organic material, and sediment. The material was crushed, sieved and rinsed with de-ionized water to remove the dust and clay minerals that could carry meteoric ^{36}Cl, and then dried at 100°C in glass beakers and stainless steel bawls. The sieved sample fractions were stored in plastic bags for later treatment. The fraction of 250-500 µm was used for further preparation because it dissolved best in the acids in the subsequent preparation steps. The chemical preparation follows mainly the method used by Stone et al. (1996b) (see Appendix B for the preparation protocol). The samples were processed in batches of four and each batch contained two different flows in changing combinations, so that possible irregularities in the preparation of the samples could be detected. Since the samples were in general of the same composition and the ones prepared together were of a similar age, cross contamination was not an issue for the process. Process blanks included in the procedure of sample preparation comprised some made of the pure blank solutions and others made of rock samples, which were too young for any measurable build-up of ^{36}Cl (Etna, eruption 2002). Both types of blanks were processed like the rock samples from Fuerteventura. These blanks, which are samples that do not contain the isotope of interest, are needed in the measurement to determine the background caused mainly by ^{36}S but also by other particles that leak into the AMS particle detector. For the sample preparation about 60 g of rock sample were leached in water overnight and after that leached in acid for five hours (2 M HNO_3, 100 ml per gram sample dissolved 10-15 % of the grains) to remove meteoric[4] ^{36}Cl and secondary carbonates, which are common in arid climates (Zreda & Phillips, 1994). Chlorine is hydrophilic, and thus any contamination with meteoric chlorine was removed after these leaching steps (Ivy-Ochs et al., 2007).

3.5 ml HF (50%) and 6 ml 2M HNO_3 were added per gram of sample to dissolve the sample. Since the basalt samples often dissolved only very slowly and fluoride gel coating the grains hindered the continuation of the reaction, the calculated amount of acid was added to the sample step by step. On the first day a certain portion of the acid mix was added to the (unspiked!) sample, and after cooling down the reaction bottle, it was placed onto the shaker table for the rest of the day and overnight to avoid the fluoride gel caking together and coating undissolved grains. The next day the sample was allowed to rest for one to three hours

[4] Apart from production in rock ^{36}Cl is also formed from ^{36}Ar in the higher atmosphere due to interactions with cosmic ray neutrons (Fabryka-Martin, 1988). Attached to submicron-sized aerosols it reaches the earth surface and the groundwater by precipitation and forms the meteoric component that has to be removed from the sample by leaching in the first preparation steps.

depending on how quickly the undissolved fraction settled, and thereafter the supernatant liquid was decanted into another storage bottle. Then the second portion of acid was added and the whole process repeated until all the acid had been added and had reacted. Only after this procedure was 3 mg of a spike enriched in ^{35}Cl (NIST, Oak Ridge, 99.900% ^{35}Cl) added and the whole solution was carefully mixed to achieve isotopic homogenization between the sample and the spike. If one or two days after the last reaction step some undissolved material was still found, then another 50 ml of HF was added and left for another day for further dissolution. The solution finally obtained was separated from the fluoride gel and undissolved material by centrifuging. The HF gel obtained was checked for its homogeneity and for remaining undissolved grains. If undissolved grains were found in the gel besides insoluble material or there where other doubts about the dissolution process the samples were rejected from the measurements. 2-3 ml 10 % $AgNO_3$ solution was added to the supernatant liquid. After the AgCl precipitate had been allowed to settle for at least three days, most of the supernatant was carefully pumped off and the reminder was centrifuged. The AgCl was rinsed and centrifuged several times to remove as much HF as possible and then re-dissolved in 3 to 5 ml 1:1 NH_4OH solution. 2-3 ml concentrated $Ba(NO_3)_2$ solution was added to remove the sulphur in the sample. After a few days the solution was centrifuged and the supernatant was pressed slowly through a 0.20 μm syringe filter. The supernatant liquid was re-acidified with 1:1 HNO_3 to re-precipitate AgCl. The precipitate was rinsed and centrifuged several times to remove HNO_3 from it and finally dried overnight at 125˚C. The reproducibility of the preparation procedure was confirmed by preparing several AMS targets from the same rock sample. Samples from different sites, preferably from all the flows at once, were measured in the same batch. Generally samples, blanks and standards that have been prepared approximately at the same time under the same conditions were measured together in the same AMS-batch.

To test if the dissolution procedure suffered from a loss of chlorine, the preparation method was modified. As opposed to the method described above a number of samples was spiked first and then subsequently dissolved in one step by adding all the acid at once. If a loss occurred during dissolution, the samples that had been spiked first would have lost natural chlorine and spike at the same time and thus the ratio of natural chlorine and spike would not have changed. In contrast the samples that had been spiked after dissolution would have combined too low a natural chlorine concentration with the original amount of spike and thus would have resulted in lower natural chlorine and ^{36}Cl amounts during the AMS measurements compared with the other samples. Any loss of chlorine or AgCl that occurred

after dissolution and spiking (e.g. during AgCl collection from precipitation or rinsing) would not have affected the measurement results of the isotope ratios. Both methods were applied to samples stemming from the same rock samples to exclude any factor such as natural chemical variations of the rocks that might obscure the comparison. The results of the AMS-measurement demonstrated that the methods did not suffer any measurable chlorine loss in any of the dissolution steps.

Tests have been performed on the synthetic samples to investigate if the application of H_2O_2 to oxidise fully all the sulphur compounds resulted in a more efficient $BaSO_4$ cleaning. Also it was tested to see if significant amounts of chlorine were lost during this process from the oxidation of chlorine ions. The results of the measurements did not show any indication of an improved purity of samples after the H_2O_2 treatment and thus, further sample preparation was done without it.

The total rock density, which is needed for scaling for the sample thickness (see chapter 2.3) was determined on hand specimens by weighing them and determining their volume in a measuring cylinder. From highly vesicular samples the density of the crushed material was additionally quantified. The major and trace element analyses for each flow were performed with XRF (X-ray fluorescence) spectroscopy and ICP-MS (Inductively coupled plasma mass spectrometry) at the NITG Geolab at the Utrecht University (see table Appendix C). Mineral determination on the crushed rock and on the secondary minerals and sediment from the pore space of the samples (mainly carbonate, clays, quartz) were done with XRD (X-ray diffraction) at the CEREGE (Aix-en-Provence, France) and at the Utrecht University. Thin sections have been made from several samples of each flow to inspect the mineralogy of the rocks and the general condition of the samples in terms of alteration. A check was made to see if minerals have been replaced by secondary minerals by weathering, which could indicate an increased presence of meteoric ^{36}Cl (Zreda & Phillips 1994). Chemical spot analyses were performed with the microprobe (JXA-8600 Superprobe) at the Geosciences department of the Utrecht University. Additional measurements of ^{10}Be and/or ^{26}Al to support the ^{36}Cl measurements were not possible because the Si concentration of the samples was so low that no quartz had formed in separable grains. Olivine or pyroxene from which these isotopes also could have been extracted also did not occur in sufficient amounts of separable phenocrysts. The $^{40}Ar/^{39}Ar$ age determination for the flows was performed at the Free University in Amsterdam (Schneider et al., submitted). This method reached its limits for the very young samples and produced ages with large uncertainties, but for the older samples it worked rather well (B. Schneider and J. Wijbrans 2008, pers. comm.).

Testing the influence of the drying temperature during the chemical preparation

Two sample sets of different age and thus different ^{36}Cl contents were tested to see if the loss of chlorine from the samples depended on the temperature at which the samples were dried during the steps of pre-preparation (crushing, cleaning) and the first steps of the actual preparation (water and acid leaching). For the flows MA and VF additionally to the samples dried at (regular) 100°C (MA 05/02-2, MA 05/02-3, VF 05/04-3; open circles in Fig. 4.3) a few samples from the same rock samples were dried at 60°C (MA 05/02 (60)-2[5], VF 05/04 (60)-1; full circles in Fig. 4.3).

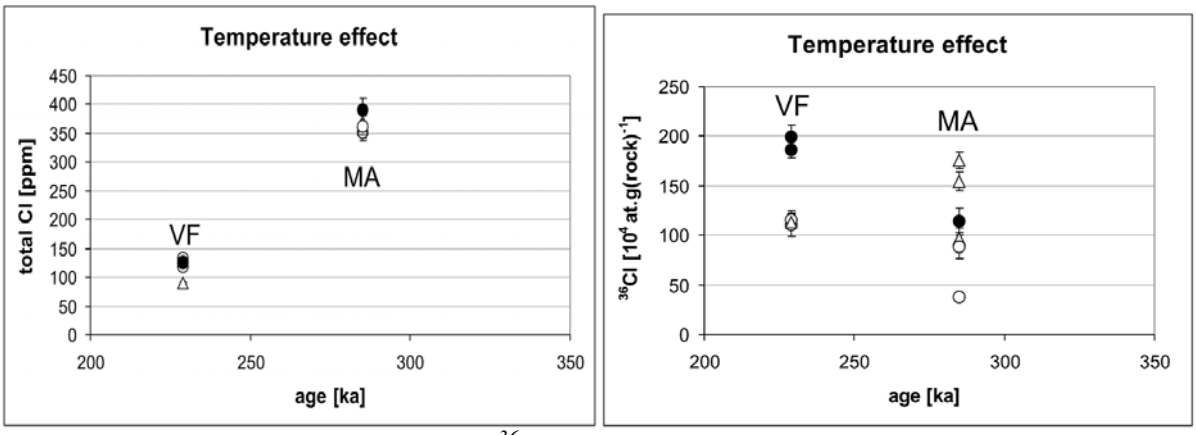

Fig. 4.3 Total chlorine (left) and ^{36}Cl (right) contents of samples dried at different temperatures during sample preparation. The full circles represent the samples dried at 60°C, the open circles the samples dried at 100°C. Triangles represent samples from other rock pieces of the same flows.

Preparing all the samples for this test for one set from the same pieces of rock from each flow (MA 05/02, VF 05/04) reduced the possible flow-internal variation of element concentrations to a minimum that otherwise could have introduced some extra scatter as indicated by the triangles in Fig 4.3. The triangles represent samples, which were made from different rock samples of the respective flows and are shown for comparison. All the subsequent preparation procedures were exactly the same for all of the samples. There were no systematic temperature dependent deviations in the total chlorine and the ^{36}Cl content for the samples tested (Fig. 4.3 and Table 4.1). The total chlorine contents were within the errors the same within both sample sets. For the VF flow the samples dried at lower temperature produced a higher ^{36}Cl content, which was not observed for the samples of the MA flow. There was thus no unequivocal indication that a drying temperature of 100°C could have affected the results of the measurements compared with the lower temperature of 60°C. The

[5] The notation is explained in Appendix D.

samples were thus generally dried at 100°C. Some of the samples are not included in the later determination of the production rate of ^{36}Cl because they did not fulfil the precision requirements for this step but they are considered to be useful to demonstrate that the temperature effect from the drying steps is not sever enough to systematically exceed all other influences from preparation and measurement.

Age	Sample	Measurement date	Total chlorine (ppm)	^{36}Cl 10^6 at.g(rock)$^{-1}$
285 ka	MA 05/02 (60)-2	27.08.2008	391 ± 17	1.15 ± 0.12
	MA 05/02-2	28.08.2008	352 ± 13	0.37 ± 0.05
	MA 05/02-3	27.08.2008	362 ± 16	0.88 ± 0.11
	MA 05/01-1	28.08.08	357 ± 14	1.54 ±0.09
	MA 05/01-1	30.08.08	370 ± 15	1.75 ±0.08
	MA 05/03-3	29.08.08	365 ± 19	0.97 ±0.10
229 ka	VF 05/04 (60)-1	29.08.2008	125 ± 3	1.87 ± 0.09
	VF 05/04 (60)-1	30.08.2008	128 ± 3	2.00 ± 0.12
	VF 05/04-3	27.08.2008	134 ± 4	1.11 ± 0.12
	VF 05/04-3	29.08.2008	119 ± 3	1.15 ± 0.09
	VF 05/06-2	28.08.08	89 ± 2	1.13 ± 0.08

Table 4.1 Total chlorine and ^{36}Cl contents of samples prepared from the same rock sample, which were dried at different temperatures during sample preparation.

Test of possible influence of weathering at the surface

The influence of weathering of the rock surface was tested for two sets of samples of different age. The alteration crust along the rock surface was very thin (2-4 mm, in a few cases up to 5-10 mm) and only visible by the slight colour change, but there was not any textural alteration. Thin chips of approximately 0.5-1 cm thickness that encompassed the whole alteration zone but not too much of the fresh material underneath it were cut with a saw from the surfaces (CG05/04w-1, MM05/04w-1) and processed like a regular sample. For comparison, fresh material from the centre of the same samples (corresponding to an effective minimum depth of 1-3 cm) was taken as separate sample (CG05/04f-1, MM05/04f-1) and processed in the same manner as all the other samples produced for AMS measurements. The results are shown in Fig. 4.4 and Table 4.2. Open circles indicate material from the unaltered centre and closed circles the material from the alteration crust. Triangles represent samples,

which were made from different rock samples of the respective flows and are shown for comparison.

The total chlorine and ^{36}Cl contents were somewhat higher for the CG 05/04w-samples (altered crust) compared with the CG 05/04f-samples (unaltered material from the same rock piece). For the MM 05/04-samples the situation was reversed and the difference between the weathered and the fresh sample parts was minute. For both flows the total chlorine and the

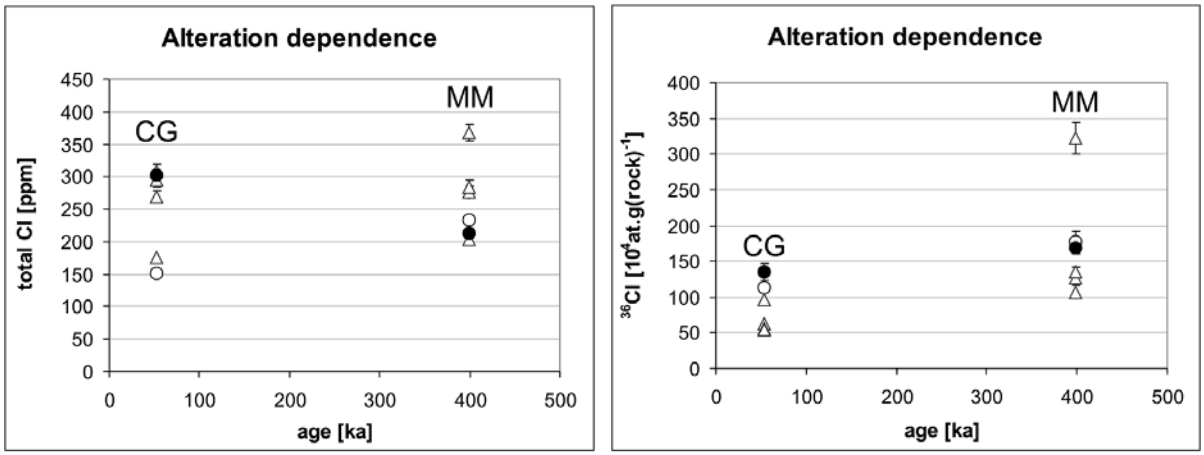

Fig. 4.4 Test of ion exchange with the environment within the thin alteration crust of the samples in comparison with very fresh material from the centre of the rocks. The full circles represent the samples of the alteration zone, the open circles the samples from fresh material. The triangles represent regular samples that included both alteration crust and fresh rock.

^{36}Cl contents of the samples from the alteration crust lay within the overall scatter of all samples of the according flows. Even though the values in this test are partly not used for the determination of the production rate of ^{36}Cl because they did not fulfil the precision requirements for this step, they are considered to support the conclusion given here. If the difference between the weathered and the fresh samples were significantly higher and had exceeded the other effects of the preparation and measurements the samples would have needed to be prepared solely without the outmost layer. Also XRF and ICP-MS measurements did not indicate any significant variations in the chemical composition of the material from the alteration zone compared with the material from the unaltered centre. There was no evidence that significant changes in the elemental composition occurred in the alteration zone on the surface. Thus, including a tiny alteration zone as found on the present samples did not introduce significant errors in the measurement.

Age	Sample	Measurement date	Total chlorine (ppm)	^{36}Cl 10^6 at.g(rock)$^{-1}$
53 ka	CG 05/04f-1	29.08.2008	151 ± 4	1.12 ± 0.09
	CG 05/04w-1	29.08.2008	303 ± 13	1.35 ± 0.12
	CG 05/01-1	28.08.08	294 ± 11	0.63 ± 0.08
	CG 05/01-3	29.08.08	269 ± 9	0.56 ± 0.06
	CG 05/05-5	30.08.08	175 ± 5	0.53 ± 0.05
	CG 05/06-1-1	16.07.08	308 ± 10	0.95 ± 0.05
	CG 05/06-1-2	16.07.08	308 ± 11	0.95 ± 0.05
399 ka	MM 05/04f-1	28.08.2008	234 ± 7	1.78 ± 0.15
	MM 05/04w-1	28.08.2008	213 ± 7	1.69 ± 0.10
	MM 05/01-3	30.08.08	276 ± 10	1.27 ± 0.06
	MM 05/02-1	27.08.08	368 ± 14	3.22 ± 0.22
	MM 05/02-2	29.08.08	284 ± 11	1.07 ± 0.09
	MM 05/04-2	28.08.08	203 ± 6	1.35 ± 0.07

Table 4.2 Total chlorine and ^{36}Cl contents of samples from the thin alteration crust and from the centre of the samples. f=fresh, w=weathered. There is no systematic effect based on chemical reactions in the alteration crust that indicates ion exchange of the sample with the environment that could affect the results of the measurements of chlorine and ^{36}Cl.

4.3 AMS technique

The AMS system is composed of an ion source, an achromatic selection spectrometer comprising a 90° electrostatic deflector and a 90° injection magnet, which together form the low-energy (LE) end, the tandem accelerator, and the high-energy end (HE) that consists of a 13° electrostatic deflector, a 90° analysing magnet, a particle detector and Faraday cups. Negative ions are produced in the ion source by sputtering the prepared target with a 0.2 mm wide Cs^+ beam of 3.7 keV. The ions are extracted from the source with energy of 20 keV. The ions are selected with the injection system according to their energy and mass, pre-accelerated to 110 keV and then injected into the tandem accelerator. The negative ions are accelerated towards the terminal of potential (V) of 6 MV where they pass through a stripper channel filled with Ar gas. In this channel they are stripped into multiply charged (q) positive ions. Subsequently the positive ions are further accelerated in the second stage of the tandem to ions of energy of (1+q)V. These ions are further E/q-selected by the electrostatic deflector and p/q-selected by the analysing magnet. The yield of the rare isotope is measured in the

ionization chamber detector and the yields of the stable isotopes are measured in the Faraday cups located in the focal plane of the magnet.

The ^{36}Cl measurements were performed at the AMS facility of the Utrecht University, which comprises an EN-Van de Graaff-Tandem accelerator with a terminal voltage of 6 MV. For the chlorine measurements we used the dried AgCl samples, which were pressed in a sample holder (Cu cathode of 6 mm diameter) prefilled with an AgBr bed. The sample holders with the AgCl samples were loaded in a 20 position sample wheel of the NEC source of the Utrecht AMS facility (van der Borg et al., 1984). Per batch 12 samples, 3 - 4 chemical blanks, and secondary standards diluted from the ^{36}Cl reference material (NIST, SRM-4349) with $^{36}Cl/^{35}Cl$ ratios of 10^{-11} and 10^{-13} (1 standard each), and of 10^{-12} (2 standards) were used. The ^{36}Cl concentrations of the standards we used were not more than two orders of magnitude higher than the one of the samples to avoid cross contamination. Negative ^{35}Cl currents of 0.5-1 μA were obtained from the ion source. A fast beam-switching device applies short high-voltage pulses to the vacuum chamber of the LE-analysing magnet to inject pulses of the isotopes ^{35}Cl and ^{37}Cl in addition to ^{36}Cl (van der Borg et al, 1984; de Haas et al., 1987). The total pulse length is 100ms, from which 0.5 ms are used for the each the injection of ^{35}Cl and of ^{37}Cl, and the remaining time of the pulse is used for ^{36}Cl. Compared with the rather slow variations of the terminal voltage these high frequency pulses of the switching element are fairly rapid and so a quasi simultaneous measurement of the isotopes can be performed independently of any system variations (van der Borg et al., 1984). Due to the short beam pulses the stability of the terminal voltage has not been affected.

For these measurements we used a terminal voltage of 6MV and stripped the chlorine ions to the 7+ charge state resulting in 48 MeV ions. In the stripping process the interfering molecules (for example $^{35}ClH^-$) were eliminated. Only the sulphur, ^{36}S, which is present everywhere in the samples as well as in the material of the sample holder, cannot be reduced in this way. After passing the 13° electrostatic deflector and the 90° analyzing magnet the ^{36}Cl ions are bent into the detector and the ^{35}Cl and ^{37}Cl ions into Faraday cups. For more details of the working principles of accelerator mass spectrometers see for example Litherland (1984). The samples, standards, and blanks were repeatedly measured in several of these short cycles. These short cycles were repeated eight to ten times to average out effects of long-term variations of the system and to control the long-term stability of the measurement. The whole batch was measured several times.

The ^{36}Cl identification was optimized with a gas ionization counter provided with a 70 nm SiN entrance window and 26 mbar propane detector gas. Using the SiN window instead of a

mylar window decreased the energy loss of the particles in the entrance window and improved the sulphur-chlorine separation in the detector. The fast moving incoming ions lose kinetic energy due to interactions with the gas molecules and produce ion-electron pairs along their track through the gas. The ionization signals produced by the stopping process in the gas are recorded by five anode plates by collecting the electrons on the plates (which are in that way a measure of the energy loss (ΔE) of the ions beneath the plates), while a cathode records the total energy (E) of the particles. The gas pressure in the detector was chosen to receive a higher energy loss of ^{36}Cl than of ^{36}S for the range of the first two anode plates and a lower energy loss for ^{36}Cl beneath the fourth and fifth anode plate according to its stopping power, which depends on the atomic number and the energy of the particle. The third anode plate was the cross-over for the ^{36}Cl- and ^{36}S-stopping power curves (which is the point of equal energy loss of the two isobars) (Fig. 4.5). All particles were stopped under the fifth plate.

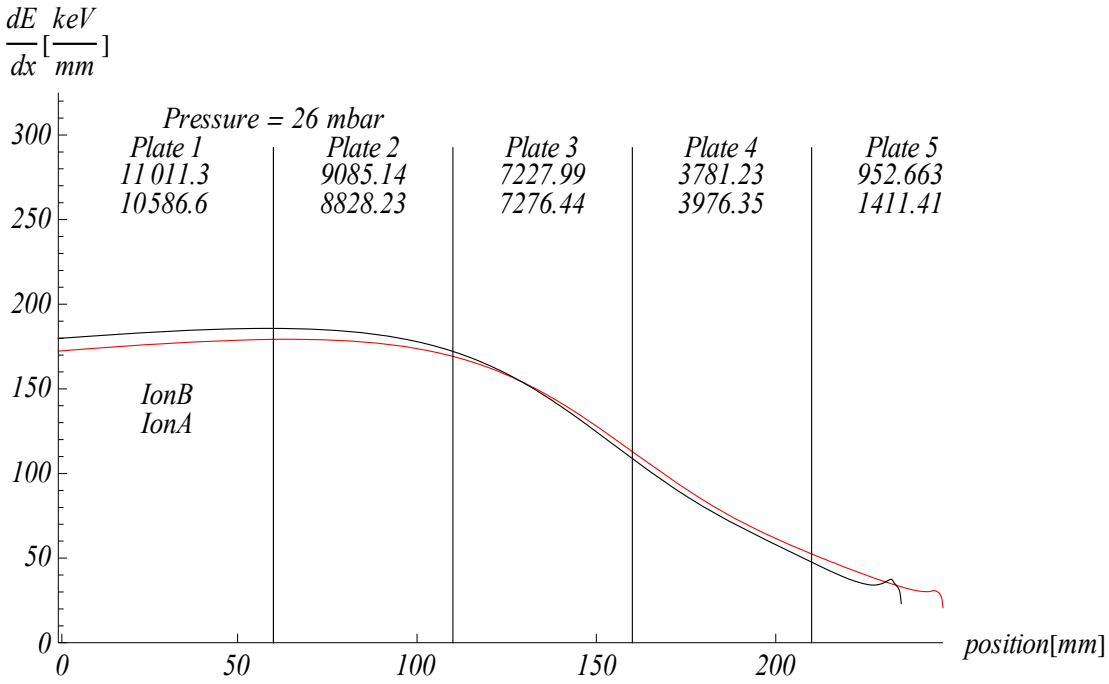

Fig. 4.5 Stopping power curve showing the dependence of the energy loss and penetration depth of particles in a propane filled detector on the detector gas pressure, here 26 mbar. The red curve represents Ion A = ^{36}S, the black curve represents Ion B = ^{36}Cl. The numbers denote the energy losses in keV for the ions.

Before starting the actual measurements, all of the samples were bombarded with the Cs-sputter beam to clean the surfaces from impurities that had settled onto them while the sample was pressed and loaded. During the measurements the ion source had to be run at a fairly low

temperature for the caesium oven and the ionizer, for the shape of the Cl^--ion beam to be best controlled.

The data acquisition and analysis was performed with the computer program UMAC (de Laat et al., 1992) that visualized E and ΔE signals as 1D and 2D spectra. The reduction of the ^{36}S background ($^{36}Cl/^{36}S$ particle separation) could be improved with the software by setting windows around the ^{36}Cl-related peaks in the pulse spectra of each of the five anode plates and the cathode. Certain restrictions could be applied to the spectra, for example allowing only events to be counted as ^{36}Cl ions when their ΔE signal fell in the specified windows for the different plates simultaneously. The difficulty with setting the software gates fairly narrowly was that it made the ^{36}Cl-^{36}S separation very sensitive to small changes in the ΔE peak positions as they occurred when high ^{36}S counting rates or ^{35}Cl and ^{37}Cl leak-in caused short-term instabilities of the detector. The ^{36}S background was determined as "$^{36}Cl/^{35}Cl$" ratio from measurement of the ^{36}Cl-free blanks. Since the blanks do not contain the isotope of interest, the signals found in the ^{36}Cl windows of the pulse spectra were to be considered to be ^{36}S-induced background. The $^{36}S/^{35}Cl$ ratio was found to be of the range of $5*10^{-15}$-$2*10^{-14}$.

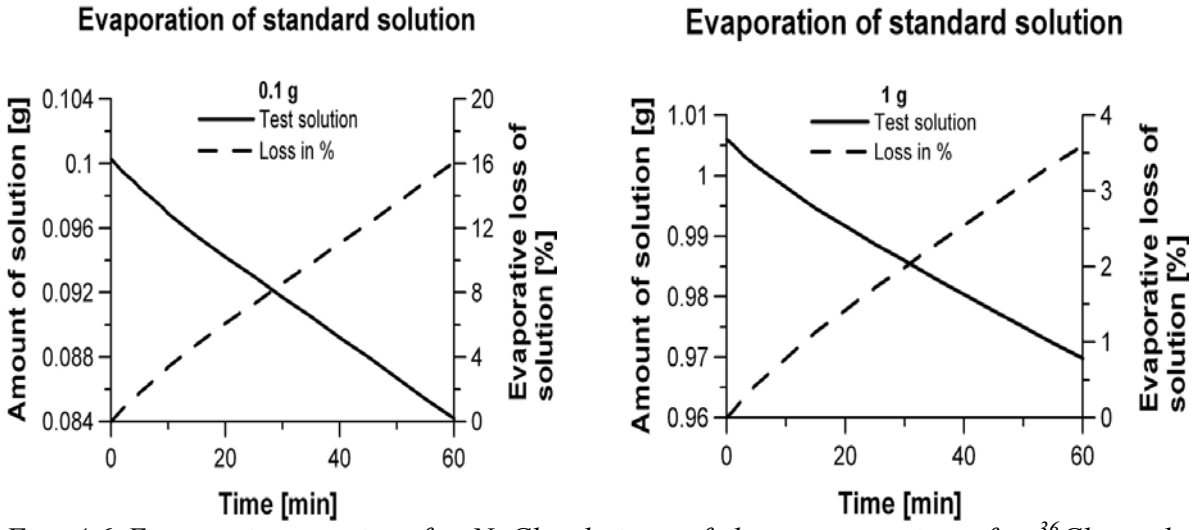

Fig. 4.6 Evaporation vs. time for NaCl solutions of the concentration of a ^{36}Cl-standard solution. Note the different scales used for the 0.1 g and the 1 g experiment. The error introduced to dilution procedures due to the evaporation-based mass loss and concentration shift in the solution is the higher the smaller the starting amount for the dilution is.

The in-house standards of ^{36}Cl were prepared starting from a NaCl solution of an original NIST standard (SRM 4943) with a concentration of 0.2 g (NaCl)/l and a calibrated activity of $(1.095\pm0.0005)*10^4$ Bq/g. Based on the half-life of 301 ka for ^{36}Cl (Faure & Mensing, 2005) a concentration of ^{36}Cl of $1.50*10^{17}$ atoms.g^{-1} was obtained. Using a Merck CertiPur chloride

standard solution a series of dilution steps was performed to produce the secondary AMS standards with certain $^{36}Cl/^{35}Cl$ ratios.

The dilution of the standard solutions has to be done very precisely. The errors introduced depend on the uncertainty in the concentration of the solutions and on the uncertainty in the mass of the portions of the combined solutions. Even a small uncertainty in the absolute mass of the portion of the standard solution that is diluted carries a relatively large contribution to the error because the amount of the standard solution used in dilutions is typically very small. The blank solution, which is added in larger amounts, is not as critical. The dilution of a standard solution into a series of standards of different strength requires the exact knowledge of the concentrations of both the standard solution and of the diluting solution. Any change in the concentration of the solutions e.g. from evaporation introduces an uncertainty in the procedure. This propagates through the whole dilution process. This is especially critical for the component, which is used in only a small quantity, i.e. the standard solution. Fig. 4.6 illustrates the results of evaporation experiments performed with different amounts of salt solutions of identical concentration, which was the same concentration as the standard solutions had. For one experiment 0.1 gram of salt solution was inserted into a small tared beaker on a precise balance (balance error 0.00005g). For the time of an hour every minute and from the tenth minute every five minutes the mass of the liquid in the beaker was recorded. For the second experiment the same procedure was repeated starting with 1 gram of salt solution. Not surprisingly, it is seen that the mass loss from evaporation of the solution causes significantly higher relative deviations from the original mass for the smaller volume and that the error for the dilution procedure increases with increasing length of time of evaporation. This enforces two conclusions: firstly it is necessary to start the dilution for standard preparation with quantities that are not too small, and secondly, the procedure has to be performed both very carefully and very rapidly. Furthermore, parent solutions of standards that have been stored for a few years should not be used as primary standards anymore since they tend to have changed their concentrations because water is lost from the bottle. Standards made from such solutions have to be re-calibrated with proper standards.

A series of spike blanks, which was made from the ^{35}Cl enriched spike diluted with known amounts of regular CertiPur NaCl solution, were measured to control possible memory effects in the ion source that would disturb the determination of $^{35}Cl/^{37}Cl$ ratios of the spiked samples due to the regular blanks in the batch being higher in ^{37}Cl. The tests demonstrated that there were no memory effects that could affect the quality of the measurements.

Systematic errors can already be introduced during the sample preparation. Some of those such as (cross) contamination can be avoided by working with carefully cleaned laboratory equipment and chemicals of high purity. Sample processing following a strict protocol guarantees reproducibility of the target preparation. Other influences such as chemical mass fractionation or the sputter behavior of the sample based on its chemical composition and structure (grain size, surface condition) are not so easily controlled (Suter, 1990). Furthermore in spiked samples the calibration of the spike solution, which for example can be affected by weighing and diluting errors or by isotopic fractionation during the analysis of the spike, determines the accuracy of the results (Bowen, 1988).

In measurements made relative to standards, most of the measuring errors cancel out. Thus, the final uncertainty of the measurement is determined by the variations of the systematic errors such as time-dependent variations coming from voltage drift in the tandem, variations in the vacuum conditions and the ion source parameters (e.g. temperature, Cs-current, sputter yield), which are recognizable by monitoring the long- and short-term stability of the system. Furthermore changes in the samples themselves by abrasion of the sample material are a source of non-canceling systematic errors (Suter, 1990). Slight isotopic fractionation due to residual magnetic fields existing along the beam path or beam deviation associated with the switching processes can be decreased radically by high and stable transmission. Large counting rates are required for low statistical errors and high precision. However, at too high counting rates systematic errors in the detector may arise, such as pulse pile-up and increased dead time, which can cause counting losses. A high background can obscure the peaks of interest and affect the resolution (Suter, 1990).

To keep the probability of undetected errors as low as possible sample preparations and measurements were performed repeatedly. A number of samples were taken from each flow and from the most suitable of them several different AgCl samples for the accelerator were prepared. From these AgCl samples two or three AMS samples were measured, either on the same run, or in different batches. In this way the reproducibility of the chemical preparation and of the measurement performance could be checked.

4.4 Data analysis

In the AMS measurements the ratios of the chlorine isotopes were determined rather than their individual concentrations. The normalized isotope ratio of a sample (R_s) was calculated from the background-corrected isotope ratios of the sample (M_s) and of the standard (M_{std}), and the absolute isotope ratio of the standard (R_{std}).

$$R_s = \left(\frac{M_s}{M_{std}} \right) R_{std} \tag{4.1}$$

The overall chlorine concentration in the basalt samples was very low in terms of preparation yield, so that only unmanageable amounts of sample material could produce sufficient AgCl for an AMS-sample. To overcome this problem and also to be able to determine the total amount of chlorine present in the sample, the method of isotope dilution was applied. A certain quantity of ^{35}Cl enriched NaCl-spike solution (NIST, Oak Ridge, 99.900% ^{35}Cl) of known concentration was added to a known amount of rock sample. Thus, the AMS sample finally contained a mixture of a known amount of spike of known isotopic composition and an unknown amount of natural chlorine of natural (known) stable isotope composition together with the ^{36}Cl. During the measurements, the ratios between ^{37}Cl and ^{35}Cl (R^{Cl}_{AMS}) and between ^{36}Cl and ^{35}Cl (R^{36}_{AMS}) were acquired. Both ratios had to be determined extremely carefully because the further calculations of age or production rate were based on them.

Based on R^{Cl}_{AMS} the quantity of the total chlorine occurring naturally in the rock can be calculated (after Faure & Mensing, 2005):

$$R^{Cl}_{AMS} = \frac{m_{Cl,nat} \cdot f^{37}_{nat} + m_{Cl,spike} \cdot f^{37}_{spike}}{m_{Cl,nat} \cdot f^{35}_{nat} + m_{Cl,spike} \cdot f^{35}_{spike}} \tag{4.2}$$

from which follows:

$$m_{Cl,nat} = \frac{M_{m,nat}}{M_{m,spike}} \left(\frac{m_{Cl,spike} \cdot \left(f^{37}_{spike} - R^{Cl}_{AMS} \cdot f^{35}_{spike} \right)}{R^{Cl}_{AMS} \cdot f^{35}_{nat} - f^{37}_{nat}} \right) \tag{4.3}$$

$m_{Cl,nat}$ = mass of natural chlorine in the sample (g)

$M_{m,\,nat}$ = molar mass of natural chlorine (35.4527 g.mole^{-1}, CRC Handbook of Chemistry & Physics Online; 2009; http://www.hbcpnetbase.com/)

$M_{m,spike}$ = molar mass of the chlorine spike (= (f^{35}_{spike}*34.969 + f^{37}_{spike}*36.966) g.mole^{-1}; molar masses from CRC Handbook of Chemistry & Physics Online)

$m_{Cl,spike}$ = mass of chlorine in the spike added during the preparation (g)

f^{35}_{spike} = fraction of ^{35}Cl in the spike

f^{37}_{spike} = fraction of ^{37}Cl in the spike

f^{35}_{nat} = fraction of ^{35}Cl in the natural chlorine

f^{37}_{nat} = fraction of ^{37}Cl in the natural chlorine

R^{Cl}_{AMS} = ratio of $^{37}Cl/^{35}Cl$ as measured with AMS

The molar masses of the natural chlorine in the sample and the spike are not equal due to their different isotopic composition. Dividing the result by the mass of the original rock sample yields the concentration of total chlorine in the rock.

To reduce the number of variables that carry uncertainties $f^{37}_{nat,spike}$ is expressed as $f^{37}_{nat,spike} = 1 - f^{35}_{nat,spike}$, so that

$$m_{Cl,nat} = \frac{M_{m,nat}}{M_{m,spike}} \left(\frac{m_{Cl,spike} \cdot \left((1 - f^{35}_{spike}) - R^{Cl}_{AMS} \cdot f^{35}_{spike} \right)}{R^{Cl}_{AMS} \cdot f^{35}_{nat} - (1 - f^{35}_{nat})} \right) \tag{4.4}$$

However, the effect of the uncertainties of f_{nat}^{35} and f_{spike}^{35} and of the molar masses of the natural and spiked chlorine are negligibly small (order of 10^{-6} – 10^{-7} grams). The mass of the spike added to the sample could introduce some errors and thus has to be determined very carefully. This is controllable by thorough work. The main contribution to the total uncertainty is the $^{37}Cl/^{35}Cl$ ratio measured by AMS:

$$\Delta m_{Cl,nat} = \frac{\partial m_{Cl,spike}}{\partial R^{Cl}_{AMS}} \cdot \Delta R^{Cl}_{AMS} \tag{4.5}$$

The natural ratio of $^{37}Cl/^{35}Cl$ is 0.320. Spiking with a spike enriched in ^{35}Cl, shifts the ratio towards smaller values as more spike is added and as less natural chlorine is present in the sample. For AMS measurements with a certain measurement error it is necessary to shift the effective $^{37}Cl/^{35}Cl$ ratio sufficiently far away from the natural ratio to reduce the influence of the measurement error on the concentrations of natural chlorine and ^{36}Cl in the sample derived from R^{Cl}_{AMS} (Fig. 4.7). The reason that the increase of spike mass decreases the error is seen from the formula for Δm (eqn. 4.5a). The numerator of the second term of the right hand side depends only on the isotope ratios f_{nat} and f_{spike}, which are constant for the natural and given spike ratios, whereas the denominator depends on R^{Cl}_{AMS}. Thus the whole fraction decreases, and even though $m_{Cl,spike}$ increases the total decrease of the whole right hand term continues.

$$\Delta m_{Cl,nat} = \frac{M_{m,nat}}{M_{m,spike}} m_{Cl,spike} \cdot \frac{-f_{spike}^{35}\left(-1+f_{nat}^{35}+R_{AMS}^{Cl}\cdot f_{nat}^{35}\right)-f_{nat}^{35}\left(1-f_{spike}^{35}-R_{AMS}^{Cl}\cdot f_{spike}^{35}\right)}{\left(R_{AMS}^{Cl}\cdot f_{nat}^{35}+f_{nat}^{35}-1\right)^2}\cdot \Delta R_{AMS}^{Cl} \tag{4.5a}$$

$$= \frac{M_{m,nat}}{M_{m,spike}} m_{Cl,spike} \cdot \frac{f_{nat}^{35}+f_{spike}^{35}}{\left(R_{AMS}^{Cl}\cdot f_{nat}^{35}+f_{nat}^{35}-1\right)^2}\cdot \Delta R_{AMS}^{Cl}$$

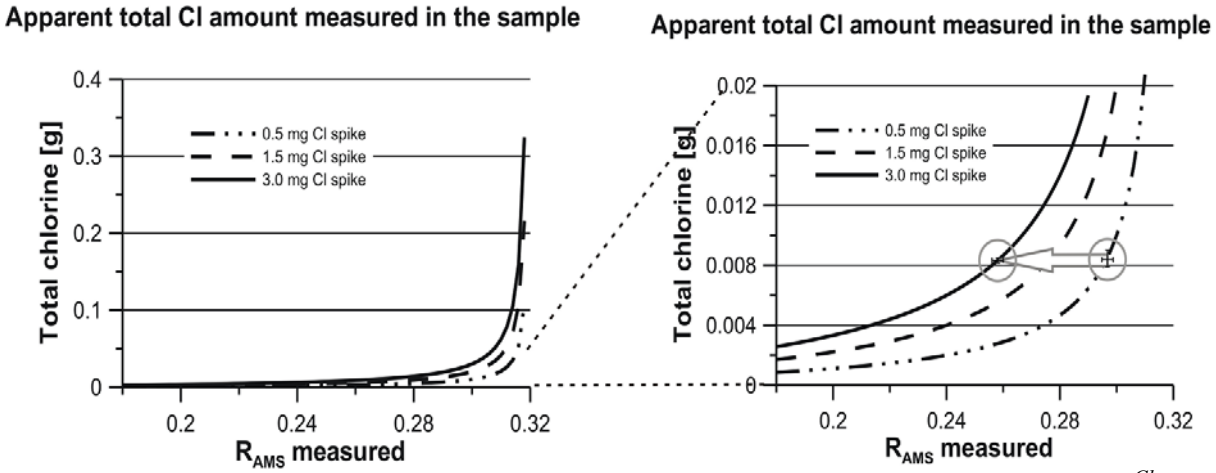

Fig. 4.7 The amount of total chlorine in the sample is obtained from the measured R^{Cl}_{AMS}.. The amount of spike added determines the measured shift in the R^{Cl}_{AMS} depending on the amount of natural chlorine in the sample. With more spike added a shift further to the lower values (arrow) is produced, and hence into a range where the calculated amount of chlorine is less sensitive for measurement errors of R^{Cl}_{AMS}. (solid line, higher amount of spike added).

A numeric example may illustrate this calculation. For the flow CA a sample has been measured, which had been prepared with 1.513 mg of spike. The measured $^{37}Cl/^{35}Cl$ ratio was 0.3170 with an error of 0.0010. The resulting uncertainty in the total mass of chlorine in the samples was then 45 %. The same method of preparation was performed for the same rock sample but with an increased amount of spike, which now was 3.583 mg. The measured $^{37}Cl/^{35}Cl$ ratio was 0.2418 with an error of 0.0014. The resulting uncertainty in the total mass of chlorine in the samples was now 3 %.

Since the R^{Cl}_{AMS} of the sample is altered by the spike, it is necessary to correct first the measured R^{36}_{AMS} value, which is the *measured* ratio $^{36}Cl/^{35}Cl$, to obtain the undisturbed (natural) ratio $^{36}Cl/^{35}Cl$ before the ^{36}Cl content is calculated:

$$R^{36}_{AMS} = \frac{N_{^{36}Cl}}{N_{^{35}Cl,nat} + N_{^{35}Cl,spike}} \tag{4.6}$$

$N_{35Cl,nat}$ and $N_{35Cl,spike}$ are the numbers of atoms of natural ^{35}Cl and of ^{35}Cl of the spike, and N_{36Cl} is the number atoms of ^{36}Cl. From that follows with some re-arrangement:

$$\frac{R^{36}_{AMS} \cdot (N_{^{35}Cl,nat} + N_{^{35}Cl,spike})}{N_{^{35}Cl,nat}} = \frac{N_{^{36}Cl,nat}}{N_{^{35}Cl,nat}} = {}^{36}Cl / {}^{35}Cl \quad , \tag{4.7}$$

which is

$${}^{36}Cl / {}^{35}Cl = R^{36}_{AMS} \cdot \left(1 + \frac{(f^{35}_{spike} m_{Cl,spike}) / M_{m,spike}}{(f^{35}_{nat} m_{Cl,nat}) / M_{m,nat}} \right) \tag{4.8}$$

$^{36}Cl/^{35}Cl$ is the natural $^{36}Cl/^{35}Cl$ ratio in the sample. If the sample is measured without spike, R^{36}_{AMS} equals $^{36}Cl/^{35}Cl$, and the correction above is not necessary. From the $^{36}Cl/^{35}Cl$ and the total mass of chlorine the amount of ^{36}Cl in the sample can be derived:

$$conc\,{}^{36}Cl = \frac{{}^{36}Cl / {}^{35}Cl \cdot m_{Cl,nat} \cdot f^{35}_{nat} \cdot N_A}{M_{m,nat} \cdot m_{sample}} \quad \text{(atoms.g (rock)}^{-1}\text{)} \tag{4.9}$$

The calculation is in principle performed in the same way when the ratio $^{36}Cl/^{37}Cl$ instead of $^{36}Cl/^{35}Cl$ has been measured with the AMS.

The errors of f^{35}_{nat} and f^{35}_{spike}, the molar masses of natural and spiked chlorine, and of the total mass of the prepared rock sample do not contribute significantly to the total error of the ^{36}Cl content that is determined (contributions in the order of 10^{-2} – 10^{1} atoms.g(rock)$^{-1}$). In contrast, the uncertainties in R^{36}_{AMS} and $m_{Cl,nat}$ and $m_{Cl,spike}$ are significant sources of error (in the order of 10^{3} – 10^{5} atoms.g(rock)$^{-1}$):

$$\Delta conc\,{}^{36}Cl = \sqrt{\left[\left(\frac{\partial conc\,{}^{36}Cl}{\partial R^{36}_{AMS}} \cdot \Delta R^{36}_{AMS} \right)^2 + \left(\frac{\partial conc\,{}^{36}Cl}{\partial m_{Cl,nat}} \cdot \Delta m_{Cl,nat} \right)^2 + \left(\frac{\partial conc\,{}^{36}Cl}{\partial m_{Cl,spike}} \cdot \Delta m_{Cl,spike} \right)^2 \right]}. \tag{4.10}$$

For the calculation of the production rate the simplest approach is tried first: No inherited ^{36}Cl is assumed because the rocks were purely volcanic. The concentration of the neutron catchers lithium, gadolinium, and boron are very low according to the ICP-MS data, so that they do not influence significantly the proportion of the neutrons available for the production of ^{36}Cl from ^{35}Cl. The well preserved surfaces of the samples indicate very little erosion. Therefore the general formula to derive the production rate is:

$$P = \frac{conc({}^{36}Cl) \cdot \lambda}{SF \cdot (1 - e^{-\lambda t})} \quad \text{(atoms.g(rock)}^{-1}\text{yr}^{-1}\text{)} \tag{4.11}$$

P is the production rate, SF stands for the scaling factors for a variety of influences discussed in chapter 2, λ is the decay constant of ^{36}Cl ($2.302*10^{-6}$ yr^{-1}), and t is the exposure age ascertained otherwise, for example by $^{40}Ar/^{39}Ar$ measurements.

The influence of the uncertainty of the age (t) on the determination of the production rate strongly varies for the given samples depending on the results of the $^{40}Ar/^{39}Ar$ dating, which is very accurate for older samples. The younger the samples are the higher the uncertainty in the age determination is for this method. The contribution lies between 0.5 and 2 atoms.g(rock)$^{-1}$yr^{-1}. Nevertheless, the main contributor (2-10 atoms.g(rock)$^{-1}$yr^{-1}) for the error of the production rate is the concentration of ^{36}Cl in the sample:

$$\Delta P = \frac{\partial P}{\partial conc^{36}Cl} \Delta conc^{36}Cl \tag{4.12}$$

Table 4.3 gives an overview over the errors and uncertainties that have the highest impact on the uncertainty of the final result.

The production rates have to be established as accurately as possible, in order to significantly decrease the error in the determination of the exposure age.

	Uncertain factor	**Total contribution to the production rate**
SF (latitude, elevation)	Magnetic dipole momentum	5->10%
	Fraction of muons	2-3%
	Fitting coefficients	2-3%
AMS Measurement	R^{Cl}_{AMS}	2-10%
	R^{36}_{AMS}	2-10%
	$m_{Cl,spike}$	2-10%
Age determination	Ar-measurement	Up to 40%

Table 4.3 Overview over the most important errors in the determination of the production rate (SLHL).

5 Results

The detailed analysis results for all samples are listed in Appendix D. Because of the wide scatter of the samples' production rates the data where examined in order to judge their reliability. Some flows like CG or MQ include a few values that are inconsistently high compared with the other values from the respective flows (e.g. CG 05/06-1-1), which cannot be explained comprehensively. Values clearly above production rates of 18 at.g(rock)$^{-1}$.yr^{-1} were generally regarded to be too high because they would suggest unreasonably high production rates for the individual production mechanisms.

sample	Ratio $^{37/35}$Cl	Ratio ^{36}Cl/^{35}Cl [10^{-15}]	conc Cl nat [ppm]	[^{36}Cl] in rock 10^4 at.g^{-1}	Prod. rate (SLHL) (at.g(rock)$^{-1}$yr^{-1})
CA 05/01-3*	0.276 ± 0.001	245 ± 21	463 ± 22	170 ± 16	16.4 ± 1.9
CA 05/03-2	0.249 ± 0.001	291 ± 16	281 ± 10	135 ± 8	12.6 ± 1.2
CA 05/03-2	0.268 ± 0.001	146 ± 28	408 ± 17	92 ± 18	8.5 ± 1.8
CA 05/05-3-1	0.241 ± 0.002	204 ± 9	273 ± 9	96 ± 5	9.4 ± 0.8
CA 05/05-3-2	0.242 ± 0.001	219 ± 8	278 ± 9	104 ± 5	10.2 ± 0.8
average			**288 ± 21**	**104 ± 7**	**10.2 ± 0.7**
CG 05/01-1	0.255 ± 0.001	133 ± 16	294 ± 11	63 ± 8	14.4 ± 5.9
CG 05/01-3	0.248 ± 0.001	125 ± 13	269 ± 9	56 ± 6	12.7 ± 5.1
CG 05/04f-1*	0.213 ± 0.001	386 ± 33	151 ± 4	113 ± 10	27.9 ± 11.1
CG 05/04w-1*	0.259 ± 0.001	281 ± 24	303 ± 12	135 ± 12	33.6 ± 13.4
CG 05/05-5	0.222 ± 0.001	165 ± 14	175 ± 5	54 ± 5	12.6 ± 5.0
CG 05/06-1-1*	0.246 ± 0.001	187 ± 9	308 ± 10	96 ± 5	22.6 ± 8.9
CG 05/06-1-2*	0.246 ± 0.002	186 ± 8	308 ± 11	96 ± 5	22.5 ± 8.8
average			**211 ± 35**	**56 ± 3**	**13.1 ± 0.5**
MA 05/01-1	0.259 ± 0.001	271 ± 14	358 ± 13	154 ± 9	8.3 ± 0.8
MA 05/01-1	0.261 ± 0.001	300 ± 9	370 ± 14	175 ± 8	9.5 ± 0.9
MA 05/02 (60)-2	0.270 ± 0.002	193 ± 18	391 ± 17	115 ± 12	6.3 ± 0.8
MA 05/02-2*	0.257 ± 0.001	66 ± 8	352 ± 13	37 ± 5	2.0 ± 0.3
MA 05/02-3	0.270 ± 0.002	160 ± 20	362 ± 16	88 ± 11	4.8 ± 0.7
MA 05/03-3	0.273 ± 0.001	176 ± 18	365 ± 17	97 ± 10	5.3 ± 0.7
average			**364 ± 5**	**136 ± 17**	**6.6 ± 0.9**
MC 05/01-2-1	0.260 ± 0.001	148 ± 7	322 ± 13	76 ± 4	7.6 ± 0.9
MC 05/01-2-2	0.259 ± 0.002	152 ± 10	315 ± 12	76 ± 6	7.6 ± 0.9
MC 05/01-3*	0.255 ± 0.001	335 ± 19	295 ± 11	160 ± 10	16.0 ± 1.9
MC 05/02-3	0.226 ± 0.001	172 ± 9	183 ± 5	57 ± 3	5.6 ± 0.6

MC 05/05-2	0.253 ± 0.001	133 ± 12	280 ± 10	61 ± 6	6.0 ± 0.8
average			**232 ± 35**	**65 ± 5**	**6.5 ± 0.5**
MM 05/01-3	0.253 ± 0.001	284 ± 11	276 ± 10	128 ± 6	6.4 ± 0.5
MM 05/02-1*	0.257 ± 0.001	549 ± 34	368 ± 13	323 ± 22	16.5 ± 1.6
MM 05/02-2	0.255 ± 0.001	233 ± 19	284 ± 10	107 ± 9	5.5 ± 0.6
MM 05/04-2	0.223 ± 0.001	362 ± 17	203 ± 6	136 ± 7	7.1 ± 0.6
MM 05/04f-1	0.241 ± 0.001	446 ± 35	234 ± 8	179 ± 15	9.3 ± 1.0
MM 05/04w-1	0.237 ± 0.001	459 ± 24	213 ± 7	170 ± 10	8.9 ± 0.8
average			**228 ± 15**	**136 ± 10**	**7.0 ± 0.6**
MN 05/03-2	0.240 ± 0.001	730 ± 25	202 ± 7	253 ± 11	11.6 ± 0.9
MN 05/04-3	0.253 ± 0.001	730 ± 19	264 ± 10	314 ± 12	15.6 ± 1.2
MN 05/05-2-1*	0.240 ± 0.001	797 ± 18	262 ± 8	358 ± 12	18.2 ± 1.3
MN 05/05-2-2*	0.243 ± 0.002	797 ± 18	273 ± 9	370 ± 12	18.8 ± 1.4
MN 05/07-1	0.236 ± 0.001	767 ± 28	249 ± 7	333 ± 14	15.8 ± 1.2
average			**231 ± 19**	**293 ± 25**	**13.7 ± 1.5**
MQ 05/03-2-1	0.197 ± 0.001	544 ± 14	168 ± 4	192 ± 6	16.9 ± 2.5
MQ 05/03-2-2	0.193 ± 0.001	548 ± 15	161 ± 4	188 ± 6	16.6 ± 2.4
MQ 05/03-3	0.213 ± 0.001	687 ± 28	151 ± 4	200 ± 9	17.7 ± 2.6
MQ 05/07-1*	0.235 ± 0.001	571 ± 22	258 ± 8	258 ± 12	21.9 ± 3.3
MQ 05/07-2*	0.245 ± 0.001	704 ± 16	251 ± 8	298 ± 10	25.2 ± 3.7
average			**160 ± 5**	**191 ± 3**	**17.0 ± 0.3**
MR 05/01-2-1	0.249 ± 0.002	545 ± 14	245 ± 9	221 ± 8	17.2 ± 1.6
MR 05/01-2-2	0.245 ± 0.001	555 ± 16	228 ± 8	213 ± 8	16.6 ± 1.6
MR 05/01-3*	0.244 ± 0.001	758 ± 28	231 ± 8	296 ± 13	23.0 ± 2.2
MR 05/01-3*	0.244 ± 0.001	753 ± 15	231 ± 8	294 ± 10	22.8 ± 2.1
MR 05/02-3*	0.239 ± 0.001	724 ± 34	213 ± 7	266 ± 14	21.1 ± 2.1
average			**236 ± 8**	**217 ± 4**	**16.9 ± 0.3**
VF 05/04-3	0.211 ± 0.001	425 ± 45	134 ± 4	111 ± 12	8.0 ± 1.0
VF 05/04-3	0.202 ± 0.001	473 ± 38	119 ± 3	115 ± 9	8.3 ± 0.9
VF 05/04-60-1*	0.202 ± 0.001	734 ± 32	125 ± 3	187 ± 9	13.4 ± 1.1
VF 05/04-60-1*	0.204 ± 0.001	773 ± 43	128 ± 3	200 ± 12	14.3 ± 1.3
VF 05/06-2	0.180 ± 0.001	551 ± 37	90 ± 2	113 ± 8	7.9 ± 0.8
average			**106 ± 13**	**113 ± 1**	**8.1 ± 0.1**

Table 5.1 The "filtered" results from all AMS analyses from Appendix D. The results given in grey and marked with (*) are considered to be unreliable and excluded from the weighted mean values and any further calculation (see text).

Zreda et al. (1991) reported about 15 at.g(rock)$^{-1}$.yr^{-1} for basalt. The presence of remainder of meteoric ^{36}Cl or unrecognised contamination may contribute to these values. These outliers were rejected from further calculations since they were considered to be unreliable. These "filtered" results of the AMS measurements are given in Table 5.1 (the rejected values have been marked in grey) together with weighted mean values for each flow. Also values that were suspiciously low (MA 05/02-2) were not accepted for calculation for consistency reasons. The AMS-measurements were fairly stable with reasonably small errors. Fig. 5.1 shows the results for the nine flows versus age.

The total chlorine concentration (Fig. 5.1a) varies within each flow, and between the flows from 110 to 370 ppm with a mean value of 230 ppm. The deviations of the concentrations of total chlorine among the flows are interpreted to be mainly natural scatter. Slight variations in the chemical composition of the basalts from the different flows given by the XRF and ICP measurements of the major, minor and trace elements accompany the variations in the chlorine concentrations and thus also indicate that the chlorine concentration shifts are natural as will be discussed in chapter 6. There is no evidence for any age dependence of the scatter as the intensity of the internal scatter of the flow is strongest for CG, MC, CA, and MM and considerably less for the other flows. The ^{36}Cl concentrations (Fig. 5.1b) increase with the age of the flows as expected but four flows (MC, VF, MA, MM) deviate from this general trend. The scatter of the ^{36}Cl content does not seem to be related to the scatter of the total chlorine content within each of the flows. The reason for the scatter in the total chlorine and ^{36}Cl contents within each flow is not fully understood and will be discussed in chapter 6.

The scatter does not appear to be a systematic error connected with a certain time of the measurements, which would suggest an instability of the measurement. Also there does not seem to be a systematic deviation for samples that have been prepared together, which would indicate irregularities in the preparation. Even though the chemical preparation procedures always suffer from some chlorine loss, there is no correlation between the loss of material and the degree of scatter. Furthermore, for some samples the measurement results are reproduced very well when a second AMS sample of the same preparation is measured in a later batch (e.g. MR 05/01-3, see Appendix D), while others show less consistency (e.g.CA 05/03-2) despite the identical treatment. Measurements of two samples that are made from the same AgCl bead and are run in the same batch always reproduce the results very well (e.g. MN 05/05-2-1 and MN 05/05-2-2). AgCl-samples prepared successively from the same rock sample do not always reproduce the measurements equally. Some do very well (e.g. CG 05/01-1, CG 05/01-3), while others scatter more (e.g. MM 05/02-1, MM 05/02-2).

Fig. 5.1c shows the production rate of ^{36}Cl in the rock (^{36}P(rock)) for each sample. All flows show some scatter as is to be expected from the ^{36}Cl data. Flow CG shows the largest scatter, but this is the youngest flow, which has largest uncertainties both in the low ^{36}Cl concentration and in the $^{40}Ar/^{39}Ar$ age (see Table 5.1). Values that are marked in grey in table 5.1 are represented as open dots in Fig. 5.1c.

From the remaining data for each flow the weighted mean production rates are listed in table 5.2 and also shown in Fig. 5.1d. The resulting production rates range between 7 and 19 at.g(rock)$^{-1}$.yr^{-1}. The total weighted mean of the production rates of all of the flows is 8.1 ± 0.9 at.g(rock)$^{-1}$.yr^{-1} (dashed line in Fig 5.1d). This includes values that are suspiciously low and others that are very high. These data have to be analysed carefully because the samples very likely have been affected by processes that influence the concentration of ^{36}Cl independently of production and decay. Excluding these flows from the mean ^{36}P(rock) results in 11.6 ± 2.8 atoms.g(rock)$^{-1}$.yr^{-1} (solid line in Fig. 5.1d). Considering that basaltic rocks from different sites can differ significantly in their composition, this production rate is in fairly good agreement with values published elsewhere (15 atoms.g(rock)$^{-1}$.yr^{-1}, Zreda et al., 1991; Phillips et al., 1996).

The expected total amount of ^{36}Cl and the relative theoretical contributions of the individual production paths to the total production rate with respect to the rock in per cent have been calculated based on the chemical compositions of the rocks, the $^{40}Ar/^{39}Ar$ ages and the production rate data for the different mechanisms (Table 2.3). Any other external influence on the production rate of ^{36}Cl such as erosion is neglected. The production of ^{36}Cl from ^{35}Cl is calculated from literature values for the thermal neutron activation in the rock following the method of Phillips et al. (1986):

$$P_{Cl,n} = \Phi_n \frac{N_{35}\sigma_{35}}{\sum_{n=i} N_i \sigma_i} \quad [\text{at.g}^{-1}.\text{yr}^{-1}] \qquad 5.1$$

where Φ_n is the thermal neutron flux in rock of (3.53 ± 0.07) .10^{5}n.kg^{-1}.yr^{-1} (Swanson, 1996)), σ_{35} is the ^{36}Cl activation cross section (barn) for thermal neutrons in ^{35}Cl, σ_i the absorption cross section (barn) for thermal neutrons of element i, and N_{35} and N_i are the numbers of atoms of ^{35}Cl and of element i (atoms.g^{-1} or mole.g^{-1}) as calculated from ICP-MS and AMS measurements, respectively.

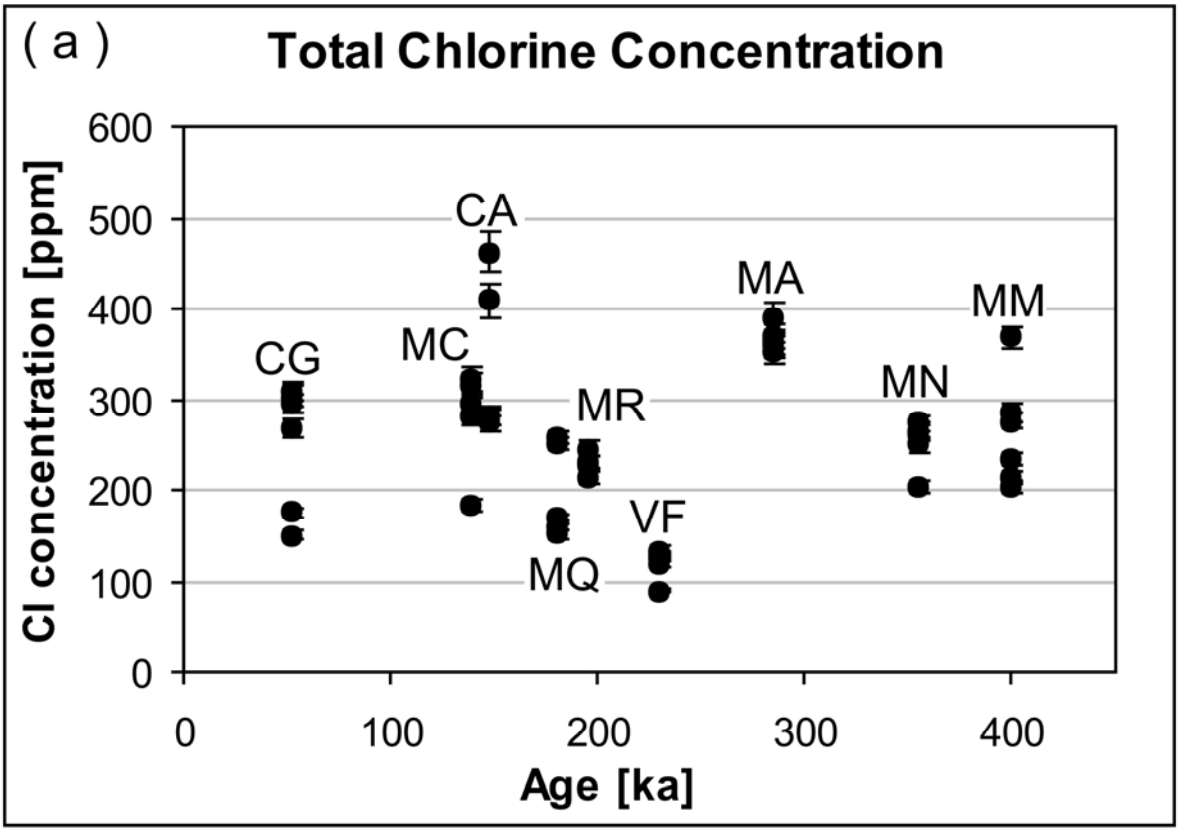
(a)
Total Chlorine Concentration
Cl concentration [ppm]
600
500
400
300
200
100
0
0
100
200
300
400
Age [ka]
CG
MC
CA
MQ
MR
VF
MA
MN
MM

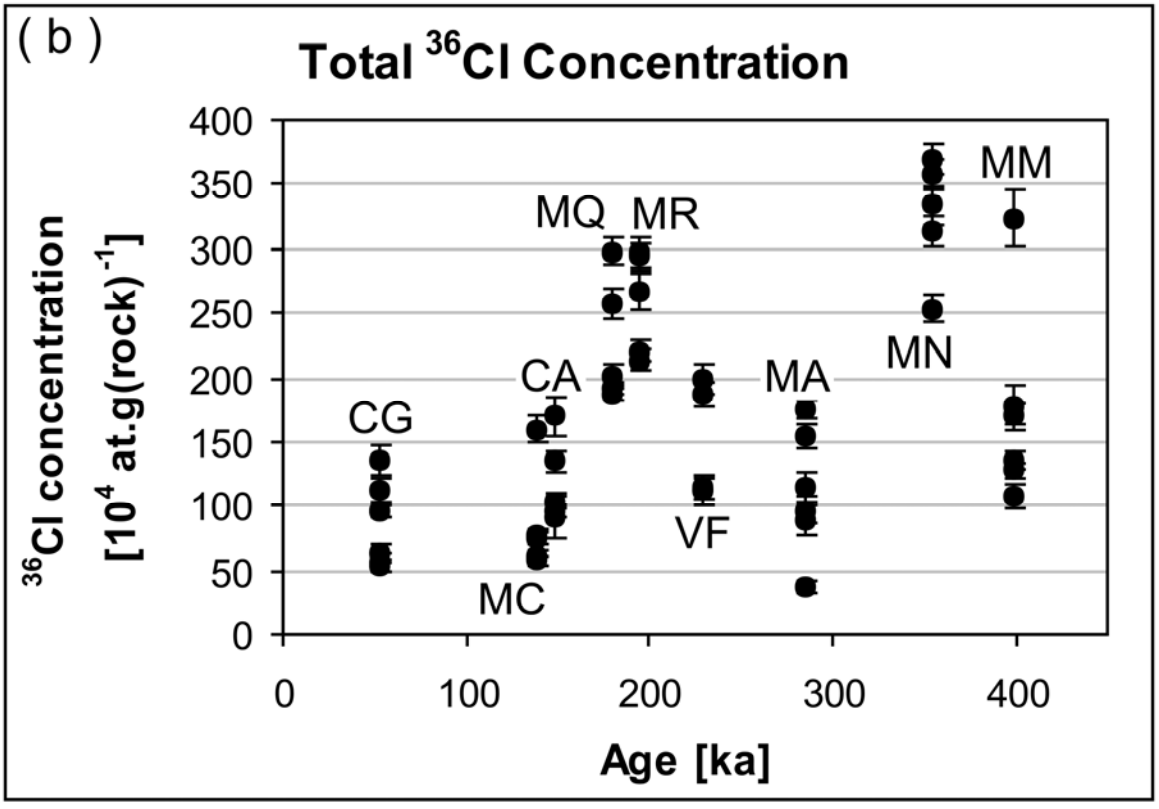
(b)
Total ^{36}Cl Concentration
^{36}Cl concentration [10^4 at.g(rock)$^{-1}$]
400
350
300
250
200
150
100
50
0
0
100
200
300
400
Age [ka]
CG
MC
CA
MQ
MR
VF
MA
MN
MM

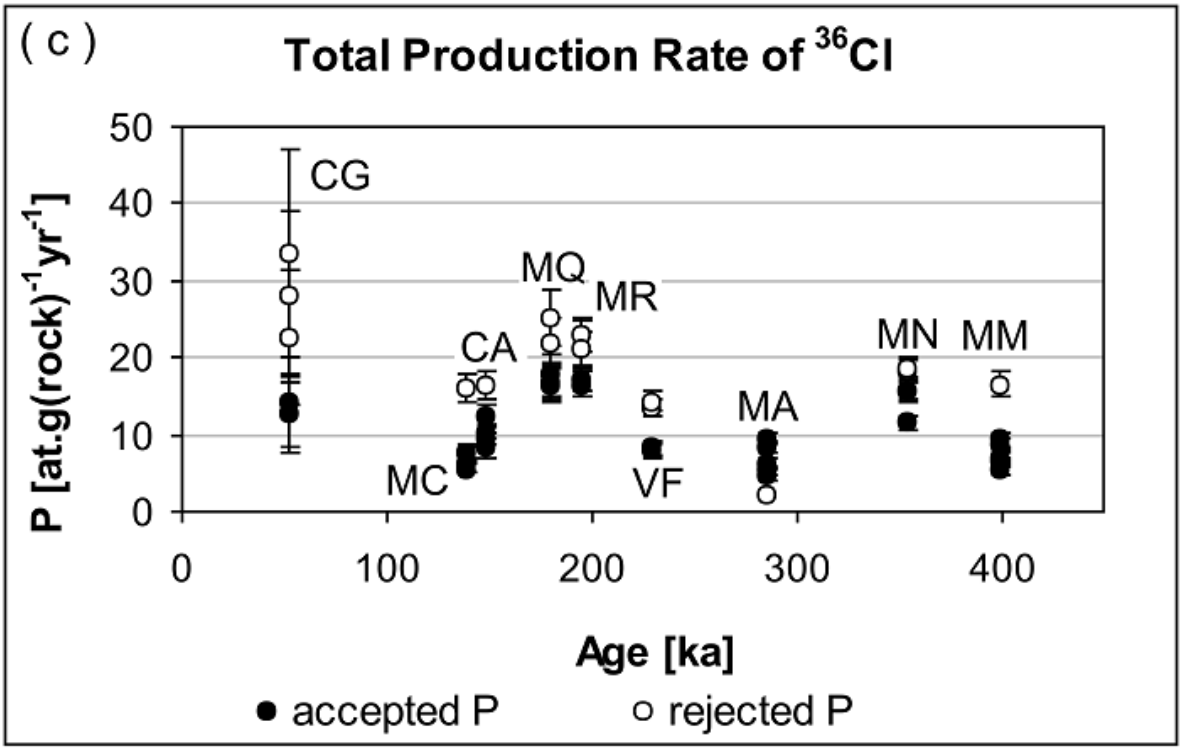

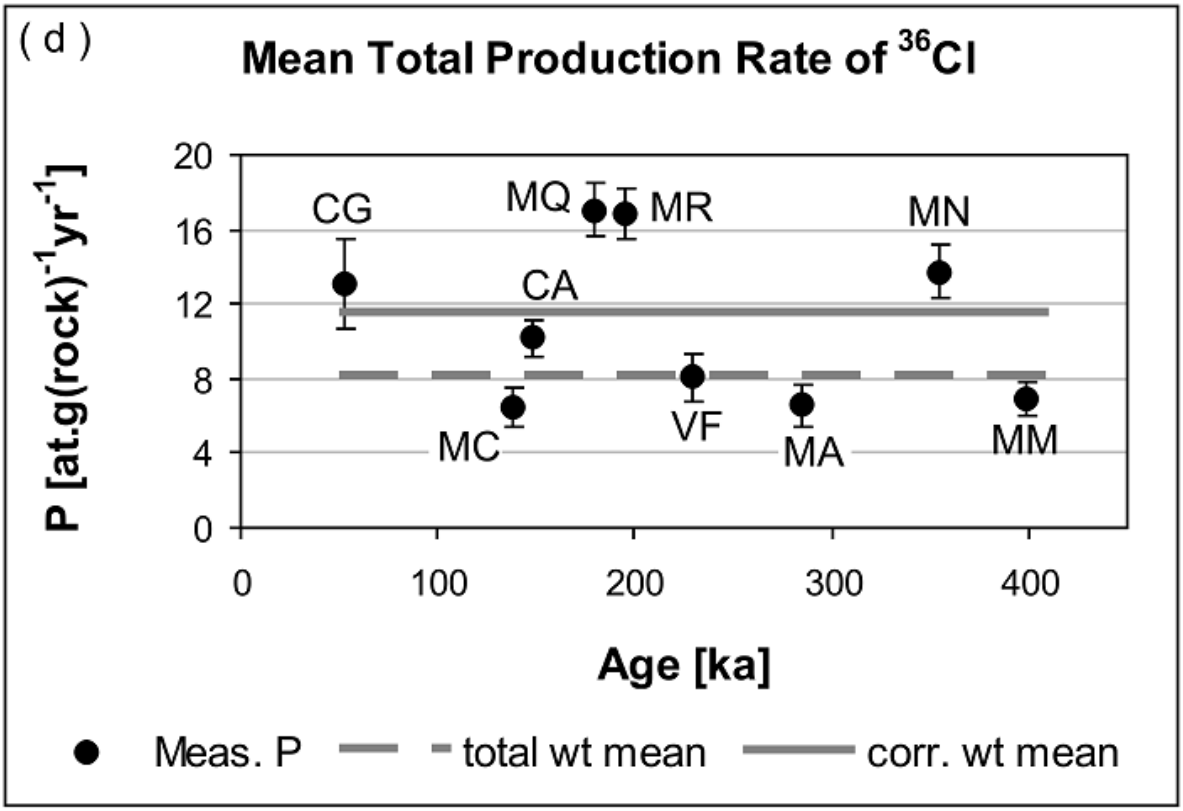

Fig. 5.1 (a) Abundances of total chlorine, (b) of ^{36}Cl, (c) total production rates, and (d) weighted mean production rates of ^{36}Cl for the samples from Fuerteventura. All samples with the same age represent samples from the same flow.

Flow	$^{40}Ar/^{39}Ar$ age [ka]	Wt mean $[Cl]_{nat}$ [ppm]	Wt mean $[^{36}Cl]$ in rock $[10^4$ at.g$^{-1}]$	Wt mean PR (SLHL) [at.g(rock)$^{-1}$.yr^{-1}]
CG	53 ± 22	211 ± 35	56 ± 3	13.1 ± 0.5
MC	138 ± 13	232 ± 35	65 ± 5	6.5 ± 0.5
CA	148 ± 8	288 ± 21	104 ± 7	10.2 ± 0.7
MQ	180 ± 29	160 ± 5	191 ± 3	17.0 ± 0.3
MR	195 ± 17	236 ± 5	217 ± 4	16.9 ± 0.3
VF	229 ± 12	106 ± 13	113 ± 1	8.1 ± 0.1
MA	285 ± 24	368 ± 5	136 ± 17	6.6 ± 0.9
MN	354 ± 20	231 ± 19	293 ± 25	13.7 ± 1.5
MM	399 ± 28	228 ± 15	136 ± 10	7.0 ± 0.6

Table 5.2 Weighted mean concentrations of total chlorine and ^{36}Cl for all flows sampled on Fuerteventura and mean weighted ^{36}Cl production rates scaled for sea level and high latitude (SLHL). The $^{40}Ar/^{39}Ar$ ages are provided by Schneider, et al, submitted.

Table 5.3 shows the expected production rates of the whole rocks for each flow, together with the weight fractions of the target elements and the relative contributions to the total ^{36}Cl production of the individual production mechanisms for all flows. As explained later, no mineral separation with focus on individual target elements was done. All elements that in principle could form ^{36}Cl by spallation but only with extremely low production rates and/or which occur in only minute concentrations like scandium are neglected. The concentrations of the target elements are given as weight per cent in Appendix C. For the main elements the data from the XRF method employing the fused disk were taken for these calculations because they were considered to be the most accurate.

For each of the production mechanisms the expected ^{36}Cl concentration was calculated depending on the target element concentration and the sample age for each flow with a simplified version of eqn. 2.5 assuming no erosion.

$$[^{36}Cl] = \left(\frac{P}{\lambda} \left(1 - \exp\left(-\lambda t\right)\right) \right) \cdot conc_{element} \qquad 5.2$$

where P is the production rate for the target element in atoms.g(target element)$^{-1}$.yr^{-1}, λ the decay constant of ^{36}Cl in yr^{-1}, t the time in yr, and $conc_{element}$ the fraction of the target element in the rock (g(target element).g(rock)$^{-1}$). The ^{36}Cl concentration is thus given in atoms.g(rock)$^{-1}$ for each of the target elements. These values were converted into production rates in atoms.g(rock)$^{-1}$.yr^{-1} for each production mechanism and then added up to obtain the

total production rate of ^{36}Cl for each flow (row "Calculated total production rate" in Table 5.3, which represents the expected production rates). Additionally, the contributions of each production mechanism to the total production in per cent (rows "contrib% (…)" in Table 5.3) were determined.

Flow	**CG**	**MC**	**CA**	**MQ**	**MR**	**VF**	**MA**	**MN**	**MM**
Calculated total production rate [at.g(rock)$^{-1}$yr^{-1}]	**14.15**	**14.40**	**15.60**	**12.44**	**13.05**	**9.63**	**16.82**	**13.39**	**13.83**
Ca (wt%) (XRF)	**7.62**	**7.76**	**7.68**	**7.30**	**7.41**	**6.68**	**7.24**	**6.85**	**7.41**
contrib% (Ca,sp)	39	39	34	43	41	50	31	37	39
contrib% (Ca,mu)	3	3	2	3	3	3	2	2	3
K (wt%) (XRF)	**1.15**	**1.09**	**0.96**	**0.59**	**0.94**	**0.69**	**0.90**	**0.85**	**0.73**
contrib% (K,sp)	14	13	11	8	12	12	9	11	9
contrib% (K,mu)	1	1	1	0	1	1	0	1	1
Fe (wt%) (XRF)	**9.94**	**10.21**	**9.79**	**9.96**	**8.98**	**9.17**	**9.02**	**9.71**	**9.34**
contrib% (Fe, sp)	1	1	1	2	1	2	1	1	1
Ti (wt%) (XRF)	**2.10**	**2.12**	**2.01**	**1.73**	**2.09**	**1.81**	**1.87**	**1.95**	**1.71**
contrib% (Ti,sp)	2	2	2	2	2	2	2	2	2
Cl cont. ppm (AMS)	**258**	**279**	**340**	**197**	**229**	**119**	**366**	**250**	**263**
contrib% (Cl,nth)	40	41	48	42	40	30	55	46	46

*Table 5.3. Calculated (expected) total production rates and contributions of the target elements according to their concentration (see Appendix C, fused disk). The first row shows the total production rates (in at.g(rock)$^{-1}$yr^{-1}) calculated from the composition of the basalts for each flow. The following rows show the concentrations of the target elements (bold) and underneath each concentration the contribution of the individual production mechanisms to the total ^{36}Cl production in %. The following literature data have been used in the calculation: P(Ca,sp) = 72 at/(g(Ca)*yr) (Zreda & Phillips, 1994), P(Ca,mu) = 5 at/(g (Ca)*yr) (Stone et al., 1996a, b), P(K,sp) = 170 at/(g(K)*yr) (Evans et al., 1997), P(K,mu) = 10 at/(g(K)*yr) (Heisinger et al., 2002), P(Fe,sp) = 2 at/(g(Fe)*yr) (Stone, 2005), P(Ti,sp) = 13 at/(g(Ti)*yr) (Fink et al., 2000), P(Cl) based on 353 n.g(rock)$^{-1}$yr^{-1}(Swanson, 1996).*

The calculated total production rates for the flows exhibit some divergence and hence show the effect that the variation of the chemical composition of the rocks has. Also the individual contributions of the production mechanisms vary considerably from flow to flow. For the VF flow the low production rate of ^{36}Cl obtained form the measurements can be explained with the low total chlorine concentration and the slightly lower calcium and potassium concentrations in the rock. In contrast, MA, MM and MC show rather low production rates, which cannot come from chemical composition because their compositions differ only very slightly from that of the flows with higher production rates. Obviously, even

for basalts from the same geological background and setting the production rates given in atoms.g(rock)$^{-1}$.yr^{-1} are not fully consistent. For this reason giving the production rate as value of whole rock production rate in atoms.g(rock)$^{-1}$.yr^{-1} is for its most a good approximation but cannot provide a parameter for accurate calculations.

The contributions of iron, titanium and the muon-based productions are relatively low either due to the low concentration of the target elements or due to the low production rate of the mechanism. The main contributors are calcium and chlorine, which together supply between 75 and 85 % of the total production. The higher both the production rates and the concentrations of the respective target elements are, the more sensitive the total ^{36}Cl production is to the variation or uncertainties in these values. Thus, the total production of ^{36}Cl in the basalts of Fuerteventura is insensitive to the uncertainties in the production rate or concentration of titanium because of its fairly low concentration. It is also insensitive to these uncertainties concerning iron and the muon-induced reactions because of their low production rates for ^{36}Cl. Repeated XRF measurements on three different samples from each flow showed that the concentrations of the target elements vary by less than one to up to four per cent for titanium and iron and by two to eight percent for calcium and potassium throughout each of the flows. Calculations based on these results show that even uncertainties in the production rate or concentration of potassium, which contributes 10 % of the total production of ^{36}Cl, do not introduce significant deviations in the concentration or the production rate of ^{36}Cl because of its low concentration. An uncertainty of 5 % in the concentration of potassium or in the production rate of ^{36}Cl from potassium introduces an uncertainty of about 1 % in the total ^{36}Cl production. For chlorine, which exhibits an extremely high production rate for ^{36}Cl, the sensitivity of the total production to uncertainties in the production rate (i.e. to the thermal neutron flux) is relatively high (2.5 % of variation in the total production for 5 % of shift in the production rate from ^{35}Cl) but it is rather low (less than 1 %) to uncertainties of 5 % in the concentration. In contrast, the total production rate reacts rather intensely to uncertainties in the production rates and/or concentration shifts when the target element is abundant and exhibits a high production rate such as calcium in this case (5 % shifts in both, production rate and concentration results in about 2.5 % of variation in the total production).

The precision of the analytical measurement routines for ^{36}Cl is about 1-2 % to date. However, many other factors add significant, but not always well defined, uncertainties to the production of cosmogenic nuclides averaged in time. The scaling factors are based on fitting procedures and so inherently carry some uncertainty. Since they correct for conditions of the earth like the earth's magnetic field and site's altitude by referring to mean annual air

pressure, they are functions of the development of these parameters in time. The production rates for the individual mechanisms are also uncertain. These uncertainties together all build up to a final error of the order of 20 % for the age and/or production rate determination (Gosse & Phillips, 2001).

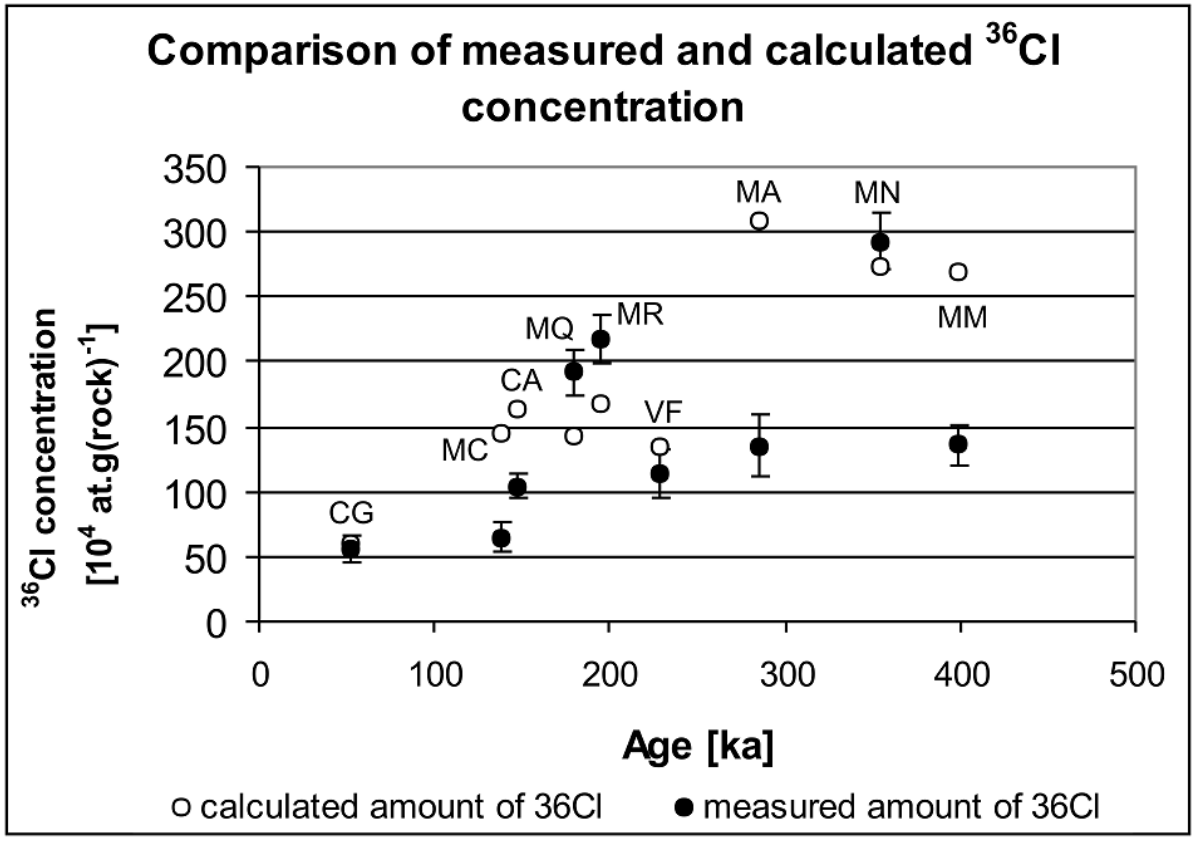

Fig 5.2 Comparison of the calculated (open dots) with measured (black dots) total ^{36}Cl contents for each of the nine flows.

Fig. 5.2 shows the concentrations calculated for ^{36}Cl (open dots) compared with the averaged measured concentrations of ^{36}Cl (black dots) produced for each flow (all in total number of atoms per gram of rock). All scaling factors are applied to the calculated values because they are compared with measured data, which refer to samples of finite thickness and density located at positions that are not sea level and high latitude. The scaling factors for sea level and high latitude are calculated according to Dunai (2001), which provides some considerable correction of the expected ^{36}Cl concentration especially for the older samples. For the flows CG, VF and MN the expected and measured ^{36}Cl concentrations are in good agreement. The flows MA and MM, and to a lesser degree the flows MC and CA, show measured values that are significantly lower than the expected ones, which indicates probably that ^{36}Cl has been lost from the system. The measured values for MR and MQ are in contrast

somewhat higher than expected. These deviations may indicate that the exposure history of the respective flows was somewhat more complicated, but also that the assumptions regarding the production rates for the individual mechanisms may have to be reviewed.

^{36}Cl is mainly generated from ^{40}Ca, ^{39}K, and ^{35}Cl by spallation and by thermal neutron capture. While calcium and potassium are integrated into many silicate minerals during the cooling and crystallization of lavas, chlorine is incorporated only to a comparatively low degree in silicate minerals. Thus the chlorine not being released from the lava during the eruption remains to a large part in the ground matrix (Schimmelpfennig, CEREGE, 2008, pers. comm.). To separate the various mechanisms of ^{36}Cl generation from each other analytically and to determine their production rates individually, samples are needed in which ^{36}Cl production can be unequivocally assigned to one of the mechanisms. Ideally, if a rock contains a significant amount of separable phenocrysts with just one of the contributing target elements (e.g. plagioclase that contains calcium, but virtually no chlorine and potassium) or in whole rock samples only one process strongly dominates the ^{36}Cl production (like in high-Ca rocks such as carbonate) then it is possible to determine the production rates of the mechanisms separately. The resulting amount of cosmogenic nuclide is then only related to one significant production mechanism. If the sample ages are known then the production rate for this mechanism could be determined without a contribution from other production paths. To separate experimentally neutron-induced mechanisms from muon-induced ones, some samples have to be taken from the earth's surface for neutron dominance and other samples have to be taken from great depth levels for muon dominance.

For the basalts from Fuerteventura only whole rock analyses could be performed for the ^{36}Cl analyses because the feldspars in these rocks occurred merely as part of the ground mass. Only very few feldspar phenocrysts were found, and these were rather small. Thus, the measured amount of ^{36}Cl originates from all mechanisms possible for these rocks together.

In spite of this difficulty, an attempt is made to make an estimate of the production rate of ^{36}Cl based on the spallation of calcium because calcium is one of the main contributors and as discussed above the total production is most sensitive to its uncertainties. The amounts of ^{36}Cl from K-spallation, thermal neutron capture by ^{35}Cl, Fe and Ti spallation and muon-induced reactions that have been calculated to estimate the total ^{36}Cl to be expected in the samples (Table 5.4) are transformed into production rates of atoms.g(rock)$^{-1}$yr^{-1} for each of the mechanisms.

Flow	Wt mean P (SLHL) at.g(rock)$^{-1}$.yr^{-1} based on AMS-measurements	Contributions of the individual mechanisms to the total ^{36}Cl production						Derived Production rate of ^{36}Cl from Ca	
		P at.g (rock)$^{-1}$yr^{-1} from K(sp)	P at.g (rock)$^{-1}$yr^{-1} from Cl	P at.g (rock)$^{-1}$yr^{-1} from Ca(mu)	P at.g (rock)$^{-1}$yr^{-1} from K(mu)	P at g(rock)$^{-1}$yr^{-1} from Fe(sp)	P at.g (rock)$^{-1}$yr^{-1} from Ti(sp)	P at.g(rock)$^{-1}$yr^{-1} from Ca(sp)	P at.g(Ca)$^{-1}$yr^{-1}
CG	13.1 ± 0.5	2.0 ± 0.3	5.8 ± 2.4	0.4 ± 0.1	0.1 ± 0.01	0.2 ± 0.02	0.3 ± 0.03	5 ± 1	69 ± 8
MC*	6.5 ± 0.5	1.9 ± 0.3	6.0 ± 0.8	0.4 ± 0.1	0.1 ± 0.01	0.2 ± 0.02	0.3 ± 0.03	-2 ± 1	-23 ± 5
CA*	10.2 ± 0.7	1.6 ± 0.2	7.5 ± 0.5	0.4 ± 0.1	0.1 ± 0.01	0.2 ± 0.02	0.3 ± 0.03	1 ± 1	19 ± 11
MQ†	17.0 ± 0.3	1.0 ± 0.1	5.4 ± 0.5	0.4 ± 0.1	0.1 ± 0.01	0.2 ± 0.02	0.2 ± 0.02	9 ± 1	121 ± 6
MR†	16.9 ± 0.3	1.6 ± 0.2	5.2 ± 0.3	0.4 ± 0.1	0.1 ± 0.01	0.2 ± 0.02	0.3 ± 0.03	11 ± 2	148 ± 20
VF	8.1 ± 0.1	1.2 ± 0.2	2.9 ± 0.2	0.3 ± 0.1	0.1 ± 0.01	0.2 ± 0.02	0.2 ± 0.02	4 ± 1	52 ± 4
MA*	6.6 ± 0.9	1.5 ± 0.2	9.2 ± 0.9	0.3 ± 0.1	0.1 ± 0.01	0.2 ± 0.02	0.2 ± 0.02	-5 ± 1	-65 ± 13
MN	13.7 ± 1.5	1.4 ± 0.2	6.2 ± 0.4	0.3 ± 0.1	0.1 ± 0.01	0.2 ± 0.02	0.3 ± 0.03	6 ± 1	84 ± 15
MM*	7.0 ± 0.6	1.2 ± 0.2	6.4 ± 0	0.4 ± 0.1	0.1 ± 0.01	0.2 ± 0.02	0.2 ± 0.02	-1 ± 1	-6 ± 13
Weighted mean of the production rate for ^{36}Cl from Ca spallation									**67 ± 11**

*Table 5.4 Experimental production rates for ^{36}Cl for total rock and the individual contributors (based on values from literature) from which the production rate for calcium are deduced. The flows for which extremely low, and even negative production rates for the calcium spallation were obtained (marked with *) and those that gave unreasonably high values (marked with †) are shown for completeness in grey. These values are not included in the calculation of the weighted mean production rate.*

These values are then subtracted from the mean production rate deduced from the whole rock measurements. The remainder is attributed to calcium spallation and converted into the elemental production rate given in atoms.g(Ca)$^{-1}$yr^{-1} (Table 5.4). The fairly large errors given for the individual production paths represent the errors of the chlorine determination and the Ar-ages and the resulting total production rates, but they disregard the uncertainties in the given production rates and in the element concentrations of the minor contributors because these have little impact.

The production rate of ^{36}Cl from calcium turns out to be very high for the flows MQ and MR. For the production rates of these flows, but also for individual samples for which the reliability of the obtained production rates were doubted (as mentioned above), a simple estimation of cross sections for nuclear reaction has been performed. This was based on the fact that the production rate is essentially the flux of a certain particle impacting a number of nuclei per cm^2 of a certain nuclide times the cross section of this nuclide for a particular nuclear reaction at a particular energy. It reveals that the observed high production rates are not supported by results of nuclear reaction experiments that determined cross sections for ^{36}Cl production from Ca spallation (e.g. Schiekel et al., 1996) because the cross section required are significantly higher than the ones obtained experimentally. Since the amount of experimental data is rather low, these estimates can only be very crude.

The very small and even negative ^{36}Cl production rates achieved for the flows MC, CA, MA and MM are a clear indication of the fact that ^{36}Cl must have been lost during the exposure history. These values whose reliability is doubted are excluded from the weighted mean production rate of ^{36}Cl from calcium, which is then 67 ± 11 atoms.g(Ca)$^{-1}$.yr^{-1} (Fig. 5.3). This agrees very well with the literature values quoted in Table 2.3. If the contributions of titanium and iron spallation and the muogenic reactions are neglected in this estimation, the production rate from calcium is significantly higher than this: 79 ± 11 atoms.g(Ca)$^{-1}$.yr^{-1}. The reason for this is that even though the individual contributions of Fe and Ti spallation and muon-induced reaction are rather small they effectively add up to 5-8 % of the total production (see Table 5.3).

The production rate for the ^{36}Cl production by neutron reaction is a function of the reaction cross section of the target nucleus for this reaction at a certain neutron energy level and of the neutron flux at this energy level. The neutron flux required in the rock, assuming a production rate of ^{36}Cl from calcium as given in the literature (72 at g(Ca)$^{-1}$yr^{-1}, see Table 2.3), is calculated. Because of the general scatter in the data, the calculated neutron fluxes

vary between 160 and 380 neutrons.g(rock)$^{-1}$.yr^{-1}, but in general they are close to the range given in the literature.

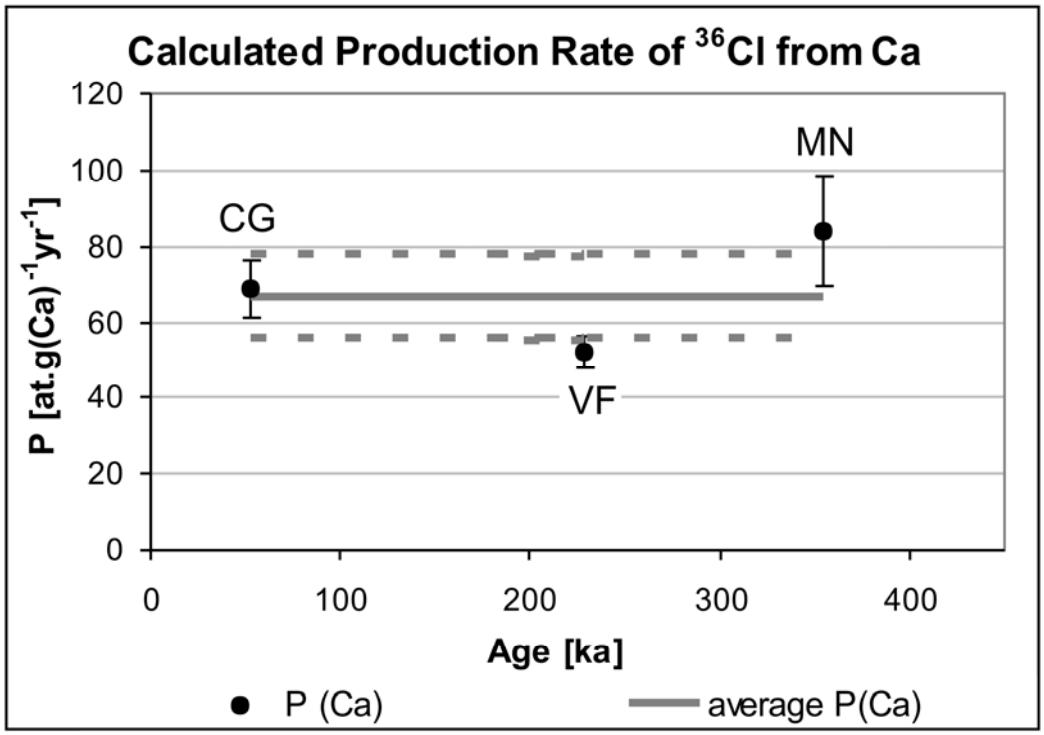

Fig. 5.3 Production rate of ^{36}Cl from calcium from the flows, which were considered to bereliable and the mean (solid line) including the standard deviation (dashed lines). See text for details.

Depth profile for the MA-flow

Two large pieces of rock (MA 05/04 P1-4 and MA 05Cl P1-4) have been taken from the MA-flow to determine the depth distribution of ^{36}Cl and so the depth-dependent production rate of ^{36}Cl. Both pieces were about 40 cm long and stuck in the earth. So they were equally shielded from all sides and only exposed to radiation at their tops. Both pieces had smooth surfaces, which indicated some erosion but they were still in their original position within the flow pinched between neighbouring pieces with which they shared deep but unmoved fractures through the flow. These pieces were cut in approximately 10 cm thick slices and then for sample preparation for AMS treated as separate samples.

In the AMS measurement the obtained R^{36}_{AMS} of the profile MA 05/04 P1 to MA 05/04 P4, which is the measured ^{36}Cl/^{35}Cl ratio, did not produce any values significantly above the background. Also the samples from profile MA 05 Cl P1 to MA 05 Cl P4 showed very low ^{36}Cl contents. The total chlorine content of these samples is like the values of all of

the samples of flow MA, so that an irregularity in the chemical preparation can be excluded as the source of error here because the chemical preparation would not exclusively lose ^{36}Cl. All the other surface samples measured contemporaneously in the same AMS-batch had R^{36}_{AMS} ratios as observed from other measurements, so that a problem during the measurement cannot be the reason for these unexpected results either. Therefore it appears obvious that these samples did not contain significant ^{36}Cl in the first place, and no depth profile of ^{36}Cl production could be obtained. The lack of ^{36}Cl is consistent with the generally very low ^{36}Cl content in all of the samples from the MA-flow.

sample	depth range (cm)	R^{Cl}_{AMS}	R^{36}_{AMS} [10^{-15}]
MA 05/04 P1-1	0-9	0.275 ± 0.002	52 ± 13
MA 05/04 P2-1	9-18	0.263 ± 0.002	54 ± 13
MA 05/04 P3-1	18-28	0.266 ± 0.002	33 ± 10
MA 05/04 P4-1	28-38	0.261 ± 0.002	32 ± 16
MA 05/Cl P1-1	0-8	0.272 ± 0.002	118 ± 20
MA 05/Cl P2-1	8-16	0.272 ± 0.002	132 ± 19
MA 05/Cl P3-1	16-24	0.285 ± 0.002	79 ± 22
MA 05/Cl P4-1	24-34	0.272 ± 0.001	136 ± 16

Table 5.4 Measurement results for the depth profiles in flow MA. The R^{36}_{AMS} ratios obtained do not sufficiently lie above the background and the resulting extremely low total ^{36}Cl is clearly not related to an undisturbed profile of known depth sequences.

6 Discussion and interpretation

Despite some random scatter of the results of the total chlorine and the ^{36}Cl determination, the results are in almost all measurements consistent for samples prepared both from the same flow and from the same rock sample. The production rates of ^{36}Cl for the whole rock are in most cases in good agreement with the literature data (e.g. 15 atoms.g(basalt)$^{-1}$yr^{-1}, Zreda et al., 1991). The final concentration of ^{36}Cl depends mainly on both the calcium and chlorine concentrations, because they are the main contributors to the total production. Therefore it should be expected that the ^{36}Cl content mirrors (age-dependent) the contents of these elements. However, the variations of the ^{36}Cl are obviously not a simple function of the chlorine and calcium contents but rather are affected by other external influences.

Parts of the scatter are certainly "technical" coming from the chemical preparation procedure. The samples are dissolved in concentrated HF and 2N HNO_3. One problem with this method is that sometimes different preparation cycles of the same rock sample performed in the same way do not work out the same. Even though the "macroscopic" conditions in the laboratory environment do not change, samples can dissolve quickly and completely in one experiment and in the next one they react slowly, even after adding extra HF, and probably dissolve incompletely. Thus, the reproducibility of the preparation is certainly subject to some minor restriction but the effect can be controlled by careful evaluation of the suitability of the samples and rejection of the ones about whose quality doubts occur. Further, the determination of the $^{37}Cl/^{35}Cl$ and $^{36}Cl/^{35}Cl$ ratios remains a critical point in the measurement procedure and certainly contributes to scatter and deviations. Since the scatter does not show any pattern systematically related to the preparation periods or the measurements, there are obviously some other components that may influence the results.

One important reason for the scatter in the ^{36}Cl data is certainly the scatter in the total chlorine concentrations. However the scatter of the concentrations of total chlorine and of ^{36}Cl does not perfectly correlate for all of the flows i.e. samples with rather high total chlorine concentrations do not necessarily exhibit high ^{36}Cl content as well. So, slight variations of the other target elements will also add in. Even though the effects of the variations of the individual target element in calculated tests is proven not to be very strong for each of them, they may well all together be a factor that contributes to the scatter and this has to be taken into account.

The degree of correlation between the total chlorine and the ^{36}Cl is maximum for flows for which the calculated and measured production rates agree very well or the data are

inherently consistent (for MN the correlation is more than 0.9). For the samples from flows for which ^{36}Cl loss (e.g. through erosion) could have been an issue the correlation is lower (between 0.6 and 0.3). The erosion may not have been the same throughout the whole flow and over time, and also the possibly overlying cover was surely not evenly thick everywhere, so that some differences in the ^{36}Cl build-up were introduced that now appear as scatter. Finally, the pore space in the rock samples was occasionally filled by sediment that had been transported into it by wind and water. The samples were cleaned carefully from the sediment but in a few cases a small portion of the sediment remained in the sample that could not be removed for technical reasons. These flows (MC, MA) had lower correlations of the total chlorine and the ^{36}Cl concentrations of 0.33 to 0.36 which may indicate that the sediment may have introduced some extra ^{36}Cl of unknown amount and thus added to the scatter. Since these samples also suffered from erosion, the possible influence by sediment cannot be estimated. Nevertheless, the amount of sediment in the samples was very small and had very little influence on the final results so that the production rates obtained for the flows are reliable.

After the extended leaching procedure applied to the samples, which removed up to 10-15 % of the rock material, it is not very likely that significant amounts of meteoric ^{36}Cl are left. However, even though the meteoric ^{36}Cl is thought to be removed well enough not to affect the reliability of the results in terms of the determination of the production rate, there may still have been a certain amount left to augment the total scatter.

As seen from Fig. 6.1 the agreement between the total production rates of ^{36}Cl deduced from the measurements and those calculated based solely on the element composition of the rocks, the age information and the production rate data published in the literature is not the same for all flows. The problem with calculating the expected amounts of ^{36}Cl based on production rates taken from the literature is that the production rates show an amazing range for the same individual mechanisms (see chapter 2, table 2.3). Thus, testing these production rates with respect to the measured data can lead to some difficulties. If one takes the most recently quoted values for Ca-spallation (49 atoms(g(Ca).yr)$^{-1}$ (Stone et al., 1996b)) and K-spallation (154 atoms(g(K).yr)$^{-1}$ (Phillips et al., 1996)) and a neutron flux of 307 n.(kg(rock).yr)$^{-1}$ (Zreda et al., 1991) (for other contributions see bold prints in table 2.3), the expected total ^{36}Cl production rates as shown in Fig. 6.1 (grey squares) are the result. Higher production rates (72 atoms(g(Ca).yr)$^{-1}$ (Zreda & Phillips, 1994), 170 atoms(g(K).yr)$^{-1}$ (Evans et al., 1997), and a neutron flux of 353 n.(kg(rock).yr)$^{-1}$ (Swanson, 1996); other contributions unchanged) for the individual mechanisms shift the expected amount of ^{36}Cl and thus the total

expected production rate upward (grey triangles). The older the samples are, the more the uncertainty in the assumed production rates for the individual mechanisms affects the total build-up of ^{36}Cl. The variation in the reaction of the expected total production rates with the changes in the applied individual production rates is also due to the rocks' composition: those with less chlorine and calcium react less intense on increase of the appropriate production rates.

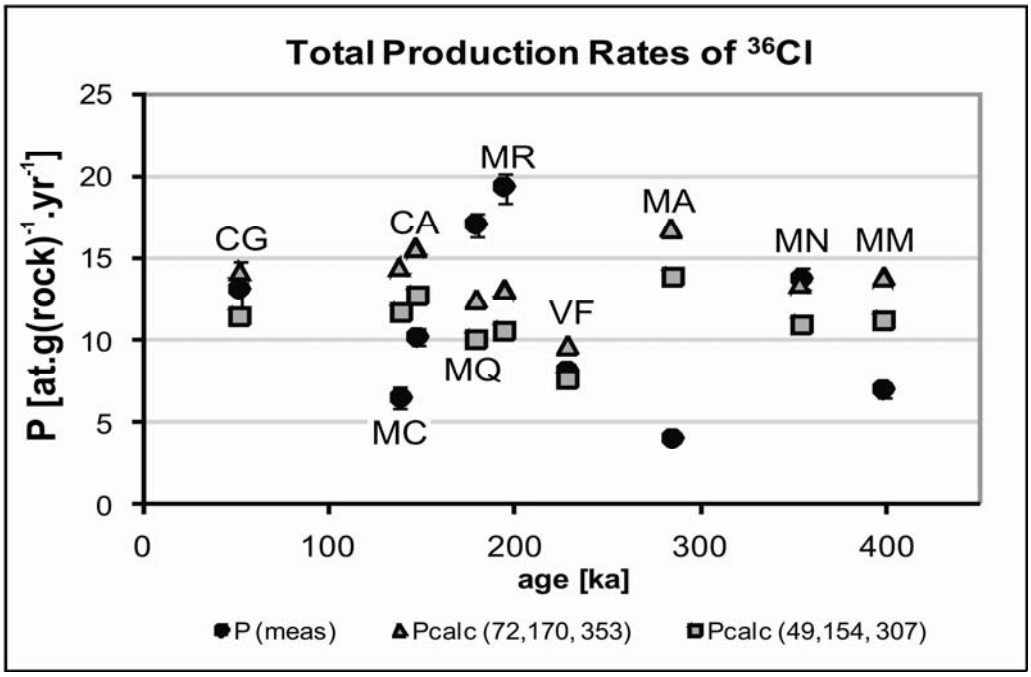

Fig 6.1 Comparison of the measured and the calculated production rates for all flows. For details of the applied production rates see text.

The whole rock production rates of the flows CG, VF and MN lie within the range of the expected production rates based on the literature data. For these samples it can be assumed that only small environmental influences have interfered with the build-up of ^{36}Cl. The production rates of the flows MR and MQ are clearly higher than the expected values. The measured results for these production rates are however internally consistent, i.e. the agreement of the measurement results within this flow is very good, so that pure measurement and preparation effects cannot be a viable explanation. The reasons which could possibly cause an increase in the samples' ^{36}Cl content in addition to the cosmogenic production will be investigated. The flows MC, CA, MA, and MM produced significantly lower production rates than expected and this also needs consideration.

There are a few factors which could lead to scatter or increased ^{36}Cl and total chlorine contents in a sample. XRF and ICP measurements reveal that the major, minor and trace

elements of the basalts vary fairly little with the flows' ages except for the flows VF and MR. This constancy of the chemical composition throughout the time indicates that the magma generation, magma storage and eruption behaviour did not change fundamentally in time. The basalts are Si-undersaturated, high-K alkali-olivine basalts and basanites (Fig. 6.2). The thin sections show extremely fine grained and locally glassy ground mass that contains mainly feldspar (primarily labradorite, in younger samples more albite), pyroxene (augite and diopside), olivine, and iron and titanium oxides. Olivines also occur as small phenocrysts in sizes between 20 µm and very rarely more than 400 µm. Occasionally pyroxene and feldspar also form very small phenocrysts. The flows VF and MR deviate from the general behaviour in that the SiO_2 content increases significantly together with increases in Al_2O_3, and decreases in MgO and slightly in Fe_2O_3 and CaO. The thin sections also show a bit coarser structure of the ground matrix. This offset may be explained with a somewhat higher degree of melting in the magmatic supply zone of the plume in contrast to the other eruptions or by a slight temporary upward shift of the melting region feeding the plume.

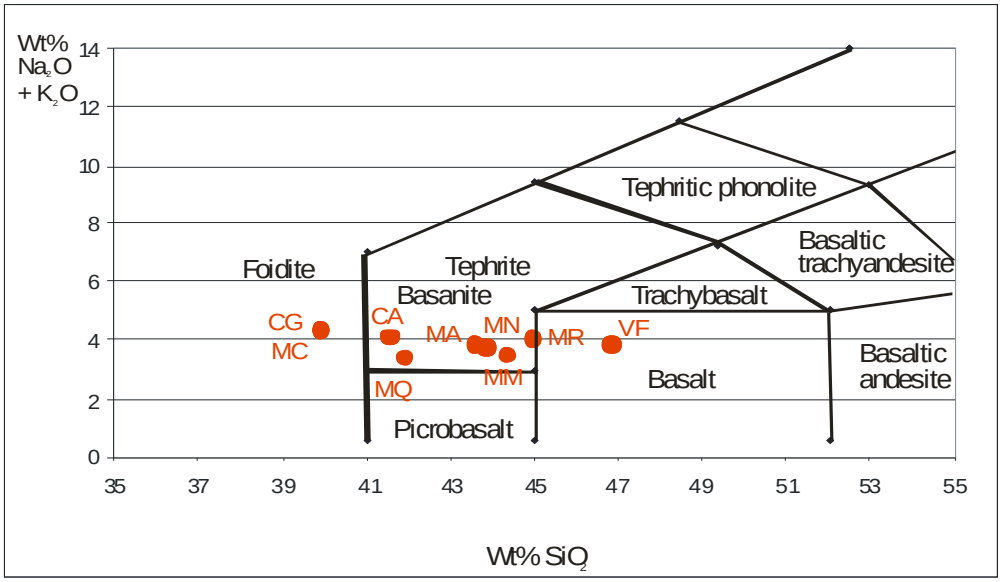

Fig. 6.2 TAS (total alkali versus silica) diagram characterizing the basalts sampled on Fuerteventura. The rocks are chemically and physically very similar.

The differences in the total chlorine content from flow to flow and within each flow are larger than the measurement errors and so they are significant and they have to be accepted as real. The rocks obviously contain naturally varying amounts of chlorine, and the variation seems fairly arbitrary. Compared with basalts from other volcanoes, the amount of chlorine in the samples from Fuerteventura is relatively high. Chlorine is a volatile component in

magmas whose abundance in the melt depends on the melt's composition, pressure, temperature, and the presence of other volatiles such as H_2O and CO_2. Chlorine escapes from the melt during the eruption due to magma degassing and during the subsequent cooling (Webster et al., 1999). The degree of loss of chlorine certainly depends on its original abundance, on the speed of the eruptive process including the speed of lava cooling, and the behaviour of the other volatiles during magma degassing. The scatter in the total chlorine concentration among the samples (also within one flow) can therefore partly be explained by the fact that the release of gases in rising magma does not occur perfectly homogeneously throughout the whole magma volume. Chlorine can also be trapped in fluid inclusions in minerals. The formation of fluid inclusions depends on the local pressure and temperature conditions during the melt formation, transport and eruption, and on the cooling process. Furthermore chloride ions can substitute OH^- groups in minerals. These processes do also not occur in the same manner everywhere in a flow and therefore have to be considered as possible sources for the scatter of the total chlorine concentrations as well. Since the total amount of chlorine is fairly large for the basalts from Fuerteventura, even small variations of very few per cent in the chlorine content can cause significant scatter throughout the samples.

Looking at all elements together for all flows (see Appendix C), the chlorine concentration seems to temporarily precede the change in the concentration of the other element seen in VF with some strong increase (flow MA), then drops significantly parallel to the deviation and then follows with another considerable increase in concentration (flow CA) before it gets back to the "normal" values before this event of changing plume-inherent melting (see Fig. 5.1a). Considering the fact that slight changes in the degree of melting at the plume base also cause variation in the magma's volatile content, the chlorine development throughout time appears to be consistent. However, this process can only introduce stable chlorine. None of the flows with higher than expected ^{36}Cl shows chemical evidence for the incorporation of crustal material or contact with brines or sea water that could contain ^{36}Cl.

^{36}Cl concentrations in a rock that are higher than would be expected from the exposure age and composition can occur in some cases like moraine boulders when they contain ^{36}Cl inherited from earlier exposures. Tera et al. (1986) describe for some back arc settings fast recycling of subducted crust including sediments on top so that magma can be erupted before the subducted cosmogenic nuclides have decayed. However, this does not apply to the Canary Islands. The presence of inherited ^{36}Cl in a basalt that erupts from a volcano on an oceanic island close to a passive continental margin is highly unlikely because the material has been at a large depth for a long time and is extracted by a deep-rooted plume. Therefore inherited ^{36}Cl

in the samples can be excluded from the list of possible contributions to the scatter within and the variations between the flows.

The uranium and thorium contents are very low for all samples from Fuerteventura (on average 0.86 ppm uranium, 3.94 ppm thorium). According to the approach by Dunai et al. (2007) the non-cosmogenic ^{36}Cl production by capturing neutrons originating from the spontaneous fission of ^{238}U, and by secondary (α,n) reactions induced by decay chains of thorium or uranium (Ivy-Ochs, 1996) provide only a minute contribution to the ^{36}Cl production in the samples and is thus considered to be negligible.

Due to the different behaviour of the components of cosmic radiation (see chapter 2), the maximum production of cosmogenic nuclides is not directly at the earth surface but in a particular depth range. Very small scale erosion can shift the peak of thermal neutron-based ^{36}Cl production towards the surface and increase the production rate. Since the surface structures of the samples did not indicate any long-time erosion and even very small rates would add up to a loss of a few centimetres throughout a few hundred kyr, only overlying covers of ash and dust could have been removed during the exposure. This could have introduced some slight scatter in the ^{36}Cl concentration. The effect and amount of low scale erosion however cannot be estimated at this point and would lead too far into speculation. It is however not able to fully explain the degree of increase of production observed from MQ and MR samples.

The climate throughout the history of the Canary Islands has been characterized by increased aridity during maximum glaciation on the northern hemisphere and more semiarid climate during the interglacials (e.g. Magaritz & Jahn, 1992). The geomorphology of Fuerteventura shows clear evidence of the temporary presence of larger amounts of water than now, e.g. ancient, now dry river beds, and fluvial valleys on the volcanoes' hill slopes (Fig. 6.3). Thus, periods with a higher water supply could possibly have caused unrecognized water cover for the samples. Thin covers of water (snow can be excluded for Fuerteventura) can increase the thermal neutron flux in the rock underneath because the peak of production is shifted upward and tightened (see chapter 2). As soon as the water layer is thicker than a few centimetres, the water itself would absorb such a large portion of the thermal neutrons that the neutron flux beneath it would decrease (Masarik & Beer, 1999). Comparison of the ages of the flows with a stratigraphic chart of the Quaternary (e.g. Gibbard et al., 2007) shows that for all the flows about half of their exposure time was affected by warmer periods and half of it by cold ones. Therefore the ratio of warm versus cold periods cannot provide an explanation for the differences in the production rates. However, the basalts, especially those from the

flows MA and MR, are very porous (up to approximately 30 %) with significant interconnected pore space within which water could have been trapped in the uppermost few centimetres. Also thin covers of ash and dust could have trapped water in their texture and so increased the thermal neutron flux underneath.

Fig. 6.3 Landscape of Fuerteventura. Ancient riverbeds and fluvial valleys indicate higher water supply in the geologic history of the island than at present.

Dep et al. (1994b) have modelled the effect of water contained in granite and showed that an increase of water from one to four per cent would increase the thermal peak flux by about 40 % and thus could increase the ^{36}Cl production by approximately 15 %. With the assumption that this approach is similarly true for basalt and with the simplification that water in the pore space is equivalent to the 4 % water content in the model by Dep et al. (1994) it is tested how much the total ^{36}Cl production could increase theoretically. The expected production rate for the flow MR increases from 13 to at most 15 atoms.g(rock)$^{-}$1.yr^{-1} (assuming the water was present throughout the whole exposure). (The measured production rate of the flow MA is very low, which indicated additional aspects of exposure and thus the flow is not included in this test.) This is still lower than the production rate obtained from the measurements on the samples from flow MR (17 atoms.g(rock)$^{-}$1.yr^{-1}), but it could reduce the discrepancy between the measured and the calculated values somewhat. Apparently water coverage can at least partly explain the “too high” production rate of the flow MR. Since there

is no possibility of improving the estimate of the amount and the duration of the water supply for the Canary Islands during the last 400 kyr, and further the effects of snow and/or water coverage cannot thoroughly be modelled with the available programs yet, the impact of water in top layers of the flows can only be roughly estimated.

Furthermore, water trapped in closed vesicles that originates from the degassing process of the magma may contribute to the thermal neutron supply in the rock as well, but this effect cannot be realistically estimated because it is not known how much of the pore space in the samples has been sealed from the environment during the exposure time. However, since the samples of all flows were porous and contained water as one of the main volatiles, the vesicular water hardly can account for the differences in the production rates.

The global climate not only affects the water supply in a region but also influences global and regional pressure and temperature conditions. As seen in chapter 2 the site's position in terms of altitude is scaled with respect to a sea level standard pressure and a mean annual temperature. Air pressure and temperature are functions of climatic conditions, which have changed repeatedly and strongly throughout the last 400 kyr. From hydrostatic equations it can be concluded that colder air is associated with higher air pressure which causes a decrease of production rates at a given height and an accelerated increase of scaling factors for increasing height. For a decrease of the standard pressure, which would correspond to a warmer climate, the production rate at the given height would be higher and the increase of the scaling factor with height is slower than for the normal standard pressure conditions. This effect is larger as the deviation of the climatically changed pressure from the standard pressure is stronger and as the scaled height difference is larger. However, the paleo-air-pressure is an especially complicated issue in paleo-climatology because besides the temperature effect (cold air leads to higher air pressure) also, among others, hydrostatic effects of the sea level changes (120 m lower during the Last Glacial Maximum, LGM), and dynamic effects due to different weather systems and different distribution of ice shields play an important role (M. Butzin, University of Bremen, 2008, written comm.). A number of models for the last 125 kyr consistently indicate that the effect on the air pressure for the region of the Canary Islands has not been severe in contrast to regions which were covered with or located close to thick ice shields. These models suggest that the climate-induced air pressure variations for the region of the Canary Islands were less than 10 hPa, i.e. less than 1% of the recent standard pressure of 1013.25 hPa (e.g. Kutzbach et al., 1998; Lohmann & Lorenz, 2007). Assuming that the variations between the Last Glacial Maximum and the Last Inter-Glacial are representative for the last 500 kyr, the air pressure very likely did only cause

a minute deviation of the scaling factors. Based on literature data, maximum global temperature variations of -5°C for cold periods and +5°C for warm periods is assumed for the analysis of the reaction of the scaling factor (e.g. Gasse, 2000; Bintanja et al., 2005). For the site of Fuerteventura the temperature-induced deviation of the scaling factor is around 0.3 % and thus negligible. Also if the temperature and pressure changes for Fuerteventura are applied together, the deviations of the scaling factors remain below 1 %. As seen from the discussion above, the variations in temperature and pressure in the region of the Canary Islands are not factors to be taken into account when analysing cosmogenic nuclide concentrations from the site of Fuerteventura in contrast to the water supply during the various climate periods. This conclusion is also supported by results from Staiger et al. (2007) who analysed atmosphere-based influences on the production rates of cosmogenic nuclides. However, the global circulation models (GCM) do not yet reach the accuracy and resolution necessary to constrain the atmospheric conditions suitably to determine their effect on the cosmogenic nuclide production throughout the time in detail.

Since the spallation of calcium is induced by high energy neutrons, tests are performed to estimate possible contributions from elements of similar mass as calcium. The behaviour of target atoms of similar mass is at these energies very similar, so that elements like scandium or manganese can also produce ^{36}Cl. The reaction cross sections obtained by Schiekel et al. (1996) for high-energy proton-induced production of ^{36}Cl from different elements (calcium, titanium, manganese, iron) are considered to be similar to those for high-energy neutrons because at energies between 50 and 1200 MeV the influence of the charge of the impacting particle is not very great any more and it is assumed to be far less than the effect of their mass. The approximate production rates for these reactions are determined from the cross sections for the target elements with atom numbers between 21 and 30 averaged over this energy range and the approximate neutron flux. The neutron flux is estimated from the known production rate of ^{36}Cl from titanium and the average cross section for this reaction. Applying this flux value (2.10^5 neutrons.cm^{-2}yr^{-1}) to the other elements yields rates for ^{36}Cl production from them and suggests values between 0.01 and 16 atoms.g(element)$^{-1}$.yr^{-1}. This is a very rough estimate because of the small amount of data available throughout the projectile energy range considered. However it still provides an insight into the order of magnitude of the contribution. The contribution of the spallation reaction in the basalts from the elements scandium to copper, and excluding iron and titanium which have been taken into account already, is in total less than 0.1% and thus negligible. Therefore the contribution from these

elements can neither cause the scatter in the ^{36}Cl concentrations nor can it be responsible for the high production rate obtained for Ca-spallation.

Despite the fact that the production rates are still debated, and the whole set of production mechanisms including all factors is not yet fully understood, it is worthwhile to examine other influences that affect all components of the incoming cosmic radiation instead of mainly the thermal neutron flux as has been discussed until now. The intensity of the total neutron flux depends on the intensity of the incoming cosmic radiation which is modulated by the earth's magnetic field. The scaling factor for latitude and elevation refers to data sets on the historic development of the earth magnetic field intensity.

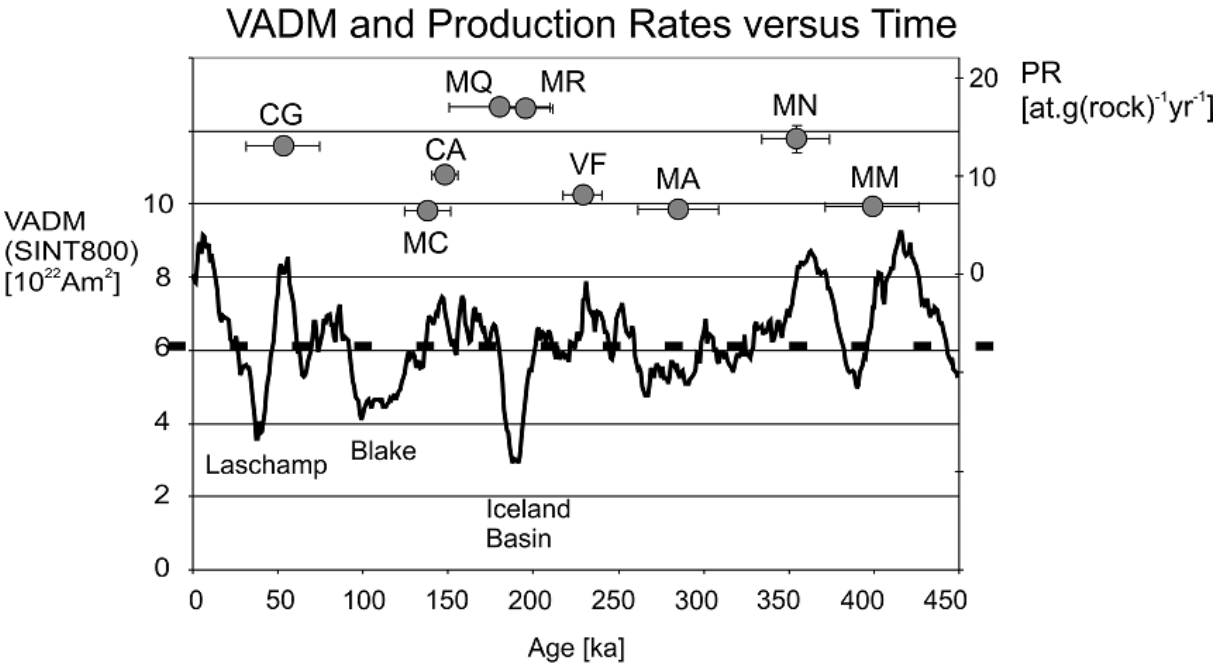

Fig 6.4 The development of the earth magnetic field during the recent 450 kyr, displayed by VADM data of the SINT 800 record (Guyodo & Valet, 1999) and the production rates of the individual flows. The dashed line represents the mean VADM.

The plot of the VADM (SINT800) versus time (Fig. 6.4) shows short episodes of a few kyr of very low and of very high field intensities, phases of extremely fast intensity changes but also longer periods of relative stability. During the last 40 kyr the magnetic field has continuously increased from a pronounced low intensity and reached a rather stable temporal intensity maximum for the last ten thousand years. Here "stability" still includes deviations of about 30 to 40 % from the present value. For the last 800 kyr the field has on average only

been about 70 % of what it has been for only the last 10 kyr. Thus, the production rate of cosmogenic nuclides must have been higher throughout most of the period of 800 kyr than in the last 10 kyr at low- and mid-latitudes (see also Masarik et al., 2001). A sample at the surface receives the incoming cosmic radiation over a given time, i.e. the total in-situ production of cosmogenic nuclides is integrated over this time[6]. Therefore the relatively short-time variations in the field strength have an impact mainly on young samples. The older the samples the more the effects of the variations are cancelled out. For the samples from Fuerteventura the averaged VADM varies only between $6.0*10^{22}$ and $6.2*10^{22}$ $A.m^2$ for the ages of all of them. The overall field intensity was fairly balanced throughout the time for each of the flows: 47-58 % of the exposure age of the samples the field was below average, while during the rest of the time the field reached considerable highs as well. The production rates for the flows MR and MQ seem to reach a peak right at a low field episode, but since the total production rate averages over the age of the samples this is no real correlation. Thus, there is no correlation between the development of the field intensity and the ^{36}Cl content. The magnetic field variations cannot be a major reason for the variations in the measured values. Even for the youngest flow (CG, 64 ka) there is no clear evidence that the slight increase in the ^{36}Cl production can be assigned to the geomagnetic low-intensity period of Laschamp.

However, the SINT records are smoothed considerably because their resolution of 1000 years is limited by the resolution of the sediment cores on which they are based. This smoothing may obscure higher frequency variations as is seen for example in the ^{10}Be records which indicate a significantly higher number of excursions (during which the field commonly weakens) than seen in the SINT records. The SINT data could thus in general be somewhat too high which would imply that the scaling for the field intensity might also be somewhat too strong. The degree of overestimation of the field intensity is unknown so that it is not possible to estimate by how much the resulting neutron flux would increase for the adjusted scaling (A. Biggin, UU, 2008, pers. comm.). The SINT records comprise values from all over the world and may include unresolved non-dipole signals from samples originating from sites of temporary magnetic anomalies (C. Constable, 2007, pers. comm.)[7]. Strong non-dipole effects

[6] This is an important difference from systems in which the isotope is formed in the atmosphere and then precipitated (e.g. ^{10}Be in ice or lake sediments). There a time record throughout the sedimentation profile is formed that relates the concentration of the isotope at a certain depth interval to a certain time span.

[7] Besides the uncertainty in the paleointensity data the time information also often turns out to be of limited reliability due to non-ideal isotopic record or to uncertainties in the non-continuous

are not only present in periods of weak dipole field but also during high field intensity and recently doubts have been expressed that they are all short-term features of the earth's magnetic field but that some of them might be rather persistent (e.g. Lifton et al., 2008). The earth's magnetic field to date is for about 90% a dipole at the surface. At the distance of the magnetosphere it is virtually a dipole so that incoming primary cosmic radiation does not experience the effect of anomalies (A. Biggin, Utrecht University, 2008, pers. comm.). In periods of weak field the dipole structure was disturbed. Deflected primary and charged secondary particles moving along field lines of the earth magnetic field might have been influenced in their path by strong anomalies causing higher particle flux at the sites of the anomalies. It appears thus conceivable that the increased flux of particles reaching the atmosphere due to the weak field could have been intensified regionally by the non-dipole pattern of deflection of charged particles that initiate cascades of particles being finally effective for cosmogenic nuclide production. However, to date there are no paleomagnetic data from the Canary Islands that cover the range of the samples' ages and which indicate a long-term anomaly in this region. So this aspect of increased particle flux is fairly speculative.

Variations of the pole positions over time ranged from slight deviations of the poles relative to the geographic pole, geomagnetic excursions (where the VGP (virtual geomagnetic pole) deviated >45˚ from the geographic poles, often coinciding with the dipole field being so low that non-dipole effects become dominant), to complete field reversals (Guyodo & Valet, 1999). Korte & Constable (2003, 2005, 2006a, 2006b) and Korte et al. (2005) produced a global field model for the last 7000 years (CALS7K), which provides insight into the variation of the geomagnetic field behaviour including pole positions. Modelling the different aspects of magnetic field variations demonstrates that for very young samples of up to 10 ka the short-term variation of the pole position has a significantly greater impact on the scaling factor than the long-term variation of the field intensity. Therefore short-term variation of the pole position can cause considerable short-term shifts in the resulting scaling factors. The positions of the geomagnetic poles average over longer periods approximately to the geographic pole. This indicates that the time-averaged geomagnetic field is a geocentric axial dipole (GAD) field (Butler, 1992). The older the samples, the more the short-term instability of the pole position and even larger excursions (which are usually accompanied by field intensity lows) are averaged out. For samples of more than 10-20 kyr the mean field intensity becomes increasingly influential for the scaling factors. It is reasonable to take the geographic

sedimentation rate. Depending on the dating methods, the material used for age determination and the absolute age of the sample, the errors easily reach the order of a few percent to a few tens of percents.

pole as the average position for the magnetic pole if long periods are involved and it is assumed that polar wander has not severely affected the average production rates on Fuerteventura. There are now doubts that non-dipole effects of higher persistence may average out to a GAD over a certain time range, which introduce some uncertainty unknown in its magnitude (e.g. Merrill, et al., 1996; Johnson & Constable, 1997; Lifton et al., 2005), but there is to date no consistent information about the pole positions throughout the time considered in this study.

Apart from the terrestrial parameters that determine the scaling factors and the effective particle flux on a local and regional scale, the extraterrestrial parameters affecting the incoming primary cosmic ray flux can also have changed over time. Assuming that the primary particle flux has been higher for longer periods, the secondary particle flux would have been higher than presumed as well. This could have been due to solar variations, to a generally higher intensity of the galactic cosmic radiation or to shifts in the spectrum of the radiation components (Lifton et al., 2008). Solar variability tends to be a short-term effect so that it would require unreasonably severe variations to introduce measurable effects on a sample over several 100 kyr. Effects of solar origin are thus restricted to very young samples. Increases of the overall radiation intensity or shifts in the spectra could be caused by supernovae whose remnants can keep up to 100 kyr (J. Heise, Utrecht University, 2008, written comm.) due to motion of the solar system within the galaxy, or due to movement of the galaxy through ionized regions of interstellar space which would rather cause long-term effects of numerous 100 kyr to several Gyr. Significantly more information is needed about the intensity and the spectrum of the radiation, the resulting neutron flux and the behaviour of the spectrum when it is subject to energy shifts. Studies on meteorites indicate that the cosmic radiation they have collected did not vary significantly throughout time (e.g. Reedy, 1987). However, there are often uncertainties about their exposure history, fragmentations during collisions, their orbital paths which change due to collisions, and finally also their cosmogenic nuclide build-up which integrates over the time of exposure to widely unknown radiation.

The above discussion of the possible causes for the increased production of ^{36}Cl shows that there are not many reasons likely for the case of the increased concentration of ^{36}Cl in the flows MR and MQ. Excluding inherited and radiogenic ^{36}Cl, and contribution from elements other than the typical target elements there are only magnetic field, climatic influences including (probably repeated) input of small amounts of water over longer periods into the pore space or in some thin ash layer on top of the lava, and (contributing only little if at all) small scale erosion left. The scaling with possibly too high VADM values may be one reason,

but this would affect all flows. The older the flows the stronger the effect would be. The main influence for the production rates for MR and MQ is likely to be very restricted in space and time because only two flows are affected. Another flow (VF) not far away from MR, and also not much older, does not show any deviation of this sort from the expected values. The input of water could explain the spatial restriction of the increase of the production rate but not at all the amount. The inherent consistency of the high production rates measured from the different samples for these flows makes it unlikely that the influence of meteoric ^{36}Cl is the only reason for the increased values. Therefore the possibility that the Ar-ages are not determined correctly has to be considered as well. If the ages for these flows are determined too low, the resulting production rates would come out too high.

Based on these considerations the exclusion of the production rates obtained for the samples from the flows MR and MQ from the weighted mean of the production rates for all flows appears reasonable. So the finally obtained total rock production rate is 12 ± 3 atoms.g(rock)$^{-1}$yr^{-1} and the resulting production rate for Ca- spallation is 67 ± 11 atoms.g(Ca)$^{-1}$yr^{-1}.

In contrast to the cases discussed so far, dealing with the possibility of an increase in the neutron flux, the flows MC, CA, MA, and MM show a production of ^{36}Cl far lower than expected. This indicates a loss of ^{36}Cl from the geological system e.g. due to erosion or prevention of ^{36}Cl production in the first place due to shielding/coverage which has now gone. To estimate the thickness of cover necessary to explain the data for each of the flows, the theoretical total ^{36}Cl production rate per gram rock without erosion is estimated from the age and the composition. Using the build-up diagram based on equations from Nishiizumi et al. (1991) (Gillespie & Bierman, 1995; Ivy-Ochs, 1996), which relates the production rate and the erosive loss to the total ^{36}Cl, an erosion rate for each flow with "too low" build-up is found iteratively (see chapter 2). This is a very simple method of estimating since the underlying assumption is that the erosion rate was approximately constant. The estimated erosion rates for the younger flows are 0.0003 cm.yr^{-1} (approximately 40 cm of loss of material) for MC and 0.0001 cm.yr^{-1} (15 cm) for CA. For the older flows they are 0.0004 cm.yr^{-1} (110 cm) for MA and 0.0002 cm.yr^{-1} (80 cm) for MM. Note that the erosion rates and the eroded layer thicknesses are smallest for a certain build-up deficit when continuous erosion at a constant rate is assumed throughout the entire exposure history. If the coverage existed only for a restricted time range, then the erosion rate and the thickness of the covering layer would have to increase to reproduce the same deficit in build-up as obtained from the samples. These values are of course only rough estimates based on the diagram, they cannot

provide secure erosion rates because for this either two or more isotope systems or samples of one isotope at different depth levels would be needed. The results are very large erosion rates which are not at all supported by field observation: the erosive loss of the sample surfaces is estimated at its largest to be about 1.5 cm, and the surface structures are in most cases still well preserved. Obviously not the actual surface of the samples has been removed but rather layers of ash and dust and of lava sheets on top the samples. The individual lava sheets could have been fairly thin (10-20 cm) and a few of them could have lain on top of each other. Ash between lava layers may facilitate flaking of the separate lava sheets from each other without significantly damaging the surface structures of the layers underneath. Thus, when the ash and dust layers are removed and the overlying lava sheets are eroded, the preserved surfaces of the lava layers underneath appear. The eroded fragments of the overlying layers are not distinguishable from any other piece of lava at the site because it is all the same type of rock and thus previous shielding is not detectable from field observation. This is supported by the consistency of the data throughout the flows. An ash cover could not affect only a few samples and others not at all but would rather spread over a wide area. The apparent coverage of the present surface seems to have been especially thick on the sites of MA: all of the ^{36}Cl values are extremely low and the profile samples did hardly contain any measurable cosmogenic ^{36}Cl.

Apart from the coverage of the samples by rock, water could also have contributed to the shielding. Even though small amounts of water can increase the thermal neutron flux in the samples and so increase the thermal-neutron induced production of ^{36}Cl, larger amounts of water e.g. in the texture of the ash cover or in the vesicles or as layers at the surface decreases the neutron flux in the material underneath. The presence of water would decrease the theoretically estimated amount of erosion considerably and thus cannot be excluded from the reasons explaining the small build-up of ^{36}Cl in these samples. Neither the amount of erosion nor the amount of water can be reasonably estimated for these flows. The modelling of the erosion rate gives only the simplest but not necessarily the true story of coverage, exposure and water content of the lava flows in consideration. Countless versions of modelled total production rates and coverage histories could be created without any possibility to decide which one is closest to the truth.

The lower production rates of ^{36}Cl cannot be explained by an unrecognized movement of the samples because they all showed undisturbed surface structures different from the structures of their bottom sides. The continuous and homogeneous distribution of lichen on top of the samples clearly indicated that they had not been buried by a recent flipping of the

rock they settled on. No indication of dense vegetation that could have caused additional shielding has been found on the sampling site either. Even though vegetation reacts fairly quickly to variations of climatic conditions and certainly smaller plants could have grown on the lava flows it would need a decent forest to shield the ground from incoming radiation severely which certainly was not the case for the sampling sites.

The data on deviations of the ^{36}Cl production seem to be supported by data from cosmogenic ^{3}He (B. Schneider, Free University Amsterdam, 2008, pers. comm.) which have been obtained from some of the flows. The ^{3}He production rates obtained are fairly close to the expected production rates for the flows CG and MR, which are also the flows with high ^{36}Cl production rates. For MC and MM the ^{3}He values are very low which corresponds well with the low ^{36}Cl production for these flows. The ^{3}He values for MQ are low as well whereas the ^{36}Cl production was close to the expected value. The reason for this discrepancy is not known but it is possible that ^{3}He is more sensitive to erosion and weathering of the olivine than is ^{36}Cl with respect to the whole rock.

7 Conclusions

In the study presented here, the concentrations of total chlorine and ^{36}Cl in basalts from the Island of Fuerteventura, Canary Islands, were measured at the AMS facility of the Utrecht University. The production rate of ^{36}Cl was determined for the whole rocks and for the production mechanism of Ca-spallation alone as a function of the individual production rates of the contributing production mechanisms and of the site parameters such as height and latitude

The measurements showed considerable variation in the total chlorine and ^{36}Cl data between the flows and also produced significant scatter in the total chlorine and ^{36}Cl contents within each flow which exceed the experimental uncertainty. The variations in the total chlorine concentrations among the flows are assumed to be mainly caused by slight variations in the chemical composition of the magma. This is supported by the variations of the other elements among the flows that also indicate changes in the melting process over time. The scatter in the total chlorine concentration within each flow may be explained with the volatile character of chlorine which escapes from the lava during the eruption and the subsequent cooling at certainly different rates for different lava pieces.

The mean production rates calculated for the individual flows range between 7 ± 1 and 17 ± 1 atoms.g(rock)$^{-}$1.yr^{-1} and are given in detail in Table 5.1. For some flows (CG, VF, MN) the ^{36}Cl contents in the samples and the resulting production rates of ^{36}Cl, which were determined on whole rock samples, reflect the expected build-up as a function of the age and the chemical composition of the rocks well, while for other flows (MC, CA, MA, MM) the ^{36}Cl concentration and the production rates are significantly smaller than expected. This discrepancy between measured ^{36}Cl content and the values calculated from the ages, the composition of the rock and published production rates for te individual production mechanisms can be explained with previous coverage with ash and thin lava layers which are removed by now. The surface structures of the samples do not indicate great erosion themselves, so that only the removal of layers that had protected the structures seen now seems the most likely explanation. The effect may have been increased temporarily by larger amounts of water trapped in the lava or the ash at the surface that would absorb a large portion of the incoming neutrons.

The ^{36}Cl content and the production rate in the flows MQ and MR are in contrast considerably higher than the values expected from the age and the composition. Small scale erosion and too strong scaling for the earth's magnetic field are considered to be possible

factors contributing to this increase. The main part of the increase is attributed to very small amounts of water that were trapped in the basalt's vesicles and in a possibly thin overlying ash layer that could have increased the neutron flux in the sample material. The effects are difficult to quantify because it is impossible to evaluate how large their effect could have been. However, they cannot fully account for the increase observed, so that other unrecognised influences may contribute to it. The $^{40}Ar/^{39}Ar$-age determination is also a factor of uncertainty because the samples are relatively young. Especially for the flows with extremely high production rates there is some suspicion that the argon ages might be too low. Since recently published isotopic abundance ratios of atmospheric argon (e.g. Lee et al., 2006) which are used as reference values for $^{40}Ar/^{39}Ar$ geochronology deviate from earlier ones (Nier, 1950), the argon-ages employed here have been re-calibrated (Schneider et al., submitted). The future will show if the new reference values remain in use.

Several sources may contribute to the scatter in the ^{36}Cl concentrations within the flows. Part of the scatter is the result of the scatter in the total chlorine concentrations. Furthermore small remainders of sediment, small variations in the target element concentrations throughout the flows, irregular distribution of water and ash or lava layers at the surfaces, or remainders of meteoric ^{36}Cl may contribute to the scatter to varying extent. However, the degree of the scatter in ^{36}Cl is in general fairly high. Neither one of the possible reasons alone nor all of them together appear to be able to fully explain it. Therefore there must be an unrecognised component contributing to the scatter additionally. It is not clear to date what this could be. This does not appear to be a problem only for samples from Fuerteventura or specifically for the preparations and measurements performed in Utrecht, but rather a more general one. Licciardi et al. (2008) obtained a similar scatter in their measurements on basalts from Iceland processed and measured elsewhere. They explain the scatter similarly to the arguments presented here (varying degrees of minor erosion, thin cover, presence of water close to the surface, and significant blank corrections for measurements on the youngest samples).

The total weighted mean production rate calculated only from the flows CG, VF, MQ, and MN that were not clearly affected by erosion or other influences was scaled to sea level, high latitude (SLHL) using the scaling model by Dunai (2001) to make the data comparable with data from other sites on earth. The total production rate is 12 ± 4 atoms.g(rock)$^{-}$1.yr^{-1} and is generally comparable with data quoted elsewhere in the literature (Zreda et al., 1991). From the total production rates for each of the considered flows the production rates for the ^{36}Cl production from Ca-spallation alone were deduced based on literature data for the other

contributing mechanisms. All possible mechanisms had to be taken into account because ignoring those led to too high values in the estimation of the production rate of ^{36}Cl from Ca-spallation. The weighted mean production rate is 67 ± 11 atoms.g(Ca)$^{-1}$.yr^{-1} for all flows considered.

Apart from the technical part of determining the production rates and scaling effects for the site of Fuerteventura it may be worthwhile to conclude with a few words appraising the site as a calibration site. During this research the question arose if and how well rocks from the island of Fuerteventura can be used as calibration material for ^{36}Cl production at a mid-latitude low-altitude site. According to the data obtained the flows of CG, VF, and MN best suit the requirements of a calibration site. They apparently have not been affected by severe erosion or shielding or any other disturbance. Even though there are still uncertainties about external influences such as the variations in the primary cosmic ray flux for which no or no sufficient corrections can be applied, the total scaling for position and the known constituents like the development of the earth magnetic field intensity work reasonably well. The flux of cosmogenic particles as it interacts with terrestrial material needs to be better determined and described physically. Broad understanding of these interactions would ideally help to improve the scaling models considerably and may even help to replace fitting-based models by physically descriptive ones.

For calibration reasons ^{36}Cl is best applied to samples in which only one production mechanism strongly dominates (e.g. carbonate) or in rocks from which minerals can be separated that contain essentially only one target element. An alternative could be to employ artificial samples of for example pure CaO, which can be installed for known time periods and under known conditions. However, apart from that carbonates are not necessarily chemically and geologically simple systems, they are not as widely spread as basalt throughout the last million years, and the older surfaces are usually less well preserved. Thus carbonate rocks are not a workable alternative for basalts as a calibration material. It is important to determine first of all the individual production rates for all the production mechanisms. When several mechanisms, which are insufficiently well determined, contribute to the total production of ^{36}Cl and they cannot be separated in the preparation, then the analysis ends up in an equation with too many unknowns. In that respect Fuerteventura is probably not an optimum site for calibration for ^{36}Cl because the production paths could not be separated experimentally. None of the samples contained suitable phenocrysts to shed light onto at least one of the individual candidate paths of production. It may however be a manageable calibration site when the production rates for all the individual production

mechanisms are well determined. Cosmogenic nuclides cover a range of ages that cannot be covered by most of the other dating methods. Although ^{36}Cl is a rather troublesome method, it is often the only method reasonably possible when no quartz for ^{26}Al or ^{10}Be is present, and the material is too old for radiocarbon and too young for argon-based measurements. Cosmogenic nuclides further provide a means of dating the surface exposure and exposure history as it is not easily possible for other isotope systems. So even though they are often problematic in performance and interpretation they are occasionally the only way to obtain the information needed. It is however clearly necessary to judge the results critically in terms of the quality and a reasonable interpretation.

Appendix A1: Overview over the samples

Place	Samples	Coordinates (UTM, WGS 84)	Height (m asl)	Total mass of the sample (kg)	Thick-ness, aver. (cm)	Density of hand specimen (g/cm³)	^{40}Ar-^{39}Ar Age (ka) (Schneider et al., 2009, submitted)	SF_{Topo}	$SF_{Thickness}$	$SF_{El,Lat}$ (Dunai, 2000, 2001)
Caldera de	CA 05/01	X=599491	127	13.17	14	2.43	148.0 ± 7.8	1.00 ± 0.01	0.90 ± 0.03	0.92 ± 0.03
los Arrables	CA 05/02	Y=3131878		14.89	15	2.33			0.90 ± 0.02	
	CA 05/03A			6.06	9	2.36			0.94 ± 0.03	
	CA 05/03B			9.15	15	2.31			0.90 ± 0.02	
	CA 05/04			9.95	17	2.51			0.88 ± 0.02	
	CA 05/05			17.04	14	2.77			0.89 ± 0.03	
	CA 05/06			10.01	13	2.25			0.91 ± 0.03	
	CA 05/07			9.17	14	2.48			0.90 ± 0.02	
Caldera de	CG 05/01	X=597494	213	5.76	7	2.33	52.7 ± 21.6	0.98 ± 0.06	0.95 ± 0.02	0.98 ± 0.04
Gairia	CG 05/02	Y=3138100		12.75	12	2.86			0.88 ± 0.02	
	CG 05/03			9.69	10	2.82			0.92 ± 0.02	
	CG 05/04			12.50	18	2.55			0.87 ± 0.02	
	CG 05/05			7.11	12	2.17			0.92 ± 0.02	
	CG 05/06			6.12	11	2.56			0.92 ± 0.02	
	CG 05/07			5.08	8	2.45			0.94 ± 0.02	
Montaña de	MA 05/01	X=603142	185	8.82	14	1.88	285.2 ± 23.8	0.93 ± 0.03	0.92 ± 0.03	0.97 ± 0.04
Arena	MA 05/02	Y=3168401		13.82	14	2.04			0.92 ± 0.02	
	MA 05/03			11.43	13	2.35			0.91 ± 0.02	
	MA 05/04-P (profile)			20.95	38	2.05-2.27			0.94 ± 0.03 0.79 ± 0.02	
	MA 05/05			10.98	14	2.46			0.90 ± 0.02	
	MA 05/06			8.65	11	2.1			0.92 ± 0.03	
	MA 05/07			6.38	9	1.40			0.96 ± 0.03	
	MA 05/08			8.02	12	1.62			0.94 ± 0.03	
	MA 05 Cl-P (profile)			19.34	34	1.48-2.37			0.95 ± 0.05 0.80 ± 0.03	

Malpaís	MC 05/01	X=596995	199	16.60	15	2.85	138.8 ± 13.4	0.99 ± 0.04	0.88 ± 0.02	0.97 ± 0.04
Chico	MC 05/02	Y=3135947		16.21	12	2.73			0.90 ± 0.02	
	MC 05/03			10.44	10	2.68			0.92 ± 0.02	
	MC 05/04			14.52	11	2.67			0.91 ± 0.02	
	MC 05/05			16.69	13	3.06			0.89 ± 0.02	
	MC 05/06			14.04	13	2.67			0.90 ± 0.02	
	MC 05/07			20.63	15	2.50			0.89 ± 0.03	
Montaña de	MM 05/01	X=607317	24	11.95	12	2.45	398.6 ± 27.6	1.00 ± 0.01	0.91 ± 0.02	0.85 ± 0.03
la Mancha	MM 05/02	Y=3180737		9.65	14	2.43			0.90 ± 0.02	
	MM 05/03			10.81	11	2.43			0.92 ± 0.02	
	MM 05/04			13.62	16	2.58			0.88 ± 0.02	
	MM 05/05			9.55	12	2.68			0.91 ± 0.02	
	MM 05/06			8.63	11	2.24			0.93 ± 0.03	
	MM 05/07			9.12	11	2.45			0.92 ± 0.03	
Montaña	MN 05/01	X=609388	228	4.69	10	2.23	354.4 ± 19.9	0.98 ± 0.05	0.93 ± 0.02	1.00 ± 0.04
Negra	MN05/02	Y=3168817		7.35	15	2.48			0.89 ± 0.02	
	MN 05/03			9.61	9	2.72			0.93 ± 0.02	
	MN 05/04			19.86	20	2.58			0.85 ± 0.02	
	MN 05/05			12.41	22	2.62			0.83 ± 0.02	
	MN 05/06			9.69	15	2.05			0.91 ± 0.02	
	MN 05/07			7.97	15	2.46			0.89 ± 0.02	
	MN 05/08			17.85	17	2.42			0.88 ± 0.02	
Montaña	MQ 05/01	X=597389	167	7.17	*20-30*	2.63	179.8 ± 29.4	1.00 ± 0.02	0.82 ± 0.07	0.95 ± 0.04
Quemada	MQ 05/02	Y=3160187		7.35	*15-25*	2.60			0.85 ± 0.07	
	MQ 05/03			11.63	*15-30*	2.73			0.81 ± 0.07	
	MQ 05/04			5.83	*10-20*	2.93			0.87 ± 0.08	
	MQ 05/05			10.76	*10-15*	2.87			0.89 ± 0.08	
	MQ 05/06			12.46	*10-20*	2.58			0.89 ± 0.07	
	MQ 05/07			12.11	*20*	2.72			0.85 ± 0.07	
Malpaís de	MR 05/01	X=611020	185	6.03	15	2.65	195.0 ± 16.7	0.96 ± 0.10	0.89 ± 0.02	0.97 ± 0.04
Roja	MR 05/02	Y=3167587		8.64	20	2.31			0.87 ± 0.02	
	MR 05/03			12.85	17	2.14			0.89 ± 0.02	

	MR 05/04			4.33	18	2.24			0.88 ± 0.02	
	MR 05/05			4.80	11	2.18			0.92 ± 0.02	
	MR 05/06			9.65	20	2.15			0.88 ± 0.02	
	MR 05/07			6.05	14	2.26			0.91 ± 0.02	
	MR 05/08			8.94	11	2.32			0.92 ± 0.02	
Valle de	VF 05/01	X=613361	56	22.40	15	2.40	229.0 ± 11.5	1.00 ± 0.01	0.90 ± 0.02	0.87 ± 0.03
Fimapaire	VF 05/02	Y=3163377		7.13	12	2.38			0.92 ± 0.02	
	VF 05/03			12.46	12	2.29			0.92 ± 0.02	
	VF 05/04			10.07	13	2.40			0.91 ± 0.02	
	VF 05/05			6.49	9	2.48			0.93 ± 0.03	
	VF 05/06			7.31	11	2.15			0.93 ± 0.03	
	VF 05/07			7.85	10	2.64			0.92 ± 0.03	

The thickness values for the flow MQ are estimates because of technical problems.

Appendix A2: Sample description

Close to the *Caldera de los Arrables* (CA) an apparently young flow of very uneven relief was sampled. Many local highs and lows characterized its surface. The samples were taken on top of a narrow ridge and on two little highs next to it. The erosion was estimated to have been not more than 2 mm. The surface structures were well preserved but details of mm-size were affected. The weathering crust along the surface ranged between 1 and 2 mm, sometimes 3 mm. Alterations also occurred along fractures that partly were filled with sediment. The basalt showed intermediate porosity of approximately 10 to 20 % with a gradient throughout the depth to very dense material with almost no porosity. The densities of the hand specimen were determined to be between 2.11 and 2.77 g/cm³ (average 2.75 g/cm³). Sediment comprising of (mainly quartz) sand and clay minerals was washed into the samples through the pore space. Secondary carbonate of varying concentration was found in the pores. Olivine phenocrysts were found in the samples in varying but not very high amounts. In this flow no desert pavement was present and no indication of former ash cover was found. The amount of large blocks was very high in relation to the lapilli in between.

Close to the *Caldera de Gairia* (CG) a young flow was sampled that was locally interfingering with an older one. Besides the larger pieces a significant amount of lapilli characterized the flow. The amount of large, massive pieces was considerably lower than in other flows. The samples showed clear ropy structures at the surface but also the bottoms were intensely structured in ropes. The samples were fairly fresh and the mostly small pores caused an intermediate porosity of less than 10 to 15 %, rarely up to or more than 20 %. The densities of the hand specimen were determined to be between 2.17 and 2.86 g/cm³ (average 2.53 g/cm³). The weathered crust along the surface was 1-2 mm thick. Since fractures and porosity pathways reached deep into the samples, the weathering alteration and the sediment fill of the pores were located far inside the samples. The erosion of the surface was estimated to be less than 5 mm. The samples contained some olivine phenocrysts of sizes of up to 3-4 mm. Most of these phenocrysts were considerably smaller. Varying amounts of secondary carbonate were found within the pore space and along the fracture interfaces. The site was characterized by extremely little desert pavement, no soil formation and absence of caliche.

At the site of *Montaña de Arena* (MA) mainly large blocks with only little lapilli existed. Locally the lava formed a dense cover of a few square meters cut by fractures. Several collapsed channels were identified. The erosive loss of the surface was estimated to be between 5 and 10 mm. The surface showed ropes and occasionally cauliflower structures that

did not exhibit any details of the size of millimetres. The thickness of the alteration crust at the surface ranged between 2 and 5 mm, rarely somewhat more but then with only low intensity. The alteration occasionally reached inside the sample where fractures provided paths for sediment input. The samples were highly porous with porosity in the range of at least 15 to about 30 %. In extremely vesicular parts the porosity could even reach up to 40 %. Only in very few spots the material seemed to have been compressed during emplacement and the porosity was decreased to around 10 %. The densities of some of the samples of this flow were very low due to the extreme porosity (density range 1.40 to 2.46 g/cm³, average 2.00 g/cm³). The pores were mostly of <1 to 5 mm in diameter but some of them reached more than 10 mm. The pores provided path ways for sediment input in the outmost few centimetres of the samples, but locally the sediment was found throughout the whole sample. In some of the samples flow structures were found inside the samples that showed additional alteration surfaces and sediment input. Secondary carbonate occurred as in other flows but significantly less intense. Only little of the material was completely unaltered.

South of Montaña Parrado the site *Malpaís Chico* (MC) was sampled. The erosion was estimated to be 3-4 mm, the flow top structures were still clearly visible and only slightly rounded. Most of the material is fairly fresh. The weathering crust of the samples was 1-2 mm. Locally, alterations reached somewhat further into the sample due to sediment input along open pore space and fractures. Also some secondary carbonate was observed in the pores and along fracture planes. The rock exhibits only low porosity of 2-5 %. The pores were very small, often less than 1 mm. The densities of the hand specimen were determined to be between 2.50 and 3.06 g/cm³ (average 2.74 g/cm³). Some large olivine phenocrysts (up to 3 mm) were observed besides small ones. Within the flow no desert pavement occurred but in the neighbouring older flows it was well present. No indication for former ash cover was found. The flow consisted mainly of large lava blocks. The portion of lapilli was very low.

Close to *Montaña de la Mancha* (MM), a flow ca 200 m away from the shore was sampled. The location was slightly hilly. Probably several flows were interlayering throughout the area. The sample surfaces were intensely structured. Details of the ropes gave evidence that the erosion only removed 1-2 mm from the surface. The weathered crust was very thin (1-2 mm). In some of the samples alterations did not reach far in the rock, in others the alteration followed fractures and reached further into the interior. Porosity also provided only little interconnected pathways for weathering and sediment input in most of the samples. Locally, secondary carbonate occurred inside the pores throughout a restricted volume within the samples. It hardly appeared on fracture interfaces. The porosity of the sample was 10 % or

less. The pores were mostly small (1 mm in diameter), only occasionally large ones reached 4-20 mm. The densities of the hand specimen were determined to be between 2.24 and 2.68 g/cm³ (average 2.46 g/cm³). The samples contained varying amounts of olivine phenocrysts of different size (up to 2-3 mm). Olivine xenoliths of 2-4 cm of size that appeared to be somewhat altered were found in the samples. On top of the flow only little desert pavement emerged. There were no signs of large ash cover.

At the locality of *Montaña Negra* (MN) the lava blocks were relatively widely distributed. Desert pavement and some soil formation were observed. Small walls encircling field crops were present in the closer neighbourhood. Erosive loss at the surface was approximately 1 cm, with variation among the particular samples. The weathered crust along the sample surface was 2-3 mm thick but weathering alteration occasionally reached far into the samples following fractures and porous pathways. The alteration zone within the sample was partly up to 1 mm wide. Secondary carbonate was locally concentrated in pores; in some samples it had evolved to considerable amount. The porosity was fairly high, 20-25 % sometimes even more, but rarely below 15 %. The densities of the hand specimen were determined to be between 2.05 and 2.72 g/cm³ (average 2.45 g/cm³). Throughout the sample, the porosity formed gradients or sharp transitions from higher to lower porosity. The pore sizes ranged between 1 and 3 mm. Some parts of the flow showed only very little porosity and appeared almost massive. Olivine phenocrysts are in some of the samples rare and very small, while in others they are somewhat more abundant. No evidence of former ash cover was found at the flow.

The basalts from the place *Montaña Quemada* (MQ) had decent surfaces structures. The erosion of the samples was estimated to have been 5 mm or less. The rock material was generally very fresh. A crust of 1-3 mm at the upper surface and 1 mm at the bottom side of the samples showed colour alteration (from originally blackish grey to brownish) due to weathering processes. The weathering-induced alteration continued along fractures and locally in pores into the samples as a very thin, only superficial colour change. The rock showed little porosity of up to 10 %, rarely more (locally up to 15 %). The pores were very small, usually not more than 1 mm in diameter. The densities of the hand specimen were determined to be between 2.58 and 2.93 g/cm³ (average 2.72 g/cm³). Secondary carbonate occurred in almost all samples in varying abundance, partly distributed along fractures and partly concentrated in pores within a certain volume of approximately 2-3 cm³. Samples that showed more intense weathering inside also contained more carbonate. Olivine phenocrysts were mostly very small (0.2-1 mm). Only very few larger ones occurred (up to 3 mm). Within the flow locally soil caliche (a calcareous crust) was found that had evolved there. At the

edges of the flow the caliche locally crops out. At the top of the flow aerial dust has been deposited and forms desert pavement. There is no evidence of earlier ash cover or soil development of a larger scale.

Close to *Malpaís de Roja* (MR) samples from a relatively old flow were taken. The conditions of the surface structures indicated an erosion of approximately 5 mm. The flow top structures were still well preserved. The weathering crust was 2 mm wide along the sample surface. Weathering alteration continued into the samples along fractures and interconnected pore space. Sediment has been flushed into the pores. The inner part of the rock that had not been affected by water and sediment was fairly fresh. Secondary carbonate was present abundantly throughout the rock. Olivine phenocrysts were relatively small (max. 1 mm) and occurred rather rarely. The porosity ranged mainly between 10 and 15 %, occasionally up to 20 or less than 10 % were observed. Transitions between volumes of higher porosity and those of very little porosity were often quite sharp. The pore sizes varied from 1-2 mm to 10-20 mm in diameter. The densities of the hand specimen were determined to be between 2.14 and 2.32 g/cm³ (average 2.28 g/cm³). The area of the flow showed clear soil formation. The lava blocks on the surface did not have any contact with the underlying lava material of the flow anymore and lie immediately on the desert pavement/soil. No large blocks did exist; the greatest diameters were around 0.5 m. The smaller material was a mixture of lapilli and broken-off pieces. The former existence of ash cover could not be clarified completely.

Next to the *Valle de Fimapaire* (VF) samples from an apparently older flow were taken. The surface structures were more eroded than in other flows (total erosion estimated 10 mm, max. 15 mm). Generally the ropes only existed as very remnant features without any small-scale detail. The rock was generally fairly fresh. A crust of 1-2 mm at the surface showed colour alteration (from originally blackish grey to brownish) due to weathering. The rock's porosity was 5 to 10 %. The pore sizes ranged between 1 and 15 mm with locally larger pores. The densities of the hand specimen were between 2.15 and 2.64 g/cm³ (average 2.39 g/cm³). Inside the pores sediment was washed in close to the surface, but did rarely reach very deep into the samples. The samples hardly showed any internal fractures that were altered or carried sediment. Secondary carbonate occurred in some of the pores, locally in larger concentration. The samples contained quite abundant olivine and pyroxene phenocrysts, which were very small, mainly of the size of less than 1 mm. Only rarely larger ones were found. Besides large blocks of lava significant amounts of lapilli were found in the flow material. There was no evidence of earlier ash cover or extended soil formation. Desert pavement had been deposited between the lava pieces all over the flow.

Appendix B Laboratory protocol for sample preparation for ^{36}Cl analysis with AMS

The following protocol was followed during preparation of the samples for this study. It is mainly based on Stone et al. (1996b), and instructions provided by L. Benedetti during a CRONUS-EU workshop (2005).
A detailed description of the procedure is given in chapter 4.

Sample preparation for ^{36}Cl analysis by AMS

Date:

Sample: Rock type:

Sample: Whole Rock Separated Minerals

1. Pre-treatment:

Equipment: sieves, Crushing mill, 500 ml plastic bottle, Ultrasonic bath

Material: water, MΩ water

Slab, initial thickness:

Mass whole sample:

Mass of used material:

Density sample:

Density crushing:

Name	**Fraction**	Mass of Crushed/Sieved Fractions (g)	Mass after rinsing fines out (g)
	>1000 μm		
	500 -1000 μm		
	250-500 μm		
	125-250 μm		
	< 125 μm		

Condition of rock:

2 **Leaching** Date:

Equipment:500 ml HDPE wide mouth bottles Material: 2M HNO_3, MΩ water

2.a Water leaching

	1st run	2nd run
Label HDPE-bottle		
Grain size of sample	µm	µm
Tare HDPE-bottle	g	g
Mass sample initial	g	g
Volume MΩ-water	ml	ml
Mass HDPE-bottle + rinsed, dried sample	g	g
Mass of sample (final)	g	g
Mass difference	g	g

Shaking time Start: End:

2b. Acid leaching

	1st run	2nd run
Label beaker		
Tare (beaker)	g	g
Mass beaker + sample	g	g
Mass sample (initial)	g	g
Amount of HNO_3 added	ml (%)	ml (%)
Mass rinsed, dried sample + beaker	g	g
Mass of sample (final)	g	g
Mass difference	g	g
Label tube (Cl^--determin.)		
Tare tube	*g*	*g*
Mass tube with Cl^--determin. sample	*g*	*g*
Mass Cl^--determin. sample	*g*	*g*

Italics: for Cl- determination from leachate

Reaction time: Start End

3. Dissolution

Equipment: 500 ml FEP Teflon bottle, hot plate, 5 ml vial, pipette, weigh
Material: MΩ water, Carrier, 2M HNO_3, conc. HF

Sample Loading		
Label Teflon bottle		
Mass sample + bottle	g	
Mass sample	g	
Adding carrier		
Type of carrier		
Conc. mg/g		
Mass of carrier added	g	
Dissolution		
Total amount HNO_3	ml	conc.
Total amount HF	ml	conc.

Reaction time: Start: End:

4. Separation from dissolution residue and first AgCl precipitation

Equipment: 250 ml PFA Teflon bottle, parafilm cover, 50 ml centrifuge tubes (HF-standing), centrifuge, weigh
Material: MΩ water, 10 % $AgNO_3$

Label Teflon Beaker	
Mass Teflon Beaker (empty)	g
Mass beaker (full, Cl^- sol.):	g
Mass supernatant liquid	g
Mass Flouride gel	g
Amount $AgNO_3$ added	g

Reaction time: Start: End:

5. Sulfate clean-up

Equipment: pipette, polypropylene centrifuge tube, centrifuge,
Material: 1:1 NH_3 solution, MΩ water, sat. $BaNO_3$ solution

Label polypropylene centrifuge tube	
Amount NH_3 sol.	ml
Amount $Ba(NO_3)_2$ sol.	ml
Filter size for $BaSO_4$ precip.	µm

Reaction time: Start: End:

6. Final AgCl precipitation

Equipment: small (100 ml) pyrex beaker, hot plate, parafilm cover
Material: 2M HNO_3, 1% $AgNO_3$ sol., MΩ water

Label small polypropylene centrifuge tube	
Tare of centr. tube	g
Amount HNO_3 sol.	ml
Mass of final AgCl bead	g

Appendix C: XRF and ICP data for the basalt samples from Fuerteventura

XRF, tablets

wt%	CA05	CG05	MA05	MC05	MM05	MN05	MQ05	MR05	VF05
SiO2	47.13	45.58	48.73	44.95	48.56	49.08	47.26	50.93	51.94
Al2O3	14.27	12.97	13.22	12.54	14.73	13.80	12.66	15.39	15.47
TiO2	3.43	3.63	3.12	3.59	2.80	3.14	2.87	3.56	3.04
Fe2O3	13.57	13.91	12.68	14.06	12.83	13.13	13.70	12.29	12.59
MnO	0.18	0.18	0.16	0.19	0.18	0.20	0.19	0.16	0.15
CaO	12.65	12.61	11.58	12.67	11.62	10.68	11.75	11.79	10.51
MgO	16.30	17.89	15.89	18.57	15.09	15.75	19.28	11.09	11.27
Na2O	3.18	2.95	2.69	2.94	2.94	2.53	2.69	3.24	3.32
K2O	1.34	1.54	1.19	1.46	0.94	1.09	0.78	1.24	0.89
P2O5	0.79	0.88	0.68	0.91	0.67	0.46	0.69	0.52	0.51
S	0.05	*0.01*	0.10	0.06	0.34	0.19	*0.01*	*0.01*	*-0.01*
Sum	112.90	112.14	110.05	111.93	110.71	110.04	111.88	110.23	109.68
Si	22.03	21.31	22.78	21.01	22.70	22.94	22.09	23.80	24.28
Al	7.55	6.87	6.99	6.64	7.80	7.30	6.70	8.15	8.19
Ti	2.06	2.17	1.87	2.15	1.68	1.88	1.72	2.14	1.82
Fe	9.49	9.73	8.87	9.83	8.98	9.18	9.58	8.60	8.81
Mn	0.14	0.14	0.13	0.15	0.14	0.15	0.14	0.12	0.12
Ca	9.04	9.01	8.28	9.05	8.30	7.63	8.40	8.43	7.51
Mg	9.83	10.79	9.58	11.20	9.10	9.50	11.63	6.69	6.80
Na	2.36	2.19	2.00	2.18	2.18	1.88	1.99	2.40	2.46
K	1.11	1.27	0.99	1.21	0.78	0.90	0.65	1.03	0.74
P	0.34	0.38	0.30	0.40	0.29	0.20	0.30	0.23	0.22
S	0.05	0.01	0.10	0.06	0.34	0.19	0.01	0.01	-0.01

ppm	CA05	CG05	MA05	MC05	MM05	MN05	MQ05	MR05	VF05
As	3.32	*1.21*	*2.02*	*1.15*	*0.54*	*0.38*	*1.07*	*1.71*	*0.74*
Cu	116.35	99.04	104.38	101.30	163.40	114.01	134.01	122.91	99.12
Pb	*3.54*	6.05	5.11	6.73	6.82	6.51	5.64	*3.20*	5.93
Zn	154.29	139.14	142.76	141.77	178.01	131.83	150.43	150.63	155.87
Ni	340.53	409.78	370.73	429.43	358.14	438.22	481.64	211.18	253.30
Cr	378.40	462.14	487.09	455.92	658.63	496.54	584.13	363.42	372.73
V	196.14	196.14	183.72	196.49	167.16	166.66	186.40	183.90	161.14
Sn	*-3.05*	*5.89*	*7.69*	*6.18*	*-4.04*	*2.68*	*0.87*	*-1.42*	*-2.23*
Sr	875.84	932.51	674.27	935.45	794.31	588.36	804.27	675.77	541.18
Ba	371.22	421.34	272.25	402.77	349.84	357.98	380.41	392.14	221.59

Rb	26.12	31.25	24.12	29.66	19.08	20.59	13.29	22.42	13.25
Ga	19.46	18.32	18.87	19.81	19.02	19.01	16.84	20.81	19.91
Zr	260.30	305.58	246.76	305.74	221.82	257.60	247.22	281.21	250.10
Nb	66.32	88.37	52.05	88.27	56.53	59.40	68.96	66.11	50.35
Y	28.39	29.81	25.77	28.09	25.52	24.66	25.35	27.85	25.14
Sc	23.43	23.05	24.84	22.82	20.68	21.70	21.87	23.67	19.03
La	57.13	72.57	34.20	72.18	51.20	42.76	61.02	41.78	22.63
Nd	44.73	53.62	34.48	58.21	39.25	31.62	48.96	37.48	33.54
Th	9.27	*5.29*	*3.89*	*3.61*	*0.18*	*2.80*	*3.66*	*8.34*	*8.48*
U	*0.52*	*1.10*	*0.01*	*1.46*	*2.01*	3.07	*2.68*	*-0.45*	*-0.67*

Printed in italics: Values with a high error because the concentrations of the elements were close to the detection limit.

The error for the measurements of press pellets for main and trace elements is up to 5 %.

XRF fused disks

wt%	**CA05**	**CG05**	**MA05**	**MC05**	**MM05**	**MN05**	**MQ05**	**MR05**	**VF05**
SiO2	41.54	39.90	43.55	39.91	43.83	44.33	41.90	45.00	46.84
Al2O3	11.07	10.44	10.70	10.14	11.87	11.02	9.84	12.52	12.76
TiO2	3.35	3.50	3.12	3.54	2.85	3.25	2.89	3.49	3.02
Fe2O3	14.00	14.22	12.90	14.59	13.35	13.88	14.24	12.84	13.11
MnO	0.19	0.18	0.16	0.20	0.18	0.20	0.19	0.16	0.16
CaO	10.75	10.66	10.13	10.85	10.37	9.58	10.22	10.36	9.34
MgO	12.15	12.57	12.09	13.28	11.63	12.77	14.59	8.41	8.46
Na2O	3.00	3.03	2.74	2.97	2.86	2.45	2.68	2.94	3.02
K2O	1.16	1.38	1.08	1.31	0.88	1.02	0.71	1.13	0.83
P2O5	0.76	0.92	0.73	0.95	0.69	0.48	0.71	0.54	0.53
LOI	0.15	0.08	0.53	0.03	0.33	0.83	0.12	0.24	0.07
som	98.12	96.90	97.74	97.80	98.84	99.82	98.10	97.63	98.15
Si	19.42	18.65	20.36	18.66	20.49	20.72	19.59	21.03	21.90
Al	5.86	5.53	5.67	5.37	6.28	5.83	5.21	6.63	6.76
Ti	2.01	2.10	1.87	2.12	1.71	1.95	1.73	2.09	1.81
Ca	7.68	7.62	7.24	7.76	7.41	6.85	7.30	7.41	6.68
Mg	7.33	7.58	7.29	8.01	7.01	7.70	8.80	5.07	5.10
Na	2.23	2.25	2.03	2.21	2.12	1.82	1.98	2.18	2.24
K	0.96	1.15	0.90	1.09	0.73	0.85	0.59	0.94	0.69
Fe	9.79	9.94	9.02	10.21	9.34	9.71	9.96	8.98	9.17
Mn	0.14	0.14	0.13	0.15	0.14	0.16	0.15	0.13	0.13
P	0.33	0.40	0.32	0.42	0.30	0.21	0.31	0.23	0.23

The error for the measurement of fused disks is up to 2 %.

ICP-MS

ppm	CA05	CG05	MA05	MC05	MM05	MN05	MQ05	MR05	VF05
Li	6.23	6.59	7.15	7.06	7.59	9.55	5.55	6.74	8.33
Be	1.40	1.57	1.29	1.53	1.09	1.09	1.05	1.29	1.13
B	1.21	1.51	0.81	1.35	0.82	1.02	0.71	1.02	1.00
Na	21651	21223	18770	21313	20331	17162	16664	21356	23506
Mg	77251	82308	73971	85105	75046	78036	82151	58200	62325
Al	62812	58843	56902	56362	65126	59212	47916	72540	77427
P	32784	39019	29074	40649	27960	19732	25823	23392	23820
K	9489	10871	8409	10412	6891	7724	4920	9373	7128
Ca	65167	64558	57985	64837	61677	55070	53485	65190	61109
Sc	25	23	23	23	23	25	21	28	25
Ti	17548	18081	15151	17871	14666	15778	12874	18800	16528
V	259	255	222	255	214	210	204	249	226
Cr	304	411	442	421	393	457	435	324	356
Mn	1494	1448	1256	1482	1451	1563	1328	1353	1373
Fe	96228	97322	83941	97352	90849	91106	84025	91042	94086
Co	89	88	80	88	81	85	78	98	80
Ni	299	347	298	365	317	371	349	197	240
Cu	60	67	69	73	98	93	76	62	53
Zn	124	< 120.93	111	123	137	114	99	119	129
Ga	17	17	15	17	16	15	13	19	18
As	2.18	2.34	1.80	2.44	2.08	2.04	1.59	1.86	1.85
Se	0.44	0.44	0.38	0.44	0.39	0.35	0.36	0.46	0.38
Rb	25	29	22	28	18	18	9.85	22	13
Sr	774	816	570	824	711	511	621	617	518
Y	24	25	20	24	22	20	19	24	22
Zr	239	273	214	274	205	227	198	262	243
Nb	60	79	45	79	50	53	56	61	48
Mo	1.89	2.50	1.48	2.50	1.76	1.12	1.21	1.40	0.94
Ag	3.67	5.39	3.13	3.45	3.09	3.28	2.53	3.53	2.61
Cd	0.41	0.39	0.35	0.40	0.39	0.55	0.29	0.42	0.38
Sn	2.18	2.43	2.36	2.88	2.08	1.95	1.68	2.02	2.42
Sb	0.12	0.11	0.07	0.11	0.07	0.09	0.07	0.07	0.18
Te	0.04	< 0.031	0.03	< 0.026	0.03	0.04	0.02	< 0.024	< 0.021
Cs	0.22	0.37	0.38	0.34	0.22	0.28	0.20	0.27	0.13
Ba	454	524	309	502	398	410	390	464	267
La	47	62	30	63	39	32	45	35	25
Ce	94	121	66	123	78	71	88	74	54
Pr	12	14	8.24	15	9.39	8.46	10	9.43	7.05
Nd	48	57	35	58	38	35	40	39	30
Sm	9.22	10	7.13	10	7.39	7.03	7.35	8.03	6.61

Eu	2.88	3.10	2.24	3.15	2.39	2.21	2.24	2.58	2.18
Gd	8.34	8.98	6.60	9.15	6.87	6.48	6.54	7.56	6.46
Tb	1.01	1.06	0.83	1.08	0.85	0.82	0.79	0.96	0.84
Dy	5.60	5.71	4.62	5.77	4.79	4.56	4.29	5.39	4.73
Ho	0.89	0.89	0.75	0.90	0.78	0.74	0.69	0.88	0.79
Er	2.25	2.20	1.90	2.22	2.00	1.88	1.74	2.24	2.00
Tm	0.27	0.26	0.23	0.26	0.24	0.23	0.21	0.27	0.25
Yb	1.61	1.52	1.39	1.51	1.47	1.40	1.25	1.65	1.48
Lu	0.22	0.21	0.19	0.20	0.20	0.19	0.17	0.23	0.20
Hf	5.68	6.35	5.22	6.37	4.73	5.39	4.47	6.29	5.61
Ta	4.20	5.46	3.49	5.59	3.60	4.18	3.73	4.69	3.72
W	561	633	592	531	444	431	411	1135	464
Hg	1.76	2.05	2.17	2.11	2.12	1.73	1.73	4.96	2.16
Tl	0.03	0.02	0.07	0.02	0.03	0.09	0.02	0.04	0.03
Pb	2.99	3.36	2.84	3.52	3.73	2.73	2.24	1.93	2.25
Bi	0.01	0.02	0.03	0.02	0.01	0.02	0.01	0.01	0.02
Th	4.33	6.04	2.94	6.10	3.54	3.12	4.13	3.11	2.12
U	0.97	1.33	0.68	1.30	0.88	0.61	0.83	0.70	0.43

The error for the ICP measurement is less than 10 %.

The measurements were performed by NITG Geolab at the Utrecht University(2006).

Appendix D: Results of the AMS measurements

sample	Ratio $^{37/35}Cl$	Ratio $^{36}Cl/^{35}Cl$ $[10^{-15}]$	conc Cl nat [ppm]	$[^{36}Cl]$ in rock 10^4 at.g^{-1}	Prod. rate (SLHL) (at.g(rock)$^{-1}$yr^{-1})
CA 05/01-3	0.276 ± 0.001	245 ± 21	463 ± 22	170 ± 16	16.4 ± 1.9
CA 05/03-2	0.249 ± 0.001	291 ± 16	281 ± 10	135 ± 8	12.6 ± 1.2
CA 05/03-2	0.268 ± 0.001	146 ± 28	408 ± 17	92 ± 18	8.5 ± 1.8
CA 05/05-3-1	0.241 ± 0.002	204 ± 9	273 ± 9	96 ± 5	9.4 ± 0.8
CA 05/05-3-2	0.242 ± 0.001	219 ± 8	278 ± 9	104 ± 5	10.2 ± 0.8
CG 05/01-1	0.255 ± 0.001	133 ± 16	294 ± 11	63 ± 8	14.4 ± 5.9
CG 05/01-3	0.248 ± 0.001	125 ± 13	269 ± 9	56 ± 6	12.7 ± 5.1
CG 05/04f-1	0.213 ± 0.001	386 ± 33	151 ± 4	113 ± 10	27.9 ± 11.1
CG 05/04w-1	0.259 ± 0.001	281 ± 24	303 ± 12	135 ± 12	33.6 ± 13.4
CG 05/05-5	0.222 ± 0.001	165 ± 14	175 ± 5	54 ± 5	12.6 ± 5.0
CG 05/06-1-1	0.246 ± 0.001	187 ± 9	308 ± 10	96 ± 5	22.6 ± 8.9
CG 05/06-1-2	0.246 ± 0.002	186 ± 8	308 ± 11	96 ± 5	22.5 ± 8.8
MA 05/01-1	0.259 ± 0.001	271 ± 14	358 ± 13	154 ± 9	8.3 ± 0.8
MA 05/01-1	0.261 ± 0.001	300 ± 9	370 ± 14	175 ± 8	9.5 ± 0.9
MA 05/02 (60)-2	0.270 ± 0.002	193 ± 18	391 ± 17	115 ± 12	6.3 ± 0.8
MA 05/02-2	0.257 ± 0.001	66 ± 8	352 ± 13	37 ± 5	2.0 ± 0.3
MA 05/02-3	0.270 ± 0.002	160 ± 20	362 ± 16	88 ± 11	4.8 ± 0.7
MA 05/03-3	0.273 ± 0.001	176 ± 18	365 ± 17	97 ± 10	5.3 ± 0.7
MC 05/01-2-1	0.260 ± 0.001	148 ± 7	322 ± 13	76 ± 4	7.6 ± 0.9
MC 05/01-2-2	0.259 ± 0.002	152 ± 10	315 ± 12	76 ± 6	7.6 ± 0.9
MC 05/01-3	0.255 ± 0.001	335 ± 19	295 ± 11	160 ± 10	16.0 ± 1.9
MC 05/02-3	0.226 ± 0.001	172 ± 9	183 ± 5	57 ± 3	5.6 ± 0.6
MC 05/05-2	0.253 ± 0.001	133 ± 12	280 ± 10	61 ± 6	6.0 ± 0.8
MM 05/01-3	0.253 ± 0.001	284 ± 11	276 ± 10	128 ± 6	6.4 ± 0.5
MM 05/02-1	0.257 ± 0.001	549 ± 34	368 ± 13	323 ± 22	16.5 ± 1.6
MM 05/02-2	0.255 ± 0.001	233 ± 19	284 ± 10	107 ± 9	5.5 ± 0.6
MM 05/04-2	0.223 ± 0.001	362 ± 17	203 ± 6	136 ± 7	7.1 ± 0.6

MM 05/04f-1	0.241 ± 0.001	446 ± 35	234 ± 8	179 ± 15	9.3 ± 1.0
MM 05/04w-1	0.237 ± 0.001	459 ± 24	213 ± 7	170 ± 10	8.9 ± 0.8
MN 05/03-2	0.240 ± 0.001	730 ± 25	202 ± 7	253 ± 11	11.6 ± 0.9
MN 05/04-3	0.253 ± 0.001	730 ± 19	264 ± 10	314 ± 12	15.6 ± 1.2
MN 05/05-2-1	0.240 ± 0.001	797 ± 18	262 ± 8	358 ± 12	18.2 ± 1.3
MN 05/05-2-2	0.243 ± 0.002	797 ± 18	273 ± 9	370 ± 12	18.8 ± 1.4
MN 05/07-1	0.236 ± 0.001	767 ± 28	249 ± 7	333 ± 14	15.8 ± 1.2
MQ 05/03-2-1	0.197 ± 0.001	544 ± 14	168 ± 4	192 ± 6	16.9 ± 2.5
MQ 05/03-2-2	0.193 ± 0.001	548 ± 15	161 ± 4	188 ± 6	16.6 ± 2.4
MQ 05/03-3	0.213 ± 0.001	687 ± 28	151 ± 4	200 ± 9	17.7 ± 2.6
MQ 05/07-1	0.235 ± 0.001	571 ± 22	258 ± 8	258 ± 12	21.9 ± 3.3
MQ 05/07-2	0.245 ± 0.001	704 ± 16	251 ± 8	298 ± 10	25.2 ± 3.7
MR 05/01-2-1	0.249 ± 0.002	545 ± 14	245 ± 9	221 ± 8	17.2 ± 1.6
MR 05/01-2-2	0.245 ± 0.001	555 ± 16	228 ± 8	213 ± 8	16.6 ± 1.6
MR 05/01-3	0.244 ± 0.001	758 ± 28	231 ± 8	296 ± 13	23.0 ± 2.2
MR 05/01-3	0.244 ± 0.001	753 ± 15	231 ± 8	294 ± 10	22.8 ± 2.1
MR 05/02-3	0.239 ± 0.001	724 ± 34	213 ± 7	266 ± 14	21.1 ± 2.1
VF 05/04-3	0.211 ± 0.001	425 ± 45	134 ± 4	111 ± 12	8.0 ± 1.0
VF 05/04-3	0.202 ± 0.001	473 ± 38	119 ± 3	115 ± 9	8.3 ± 0.9
VF 05/04-60-1	0.202 ± 0.001	734 ± 32	125 ± 3	187 ± 9	13.4 ± 1.1
VF 05/04-60-1	0.204 ± 0.001	773 ± 43	128 ± 3	200 ± 12	14.3 ± 1.3
VF 05/06-2	0.180 ± 0.001	551 ± 37	90 ± 2	113 ± 8	7.9 ± 0.8

The results of the AMS analyses.

The numbering of the samples (e.g. MM 05/01-3) is organized as follows: The first two letters describe the locality, i.e. the flow. The two numbers following give the year of collection, and the two numbers behind the slash are the rock sample number taken from the respective flow. The number behind the hyphen gives the number of preparation for AMS. In some cases there are one more hyphen and a number, which indicate that two AMS samples made from the same preparation procedure were measured together in one batch.

Appendix E: Geological time scale.

Era	Period		Epoch	Begin (Myr ago)
Cenozoic	**Quaternary**		Holocene	0.01
			Pleistocene	2.6
	Tertiary	**Neogene**	Pliocene	5.3
			Miocene	23.0
		Paleogene	Oligocene	33.9
			Eocene	55.8
			Paleocene	65.5
Mesozoic	**Cretaceous**		Late	99.6
			Early	145.5
	Jurassic		Late	161.2
			Middle	175.6
			Early	199.6
	Triassic		Late	228.0
			Middle	245.0
			Early	251.0
Paleozoic	**Permian**		Lopingian	260.4
			Guadalupian	270.6
			Cisuralian	299.0
	Carboniferous		Pennsylvanian	318.1
			Mississippian	359.2
	Devonian		Late	385.3
			Middle	397.5
			Early	416.0
	Silurian		Pridoli	418.7
			Ludlow	422.9
			Wenlock	428.2
			Llandovery	443.7
	Ordovician		Late	460.9
			Middle	471.8
			Early	488.3
	Cambrian		Furongian	501
			Middle	513
			Early	542
Pre-Cambrian				

(Simplified, after Gradstein et al., 2004)

References

Abratis, M., Schmincke, H.-U., Hansteen, T.H., 2002. Composition and evolution of submarine volcanic rocks from the central and western Canary Islands. Int. Journ. Earth Sci. (Geol. Rundschau), v 91, pp 562-582.

Ahijado, A., Casillas, R., Hernández-Pacheco, A., 2001. The dyke swarms of the Amanay Massif, Fuerteventura, Canary Islands (Spain). Journ. Asian Earth Sci., v 19, pp 333-345.

Alfimov, V., 2005. Accelerator mass spectrometry of ^{36}Cl and ^{129}I. Analytical aspects and applications. PhD thesis, University of Uppsala, 81 p.

Allkofer, O.C., Grieder, P.K.F., 1984. Cosmic rays on earth. Physics Data, 25-1. Fachinformationszentrum, Karlsruhe.

Almendros, J., Luzón, F., Posadas, A., 2004. Microtremor analyses at Teide volcano (Canary Islands, Spain): Assessment of natural frequencies of vibration using time dependent horizontal-to-vertical spectral ratios. Pure Appl. Geophys., v 161, pp 1579-1596.

Ancochea, E., Brändle, J.L., Cubas, C.R., Hernán, F., Huertas, M.J., 1996. Volcanic complexes in the eastern ridge of the Canary Islands: the Miocene activity of the island of Fuerteventura. Journ. Volc. Geotherm Res. v 70, pp 183-204.

Anguita, F., Hernán, F., 2000. The Canary Islands origin: a unifying model. Journ. Volcan. Geoth. Res., v 103, pp 1-26.

Balogh, K., Ahijado, A., Casillas, R., Fernández, C., 1999. Contributions to the chronology of the Basal Complex of Fuerteventura, Canary Islands. Journ. Volcan. Geoth. Res., v 90, pp 81-101.

Benson, L., Madole, R., Landis, G., Gosse, J., 2005. New data for Late Pleistocene Pinedale alpine glaciation from southwestern Colorado, Quat. Sci. Rev., v 24, pp 49-65.

Bintanja, R., van de Wal, R.S.W., Oerlemans, J., 2005. A new method to estimate ice age temperatures. Clim. Dyn., v 24, pp 197-211.

Boberg, P.R., Tylka, A.J., Adams, J.H.,Jr., Flückiger, E.O., Kobel, E., 1995. Geomagnetic transmission of solar energetic protons during the geomagnetic disturbances of October 1989. Geophys. Res. Lett., v 22, no 9, pp 1133-1136.

van der Borg, K., Alderliesten, C., Haitjema, H., Hut, G., van Zwol, N.A., 1984. The Utrecht accelerator facility for precision dating with radionuclides. Nucl. Instr. Meth. Phys. Res., B5, pp 224-228.

van der Borg, K., Alderliesten, C., Houston, C.M., de Jong, A.F.M., van Zwol, N.A., 1987. Accelerator mass spectrometry with ^{14}C and ^{10}Be in Utrecht. Nucl. Instr. Meth. Phys. Res., B29, pp 143-145.

Bowen, R., 1988. Isotopes in the earth sciences. Elsevier Applied Science Publishers Ltd., London, New York, 647 p.

Brown E.T., Bourles, D.L., Colin, F., Raisbeck, G.M., Yiou, F., Desgarceaux, S., 1995. Evidence for muon-induced in situ production of ^{10}Be in near surface rocks from the Congo. Geoph. Res. Lett., v 22, pp 703-706.

Butler, R., 1992. Paleomagnetism: magnetic domains to geologic terranes. Blackwell, Boston, 319 p.

Carracedo, J.C., Day, S., Guillou, H., Rodríguez Badiola, E., Canas, J.A., Pérez Torrado, F.J., 1998. Hotspot volcanism close to a passive continental margin: the Canary Islands. Geol. Mag., v 135, no 5, pp 591-604.

Cerling, T.E., Craig, H., 1994. Geomorphology and in-situ cosmogenic isotopes. Ann. Rev. Earth Planet. Sci., v 22, pp 273-317.

Charalambus, S., 1971. Nuclear transmutation by negative stopped muons and the activity induced by cosmic-ray muons. Nucl. Phys., A166, pp 145-161.

Coello, J., Cantagrel, J-M., Hernán, F., Fúster, J-M., Ibarrola, E., Ancochea, E., Casquet, C., Jamond, C., Díaz de Téran, J-R., Cendrero, A., 1992. Evolution of the eastern volcanic ridge of the Canary Islands based on new K-Ar data. Journ. Volc. Geotherm. Res. v 53, pp 251-274.

Constable, C., 2007. Nondipole field. In: Gubbins, D., Herrera-Bervera, E. (ed.s) Encyclopedia of geomagnetism and paleomagnetism. Encyclopedia of earth sciences series, Springer, Berlin Heidelberg New York, pp 701-704.

Dep, L., Elmore, D., Lipschutz, M., Vogt, S., Phillips, F.M., Zreda, M., 1994a. Depth dependence of cosmogenic neutron-capture produced ^{36}Cl in a terrestrial rock. Nucl. Instr. Meth. Phys. Res., B92, pp 301-307.

Dep, L., Elmore, D., Fabryka-Martin, J., Masarik, J., Reedy, R.C., 1994b. Production rate systematics of in-situ produced cosmogenic nuclides in terrestrial rocks: Monte Carlo approach of investigating ^{35}Cl(n,γ)^{36}Cl. Nucl. Instr. Meth. Phys. Res., B92, pp 321-325.

Dep, L., 1995. Cosmogenic radionuclide production in terrestrial rocks: accelerator mass spectrometry measurements and Monte Carlo simulations. PhD thesis, at Purdue University, La Fayette, IN. 154 p.

Desilets, D., Zreda, M., 2003. Spatial and temporal distribution of secondary cosmic-ray nucleon intensities and applications to in situ cosmogenic dating. Earth Planet. Sci. Lett., v 206, no 1-2, pp 21-42.

Desilets, D., Zreda, M., Prabu, T., 2006. Extended scaling factors for in situ cosmogenic nuclides: New measurements at low latitude. Earth Planet. Sci. Lett., v 246, pp 265-276.

Dunai, T.J., 2000. Scaling factors for production rates of in situ produced cosmogenic nuclides: a critical reevaluation. Earth Planet. Sci. Lett., v 176, pp 157-169.

Dunai, T.J., 2001. Influence of secular variation of the geomagnetic field on production rates of in situ produced cosmogenic nuclides. Earth Planet. Sci. Lett., v 193, pp 197-212.

Dunai, T.J., Stuart, F.M., Pik, R., Burnard, P., Gayer, E., 2007. Production of ^{3}He in crustal rocks by cosmogenic thermal neutrons. Earth Planet. Sci. Lett., v 258, pp 228-236.

Easterbrook, D.J., 2003. Comment on the paper "Determination of ^{36}Cl production rates from the well-dated deglaciation surfaces of Whidbey and Fidalgo Islands, Washington" by T.W. Swanson and M.C. Caffee. Quart. Res., v 59, pp 132-134.

Elmore, D., Phillips, F.M., 1987. Accelerator mass spectrometry for measurement of long-lived Radioisotopes. Science, v 236, pp 543-550.

Evans, J.M., Stone, J.O.H., Fifield, L.K., Cresswell, R.G., 1997. Cosmogenic chlorine-36 production in K-feldspar. Nucl. Instr. Meth. Phys. Res., B123, pp 334-340.

Evans, J.M., 2002. Calibration of the production rates of cosmogenic ^{36}Cl from potassium. PhD dissertation, Australian National University, Canberra, 142 pp.

Fabryka-Martin, J.T., 1988. Production of radionuclides in the earth and their hydrogeologic significance, with emphasis on chlorine-36 and iodine-129. PhD thesis, University of Arizona, Tucson, 400 pp.

Faure, G., 2001. Origin of igneous rocks. The isotopic evidence. Springer-Verlag Berlin Heidelberg, 496 p.

Faure, G., Mensing, T.M., 2005. Isotopes. Principles and Applications. John Wiley & Sons, Inc., New Jersey, 897 p.

Fifield L.K., Evans, J.M., Stone J.O., 2002. Calibration of the production rate of Cl-36 from potassium. Geochim. Cosmochim. Acta, v 66, no 15A, pp A234**.**

Fink, D., Vogt, S., Hotchkis, M., 2000. Cross sections for ^{36}Cl from Ti at E_p=35-150 MeV: Applications to in-situ exposure dating. Nucl. Instr. Meth. Phys. Res., B172, pp 861-866.

Finkel, R.C., Suter, M., 1993. AMS in the earth sciences: Technique and applications. Advances in analytical geochemistry, v1, pp 1-114.

Freeman, S., Bishop, P., Bryant, C., Cook, G., Dougans, D., Ertunc, T., Fallick, A., Ganeshram, R., Maden, C., Naysmith, P., Schnabel, C., Scott, M., Summerfield, M., Xu, S., 2007. The SUERC AMS laboratory after 3 years. Nucl. Instr. Meth. Phys. Res. B259, pp 66-70.

Gasse, F., 2000. Hydrological changes in the African tropics since the Last Glacial Maximum. Quat. Sci. Rev., v 19, pp 189-211.

Gee, M.J.R., Masson, D.G., Watts, A.B., Mitchell, N.C., 2001. Offshore continuation of volcanic rift zones, El Hierro, Canary Islands. Journ. Volcan. Geoth. Res.,v 105, pp 107-119.

Gibbard, P.L., Cohen, K.M., Boreham, S. & Moscariello, A. 2007. Global chronostratigraphical correlation table for the last 2.7 million years. Subcommission on Quaternary Stratigraphy, International Commission on Stratigraphy, Cambridge.

Gillespie, A.R., Bierman, P.R., 1995. Precision of terrestrial exposure ages and erosion rates estimated from analysis of cosmogenic isotopes produced in situ. Journ. Geophys. Res., v 100, no B12, pp 24,637-24,649.

Gosse, J.C., Phillips, F.M., 2001. Terrestrial in situ cosmogenic nuclides: theory and application. Quat. Sci. Rev., v 20, pp 1475-1560.

Gradstein, F.M., Ogg, J.G., Smith, A., (eds.) 2004. A geologic time scale 2004. Cambridge University Press, Cambridge, 589 p.

Granger, D.E., Kirchner, J.W., Finkel, R., 1996. Spatially averaged long-term erosion rates measured from in situ-produced cosmogenic nuclides in alluvial sediment. Journ. Geol., v 104, no 3, pp 249-257.

Granger, D.E., Smith, A.L., 2000. Dating buried sediments using radioactive decay and muogenic production of 26Al and 10Be. Nucl. Instr. Meth. Phys. Res., B172, pp 822-826.

Guillou, H., Carracedo, J.C., Paris, R., Pérèz Torrado, F.J., 2004. Implications for the early shield-stage evolution of Tenerife from K/Ar ages and magnetic stratigraphy. Earth Planet. Sci. Lett., v 222, pp 599-614.

Gurenko, A.A., Hoernle, K.A., Hauff, F., Schmincke, H.-U., Han, D., Miura, Y.N., Kaneoka, I., 2006. Major, trace element and Nd-Sr-Pb-O-He-Ar isotope signatures of shield stage lavas from the central and western Canary Islands: insights into mantle and crustal processes. Chem. Geol., v 233, pp 75-112.

Guyodo, Y, Valet, J.-P., 1999. Global changes in intensity of the Earth's magnetic field during the past 800 kyr. Nature, v 399, pp 249-252.

De Haas, A.F., Langerak, J.J., Oskamp, G.J., de Vries, H., van der Borg, K., 1987. Pulsed beam measurement system. Nucl. Instr. Meth., B29, pp 91-93.

Hart, S.R., Hauri, E.U., Oschmann, L.A., Whitehead, J.A., 1992. Mantle plumes and entrainment: isotopic evidence. Science, v 256, pp 517-520.

Heisinger, B., Lal, D., Jull, A.J.T., Kubik, P., Ivy-Ochs, S., Neumaier, S., Knie, K., Lazarev, V., Nolte, E., 2002a. Production of selected cosmogenic radionuclides by muons: 1. Fast muons. . Earth Planet. Sci. Lett., v 200, pp 345-355.

Heisinger, B., Lal, D., Jull, A.J.T., Kubik, P., Ivy-Ochs, S., Knie, K., Nolte, E., 2002b. Production of selected cosmogenic radionuclides by muons: 2. Capture of negative muons. Earth Planet. Sci. Lett., v 200, pp 357-369.

Hoernle, K., 1998. Geochemistry of Jurassic oceanic crust beneath Gran Canaria (Canary Islands): Implications for crustal recycling and assimilation. Journ. Petrol., v 39, no 5, pp 859-880.

Ivy-Ochs, S., 1996. The dating of rock surfaces using in situ produced ^{10}Be, ^{26}Al and ^{36}Cl, with examples from Antarctica and the Swiss Alps. PhD thesis, ETH Zürich, 196 p.

Ivy-Ochs, S., Schlüchter, C., Kubik, P.W., Denton, G.H., 1999. Moraine exposure dates imply synchronous Younger Dryas glacier advances in the European Alps and in the Southern Alps of New Zealand. Geograf. Annaler, 81A, pp 313-323.

Ivy-Ochs, S., Kober, F., Alfimov, V., Kubik, P.W., Synal, H.-A., 2007. Cosmogenic ^{10}Be, ^{21}Ne and ^{36}Cl in sanidine and quartz from Chilean ignimbrites. Nucl. Instr. Meth. Phys. Res., B259, pp 588-594.

Johnson, C.L., Constable, C.G. 1997. The time-averaged geomagnetic field: global and regional biases for 0-5 Ma. Geophys. Journ. Int., v 131, pp 643-666.

Klein, J., Gosse, J., 1996. Terrestrial factors that influence production rates. Radiocarbon, v. 38, pp 161-162.

Korte, M., Constable, C.G., 2003. Continuous global geomagnetic field models for the past 3000 years. Phys. Earth Planet. Int., v 140, pp 73-89.

Korte, M., Constable, C.G., 2005. The geomagnetic dipole moment over the last 7000 years-new results from a global model. Earth Planet. Sci. Lett., v 236, pp 348-358.

Korte, M., Genevey, A., Constable, C.G., Frank, U., Schnepp, E., 2005. Continuous geomagnetic field models for the past 7 millennia: 1. A new global data compilation. G3, v 6, no 2, doi: 10.1029/2004GC000800.

Korte, M., Constable, C.G., 2006a. Centennial to millennial geomagnetic secular variation. Geophys. Journ. Int. v 167, pp 43-52.

Korte, M., Constable, C.G., 2006b. on the use of calibrated relative paleointensity records to improve millennial-scale geomagnetic field models. G3, v 7, no 9. doi:10.1029/2006GC001368.

Kutzbach, J., Gallimore, R., Harrison, S., Behling, P., Selin, R., Laarif, F., 1998. Climate and biome simulations for the past 21,000 years. Quat. Sci. Rev., v 17, pp 473-506.

de Laat, C.T.A.M., Kuijer, P.G., Mutsaers, P., 1992. Conf. Proc. of the 2nd Int. Workshop of software engineering, artificial intelligence and expert systems for high-energy and nuclear physics, La-Londe-les-Maures, France, World Scientific Publ. Co. Pte. Ltd., Singapore.

Lal, D., 1987. Cosmogenic nuclides produced in situ in terrestrial solids. Nucl. Instr. Meth. Phys. Res., B 29, pp 238-245.

Lal, D., 1988. In situ produced cosmogenic isotopes in terrestrial rocks. Ann. Rev. Earth Planet. Sci., v 16, pp 355-388.

Lal, D., Peters, B., 1967. Cosmic ray produced radioactivity on the earth. *in* Sitte, K., ed., Handbuch der Physik: New York, Springer-Verlag, p. 551-612.

Lal, D., 1991. Cosmic ray labeling of erosion surfaces : in situ nuclide production rates and erosion models. Earth Planet. Sci. Lett., v 104, pp 424-439.

Leavy, B.D., Phillips, F.M., Elmore, D., Kubik, P.W., Gladney, E., 1987. Measurement of cosmogenic 36Cl/Cl in young volcanic rocks: an application of accelerator mass spectrometry in geochronology. Nucl. Instr. Meth. Phys. Res., B 29, pp 246-250.

Le Bas, M.J., Rex, D.C., Stillman, C.J., 1986. The early magmatic chronology of Fuerteventura. Geol. Mag., v 123, 287-298.

Lee, J.-Y., Marti, K., Severinghaus, J.P., Kawamura, K., Yoo, H.-S., Lee, J.B., Kim, J.S., 2006. A redetermination of the isotopic abundances of atmospheric Ar. Geochim. Cosmochim. Acta, v 70, pp 4507–4512.

Licciardi, J.M., Denoncourt, C.L., Finkel, R.C., 2008. Cosmogenic ^{36}Cl production rates from Ca spallation in Iceland. Earth Planet. Sci. Lett., v 267, pp 365-377.

Lifton, N.A., Bieber, J., Clem, J., Duldig M., Evenson, P., Humble, J., Pyle, R., 2005. Addressing solar modulation and long term uncertainties in scaling secondary cosmic rays for in situ cosmogenic nuclide applications. Earth Planet. Sci. Lett., v 239, pp 140-161.

Lifton, N.A., Smart D.F., Shea, M.A., 2008. Scaling time-integrated in situ cosmogenic nuclide production rates using a continuous geomagnetic model. Earth Planet. Sci. Lett., v 268, pp190-201.

Lingenfelter, R.E., 1963. Production of ^{14}C by cosmic ray neutrons. Rev. Geophys., v 1, pp 35-55.

Lingenfelter, R.E., Flamm, E.J., 1964. Solar neutrons and the earth radiation belts. Science, v 144, pp 292-294.

Litherland, A.E., 1984. Accelerator mass spectrometry. Nucl. Instr. Meth. Phys. Res., B 5, pp 100-108.

Lohmann, G., Lorenz, S.J., 2007. Orbital Forcing on Atmospheric Dynamics During the Last Interglacial and Glacial Inception, in: Developments in Quaternary Science Volume 7, The Climate of Past Interglacials, pp 527-545,

Lundstrom, C.C., Hoernle, K., Gill, J., 2003. U-series disequilibria in volcanic rocks from the Canary Islands: plume versus lithospheric melting. Geochim. Cosmochim. Acta, v 67, no 21, pp 4153-4177.

Maden, C., Anastasi, P.A.F., Dougans, A., Freeman, S.P.H.T., Kitchen, R., Klody, G., Schnabel, C., Sundquist, M., Vanner, K., Xu, S., 2007. SUERC AMS ion detection. Nucl. Instr. Meth. Phys. Res., B259, pp 131-139.

Magaritz, M., Jahn, R., 1992. Pleistocene and Holocene soil carbonates from Lanzarote, Canary Islands, Spain: Paleoclimatic implications. Catena, v 19, pp 511-519.

Masarik, J., Reedy, R.C., 1995. Terrestrial cosmogenic-nuclide production systematics calculated from numeric simulations. Earth Planet. Sci. Lett., v 136, pp 381-395.

Masarik, J., Beer, J., 1999. Simulation of particle fluxes and cosmogenic nuclide production in the earth's atmosphere. Journ. Geophys. Res., D104 (10), 12099-13012.

Masarik, J., Frank, M., Schäfer, J.M., Wieler, R., 2001. Correction of in-situ cosmogenic nuclide production rates for geomagnetic field intensity variations during the past 800,000 years. Geochim. Cosmochim. Acta, v 65, pp 2995-3003.

McMillan, D.G., Constable, C.G., Parker, R.L., 2004. Assessing the dipolar signal in stacked paleointensity records using a statistical error model and geodynamo simulations. Phys. Earth Planet. Int., v 145, pp 37-54.

Merrill, R.T., McElhinny, M.W., McFadden, P.L., 1996. The magnetic field of the earth. Paleomagnetism, the core, and the deep mantle. Academic Press, San Diego, USA, 531 p.

Middleton, R., 1989. A negative-ion cookbook. Dept. of Physics, University of Pennsylvania, Philadelphia.

Millikan, R.A., Neher, H.V., 1935. The equatorial longitude effect in cosmic rays. Phys. Rev., v 47, no 3, pp 205-315.

Montelli, R., Nolet, G., Dahlen, F.A., Masters, G., Engdahl, E.R., Hung, S.-H., 2004. Finite-frequency tomography reveals a variety of plumes in the mantle. Science, v 303, pp 338-343.

Muñoz, M., Sagredo, J., de Ignacio, C., Fernández-Suárez, J., Jeffries, T.E., 2005. New data (U-Pb, K-Ar) on the geochronology of the alkaline-carbonatitic association of Fuerteventura, Canary Islands, Spain. Lithos, v 85, pp 140-153.

Niedermann, S., Graf, T., Marti, K., 1993. Mass spectrometric identification of cosmic-ray produced neon in terrestrial rocks with multiple neon components. Earth Planet. Sci. Lett., v 118, no 1-4, pp 65-73.

Niedermann, S., 2002. Cosmic-ray-produced noble gases in terrestrial rocks: Dating tools for surface processes. Rev. Min. Geochem., v 47, pp 731-784.

Nier, A.O., 1950. A redetermination of the relative abundances of the isotopes of carbon, nitrogen, oxygen, agron and potassium. Physical Review, v 77, no 6, pp 789-793.

Nishiizumi, K., Winterer, E.L., Kohl, C.P., Klein, J., Middleton, R., Lal, D., Arnold, J.R., 1989. Cosmic ray production rates of ^{10}Be and ^{26}Al in quartz from glacially polished rocks. Journ. Geophys. Res., v 94, no B 12, pp 17907-17915.

Nishiizumi, K., Arnold, J.R., Fink, D., Klein, J., Middleton, R., Brownlee, D.E., Maurette, M., 1991. Earth Planet. Sci. Lett., v 104, pp 315-324.

O'Connor, J.M., Stoffers, P., van den Bogaard, P., McWilliams, M., 1999. First seamount age evidence for significantly slower African plate motion since 19 to 30 Ma. Earth Planet. Sci. Lett., v 171, pp 575-589.

Phillips, F.M., Leavy, B.D., Jannik, N.O., Elmore, D., Kubik, P.W., 1986. The accumulation of cosmogenic chlorine-36 in rocks: a method for surface exposure dating. Science, v 231, no 4733, pp 41-43.

Phillips, F.M., Zreda, M.G., Flinsch, M.R., 1996. A reevaluation of cosmogenic ^{36}Cl production rates in terrestrial rocks. Geoph. Res. Lett., v 23, no 9, pp 949-952.

Phillips, F.M., Stone, W.D., Fabryka-Martin, J.T., 2001. An improved approach to calculating low-energy cosmic-ray neutron fluxes near the land/atmosphere interface. Chem. Geol., v 175, pp 689-701.

Pigati, J.S., Lifton, N.A., 2004. Geomagnetic effects on time-integrated cosmogenic nuclide production with emphasis on in-situ ^{14}C and ^{10}Be. Earth Planet. Sci. Lett., v 226, pp 193-205.

Quenby, J.J., Wenk, G.J., 1962. Cosmic ray threshold rigidities and the earth's magnetic field. Philosophical Magazine, v7, no 81, pp 1457-1471.

Raisbeck, G.M., Yiou, F., 1989. Cosmic-ray exposure ages of cosmic spherules. Meteoritics, v 24, no 4, pp 318-318.

Reedy, R.C., Arnold, J.R., 1972. Interaction of solar and galactic cosmic-ray particles with the moon. Journ. Geophys. Res., v 77, no 4, pp 537-555.

Reedy, R.C., Arnold, J.R. Lal, D., 1983. Cosmic ray record in solar system matter. Science, v 219, no 4581, pp 127-135.

Reedy, R.C., 1987. Predicting the production rates of cosmogenic nuclides in extraterrestrial matter. Nucl. Instr. Meth. Phys. Res. B, v 29, pp 251-261.

Rothe, P., 1986. Sammlung geologischer Führer 81. Kanarische Inseln. Gebr. Bornträger, Berlin, Stuttgart, pp 70-100.

Salis, J.-S., Bonhommet, N., Levi, S., 1989. Paleointensity of the geomagnetic field from dated lavas of the Chaîne des Puys, France 1.7 – 12 thousand years before present. Journ. Geophys. Res., v 94, no B11, pp 15771-15784.

Schiekel, T., Sudbrock, F., Herpers, U., Gloris, M., Leya, I., Michel, R., Synal, H.-A., Suter, M., 1996. On the production of ^{36}Cl by high energy protons in thin and thick targets. Nucl. Instr. Meth. Phys. Res. B113, pp 484-489.

Schmincke, H.U., 1982. Geology of the northwest African continental margin. Volcanic and chemical evolution of the Canary Islands. Springer Berlin, pp 273-308.

Schmincke, H-U., Klügel, A., Hansteen, T.H., Hoernle, K., Bogaard, P. vd, 1998. Samples from the Jurassic ocean crust beneath Gran Canaria, La Palma and Lanzarote (Canary Islands). Earth Planet. Sci. Lett., pp 343-360.

Schneider, B., Kuiper, K.F., Wijbrans, J.R., Mai, K., (2009) ^{40}Ar/^{39}Ar geochronology on upper Pleistocene basalts from Fuerteventura. Submitted to Quartenary Geochronology CRONUS-EU special issue.

Simpson, J.A., 1983. Elemental and isotopic composition of the galactic cosmic rays. Ann. Rev. Nucl. Part. Sci., v 33, pp 323-381.

Simpson, J.A., 2000. The cosmic ray nucleonic component: the invention and scientific uses of the neutron monitor. Space Sci. Rev., v 93, pp 11-32.

Staiger, J., Gosse, J., Toracinta, R., Oglesby, B., Fastook, J., Johnson, J.V., 2007. Atmospheric scaling of cosmogenic nuclide production: Climate effect. Journ. Geophys. Res., v 112, B02205, doi:10.1029/2005JB003811.

Steiner, C., Hobson, A., Favre, P., Stampfli, G.M., Hernandez, J., 1998. Mesozoic sequence of Fuerteventura (Canary Islands): Witness of early Jurassic sea-floor spreading in the central Atlantic. GSA Bull., v 110, no 10, pp 1304-1317.

Stillman, C.J., 1999. Giant Miocene landslides and the evolution of Fuerteventura, Canary Islands. Journ. Volcan. Geoth. Res., v 94, pp 89-104.

Stone, J.O.H., Evans, J.M., Fifield, L.K., Cresswell, R.G., Allan, G.L., 1996a. Cosmogenic Cl-36 production rates from calcium and potassium. Radiocarbon, v 38, pp 170-171.

Stone, J.O.H., Allan, G.L., Fifield, L.K., Cresswell, R.G., 1996b. Cosmogenic chlorine-36 from calcium spallation. Geochim. Cosmochim. Acta, v 60, no 4, pp 679-692.

Stone, J.O.H., Evans, J.M., Fifield, L.K., Allan, G.L., Cresswell, R.G., 1998. Cosmogenic chlorine-36 production in calcite by muons. Geochim. Cosmochim. Acta, v 62, no 3, pp 433-454.

Stone, J.O., 2000. Air pressure and cosmogenic isotope production. Journ. Geophys. Res., v 105, no B10, pp 23,753-23,759.

Stone, J.O., 2005. Terrestrial chlorione-36 production from spallation of iron. 10th International Conference on Accelerator Mass Spectrometry, Berkeley, Calif., Sept. 5-10.

Störmer, C., 1935. On the trajectories of electric particles in the field of a magnetic dipole with applications to the theory of cosmic radiation: fourth communication. Astrophysica Norwegica, v1, no 4, pp 115-184.

Suter, M., 1990. Accelerator mass spectrometry: state of the art in 1990. Nucl. Instr. Meth. Phys. Res., B 52, pp 211-223.

Swanson, T., 1996. Determination of ^{36}Cl production rates from the deglaciaton history of Whidbey and Fidalgo Islands, Washington. In: Santa Fe Workshop Abstracts, Radiocarbon, v 38, no 1, pp 172.

Swanson, T.W., Caffee, M.L., 2001. Determination of ^{36}Cl production rates derived from the well-dated deglaciation surfaces of Whidbey and Fidalgo Islands, Washington. Quart. Res., v 56, pp 366-382.

Synal, H.A., Beer, J., Bonani, G., Hofmann, H.J., Suter, M., Wölfli, W., 1987. Detection of ^{32}Si and ^{36}Cl with the ETH/SIN EN-Tandem. Nucl. Instr. Meth. Phys. Res., B29, pp 146-150.

Templeton, D.H., 1953. Nuclear reactions induced by high energy particles. Ann. Rev. Nucl. Sci, v 2, pp 93-104.

Tera, F., Brown, L., Morris, J., Sacks, I.S., 1986. Sediment incorporation in island-arc magmas: Inferences from ^{10}Be. Geochim. Cosmochim. Acta, v 50, pp 535-550.

Tuniz, C., Bird, J.R., Fink, D., Herzog, G.F., 1998. Accelerator mass spectrometry. Ultrasensitive analysis for global science. CRC Press LLC. Boca Raton, USA, 371 p.

Usoskin, I.G., Solanki, S.K., Korte, M., 2006. Solar activity reconstructed over the last 7000 years: The influence of geomagnetic field changes. Geophys. Res. Lett., v 33, doi:10.1029/2006GL025921.

Valet, J.-P., Meynadier, L., Guyodo, Y., 2005. Geomagnetic dipole strength and reversal rate over the past two million years. Nature, v 435, pp. 802–805.

Webster, J.D., Kinzler, R.J., Mathez, E.A., 1999. Chloride and water solubility in basalt and andesite melts and implications for magmatic degassing. Geochim. Cosmochim. Acta, v 63, no5, pp 729-738.

Yamashita, M., Stephens, L.D., Patterson, H.W., 1966. Cosmic-ray-produces neutrons at ground level: neutron production rate and flux distribution. Journ. Geophys. Res., v 71, no 16, pp 3817-3834.

Yang, Q., Snyder, J.P., Tobler, W.R., 2000a. Map projection transformation. Principles and applications. Taylor & Francis, London, UK. 367 p.

Yang, S., Odah, H., Shaw, J., 2000b. Variations in the geomagnetic dipole moment over the last 12000 years. Geophys. Journ. Int., v 140, pp 158-162.

Ziegler, J.F., 1996. Terrestrial cosmic rays. IBM J. Res. Develop. v 40, no 1, pp 19-39.

Zreda, M.G., Phillips, F.M., Elmore, D., Kubik, P.W., Sharma, P., Dorn, R.I., 1991. Cosmogenic chlorine-36 production rates in terrestrial rocks. Earth Planet. Sci. Lett., v 105, pp 94-109.

Zreda, M.G., Phillips, F.M., Kubik, P.W., Sharma, P., Elmore, D., 1993. Cosmogenic ^{36}Cl dating of a young basaltic eruption complex, Lathrop Wells, Nevada. Geology, v 21, pp 57-60.

Zreda, M.G., Phillips, F.M., 1994. Surface exposure dating by cosmogenic chlorine-36 accumulation. In Beck, C. (ed.) Dating in exposed and surface contexts. Albuquerque, NM, University of New Mexico Press, pp 161-183.

Zreda, M.G., Phillips, F.M., 1995. Insights into alpine moraine development from cosmogenic ^{36}Cl buildup dating. Geomorphology, v 14, pp 149-156.

Zreda, M.G., Phillips, F.M., 2000. Cosmogenic nuclide buildup in surficial materials. Quarternary Geochronology. Methods and applications. AGU Reference shelf 4, editors: Stratton Noller, J., Sowers, J.M., Lettis, W.R., pp 61-76.

Summary

Age determination based on cosmogenic nuclides is an important tool to investigate landscape development and age relations of geologically very young materials. The aim of this study is to contribute data to establish age determination on the basis of cosmogenic ^{36}Cl production as a generally reliable method. Basalt samples from the mid-latitude, low-altitude calibration site of Fuerteventura, Canary Islands were collected and the production rates of ^{36}Cl were determined. These data were then compared with data from other analyses published in the literature.

As described in chapter 2, ^{36}Cl is a radionuclide that is produced by secondary cosmic radiation at the earth surface. The secondary radiation is produced by interaction of atoms of the atmosphere with that part of the primary cosmic radiation that possessed enough energy to penetrate the earth magnetic field. ^{36}Cl is formed by spallation from Ca, K, Ti, and Fe, by thermal neutron capture in ^{35}Cl, and by muogenic production from Ca and K. The concentration of the cosmogenic nuclide provides a measure of the exposure age of the surface, but also of the exposure history which may include periods of burial or erosion. It also may present information about the intensity of the secondary radiation throughout the time depending on the strength of the earth magnetic field, climatic variations, or about the intensity of the incoming primary radiation. Several factors such as topographic shielding and the thickness or sampling depth influence the effective amount of radiation hitting the surface and are taken into account by applying appropriate scaling factors. Also the effects of uncertainties in the collected data necessary for the determination of the scaling factors are discussed.

Chapter 3 gives an overview over the geologic development of the Canary Islands. The volcanic activity of the archipelago has lasted very long and extends to recent time. Geologically young samples covering an age range of approximately 60 to 400 ka could be collected from a number of flows, which suit the time span that can be covered with ^{36}Cl age determination. The age was independently determined with the $^{40}Ar/^{39}Ar$ method.

Chapter 4 describes the sampling strategy, the preparation procedure, the AMS technique applied, and details on the data analysis including calculations and error estimation. From each flow 7 or 8 samples were collected whose surface structures indicated as little erosion as possible. ICP and XRF measurements proved that the basalts were very similar in chemical

composition. The preparation followed generally the procedure established by Stone et al. (1996b).

Chapter 5 reports on the results of the measurements and the deduced total chlorine concentrations, the amount of ^{36}Cl, and the production rates. Despite some scatter which is due to the preparation, the measurement and mainly to the natural variability of chlorine contents in rock, the data are consistent for each flow. The production rates for the total rock compare fairly well with data presented elsewhere in the literature. The high variability of the production rates for the individual production mechanisms given in the literature make the estimation of expected total production rates rather difficult. Production rates for individual production mechanisms of ^{36}Cl could not be obtained due to the lack of suitable phenocrysts. Thus, the calculation of the production rate of ^{36}Cl from Ca and of the thermal neutron flux had to be based on literature data for the other production paths involved in the total ^{36}Cl production. These data indicate loss of ^{36}Cl in some of the samples while other samples even show increased ^{36}Cl contents compared to the expected amounts. The determination of a ^{36}Cl depth profile failed because the samples did hardly contain ^{36}Cl.

In chapter 6 the results are discussed. The ^{36}Cl concentrations lower than expected are interpreted to indicate shielding by overlying ash, dust and lava sheets, which during the exposure time have been eroded. For the samples of ^{36}Cl concentrations higher than expected a number of possible reasons is evaluated which in combination may cause increased ^{36}Cl build-up, such as thin water layers trapped in the uppermost vesicles in the rock, or an earth magnetic field weaker than assumed based on the time record used for scaling its effect.

Due to the in many cases unclear erosion/exposure history (only the flows VF and MQ appear to have experienced a simple exposure history) and the fact that it is impossible to analytically determine the production rate for individual production mechanisms, Fuerteventura is probably not a perfect calibration site. However, taking the given restriction into account it will provide useful data especially once all individual production rates are securely determined.

Samenvatting

Kosmogene nuclides zijn heel belangrijk hulpmiddelen om landschapsontwikkeling en de relatieve ouderdom van geologisch heel jonge materialen te bepalen. Het doel van dit onderzoek is gegevens te verkrijgen voor het bepalen van leeftijden op de basis van kosmogeen ^{36}Cl. Daarvoor zijn basaltmonsters van Fuerteventura, Canarische Eilanden, verzameld en daarin de productiesnelheden van ^{36}Cl bepaald. Fuerteventura was gekozen als een calibratieplek op een middelbare breedtegraad en op geringe hoogte. Deze data werden vervolgens vergeleken met resultaten van andere onderzoeken die in de literatuur zijn gepubliceerd.

Zoals in hoofdstuk 2 is beschreven, is ^{36}Cl een radionuclide die gevormd word door secundaire kosmische straling aan de oppervlakte van de aarde. Deze secundaire straling is afkomstig van de wisselwerking van atomen van de atmosfeer met het deel van de primaire kosmische straling dat voldoende energie heeft om het magnetische veld van de aarde te kunnen binnendringen. ^{36}Cl wordt gevormd door spallatie van Ca, K, Ti en Fe, door invang van thermische neutronen door ^{35}Cl en door wisselwerking van muonen met Ca en K. De concentratie van de kosmogene nuclide is een maat voor de bestralingstijd, die echter ook periodes van bedekking kan bevatten en waarin ook erosie kan optreden. De concentratie geeft ook informatie over de intensiteit van de straling over de tijd die afhankelijk is van de sterkte van het aardmagnetische veld, klimaatveranderingen en de intensiteit van de primaire kosmische straling. Er zijn meerdere factoren die de effectieve bestraling van de monsters beïnvloeden, bijvoorbeeld topografische afscherming of de dikte van het monster. Hiervoor wordt gecorrigeerd door het toepassen van schalingsfactoren. Onzekerheden in de schalingsfactoren worden ook bediscussiëerd.

Hoofdstuk 3 geeft een overzicht van de geologische ontwikkeling van de Canarische Eilanden. De archipel was geologisch heel lang vulkanisch actief en is dat nog steeds. Geologisch heel jonge monsters met een ouderdom tussen ongeveer 50 en 400 ka zijn verzameld van enkele verschillende lavastromen die geschikt zijn voor ouderdomsbepalingen op basis van ^{36}Cl en voor het bepalen van productiesnelheden van ^{36}Cl in het basalt. De ouderdom van de monsters was onafhankelijk bepaald met hulp van de ^{40}Ar/^{39}Ar methode.

Hoofdstuk 4 beschrijft de manier van het bemonsteren, de preparatieprocedure, de AMS techniek en details van de analyse van de data (berekeningen en foutendiscussie). Van iedere lavastroom zijn zeven of acht monsters genomen die zo weinig mogelijk indicatie van erosie vertoonden. Volgens de ICP en XRF metingen kwamen de basalten sterk overeen in hun

chemische samenstelling. De preparatie volgde over het algemeen het protocol van Stone et al. (1996b).

Hoofdstuk 5 behandelt de meetresultaten en de daarvan afgeleide totale concentraties van stabiel chloor en van ^{36}Cl en de productiesnelheden van ^{36}Cl. Ondanks de variatie in de gegevens die uit de preparatie, de meting en voor het grootste gedeelte uit de natuurlijke variabiliteit van de chloorconcentratie in het gesteente voortkomt, zijn deze resultaten consistent voor elke lavastroom. De productiesnelheden voor het gehele gesteente zijn vergelijkbaar met waarden in de literatuur. De sterke variatie van de gepubliceerde productiesnelheden voor enkele productiemechanismen maken het moeilijk om de verwachte totale productie af te schatten. Het was niet mogelijk om de productiesnelheden voor de individuele productiemechanismen van ^{36}Cl te bepalen omdat er geen daarvoor geschikte mineraalkorreltjes van voldoende grootte in het gesteente zaten. De berekening van de productiesnelheden van ^{36}Cl uit Ca en van de flux van de thermische neutronen zijn dus gebaseerd op data uit de literatuur voor alle andere productiemechanismen die in de totale productie een rol spelen. De getallen geven aan dat voor enkele van de monsters ^{36}Cl moet zijn verloren gegaan. Echter voor andere monsters zijn de ^{36}Cl hoeveelheden wat groter dan verwacht. Er is geen diepteprofiel van ^{36}Cl worden omdat de daarvoor selecteerde monsters onvoldoende ^{36}Cl bevatten.

In hoofdstuk 6 worden de resultaten besproken. De ^{36}Cl concentraties die lager zijn dan verwacht wiizen op bedekking van de monsters door as, stof en lava die gedurende de expositietijd weggeërodeerd zijn. Er zijn verschillende mogelijkheden ter verklaring van de ^{36}Cl concentraties die hoger zijn dan verwacht, zoals dunne waterlaagjes binnen de bubbeltjes in de bovenste laag van het basalt of een lagere intensiteit van het aardmagnetisch veld dan aangenomen voor de berekening van de schalingsfactoren.

Fuerteventura is geen perfecte calibratielocatie omdat in vele gevallen de erosie- en blootstellingsgeschiedenis niet erg duidelijk is (alleen de lavastromen VF en MN lijken een eenvoudige bestralingsgeschiedenis te hebben) en omdat het niet mogelijk was om de snelheden voor enkele productiemechanismen analytisch te bepalen. Indien deze individuele productiesnelheden goed bekend zouden zijn kunnen gegevens van Fuerteventura van groot belang worden.

Acknowledgements

The research presented here was made possible by the support of many people in and outside of the Van de Graaff lab. First of all I wish to thank Klaas van der Borg for attracting my attention to cosmogenic nuclide based dating, for introducing me to accelerator measurements and for bodaciously supervising my research. Especially his inexhaustible patience to get principles of accelerator physics into a geologist's head is greatly appreciated. Countless discussions about questions occurring during the research gave me the great opportunity to focus on issues not "just geology".

René Kamermans is also thanked for supervising my work, and for many enlightening and pleasurable discussions. He read many versions of the manuscript while it still was under construction and gave valuable advice.

Arie de Jong and Cees Alderliesten are also thanked for many helpful discussions on chemical problems as well as on accelerator and cosmogenic nuclide issues. Arie greatly helped me to set up my preparation lab when I started my research and also later on to keep it running. Without his advice in general lab issues as well as in specific problems of chemical preparation this research would not have worked - lacking reasonable samples. Cees was an invaluable source – a true artesian spring - of information on what can go wrong in accelerator measurements and on many questions about particle physics. He also checked with eagles' eyes the final version of this thesis for typing errors, missing references and all sorts of inconsistencies. He, together with Kejun Dong took care of the measurements at the accelerator. David Heesbeen and Erik Maddox took care of the measurements earlier in the research and their help and good humor even if things went wrong are greatly appreciated, too.

Ruud van Stappershoef, Gerard van Gelder, Henk Kersenmaeker, Wim Arnold Bik, Philip van de Vliet, Remko van Hal, and Hans Heesen repaired the accelerator countless times with never-ending patience and solved even the most obscure problems. Ruud and Gerard passed away way too early and left behind a painful gap.

Lucilla Benedetti and Irene Schimmelpfennig introduced me to the mysteries of chemical sample preparation during a two weeks practical training at CEREGE. I gained much practical experience in the labs of CEREGE and major inspiration how to install my own lab at Utrecht University. Especially Irene is also thanked for making the time in Aix-en-Provence most enjoyable.

Tibor Dunai and Jan Wijbrans introduced my colleague Björn Schneider and me into the field methods of sample collection for cosmogenic nuclide dating.

I further wish to express my gratitude to all the people who contributed to the research outside of the AMS lab: The people from NITG for the XRF and ICP measurements, Frans Bakkers, Wynanda Koot, en Bouk Laçet from the VU-laboratory for rock preparation for fantastic thin sections and the opportunity to work in their lab, Tilly Bouten (UU) for the chance to perform measurements at the microprobe and Marjan Versluijs (UU) for XRD measurements.

From many other people I could learn a lot about fields related to cosmogenic nuclides: Monika Korte (GFZ Potsdam), Cathy Constable (University of California) and Andy Biggin (Utrecht University) taught me many important details about paleomagnetics, Susan Ivy-Ochs (ETH Zurich) and Christoph Schnabel (SUERC, Glasgow) gave valuable advice on practical experimental questions ad data analysis.

Further I wish to express my gratitude to the members of the commissie, Prof. Thomas Peitzmann, Prof. Andy Lotter, Prof. Paul Andriessen and Prof. Cor Langereis who gave valuable advice to improve the manuscript.

This research was made possible with generous financial support from the Marie Curie Fellowship, EU, funded by the European Community's Program: Improving the Human Research Potential and the Socio-economic Knowledge Base.

Finally I wish to thank my parents Birgit and Matthias Mai and my friends, especially Elisabeth Beer and Tony Hearn for their inexhaustible support and patience with me during my research but also for their successful attempts to now and then get me out of science and enjoy life e.g. with opera, concerts and visits to towns and countryside. Tony spent days on correcting the grammar and wording of this thesis.

Curriculum Vitae

I was born in Berlin, Germany on the 10th of August 1975. After finishing my Abitur at the Alexander v. Humboldt- Gymnasium, Berlin-Köpenick, in 1995 I did an apprenticeship as a surveyor by the ÖbVI Noormann-Wachs. In 1998 I started my studies of geophysics at the Technical University of Berlin. In 2001 and 2002 I studied geology at the University of Oklahoma based on an exchange program, where I earned the degree of Master of Science in Geology (thesis: “Microstructural and kinematic analyses of a proterozoic quartzite-schist sequence in Blue Ridge, Colorado”). Back in Berlin I finished my studies of geophysics in 2005 and earned the degree of Diplom-Ingenieur of Applied Geophysics (thesis: “The Altiplano (Central Andes) High Conductivity Zone: Interpretation and Modeling”).
Since 2005 I have been AiO at the Utrecht University, based on the Marie Curie Fellowship, participating on the CRONUS-EU programme, which is supported by the European Community's Program: Improving the Human Research Potential and the Socio-economic Knowledge Base.